12-2013

An Experimental and Computational Evaluation of the Importance of Molecular Diffusion in Gas Gravity Currents

Jeremy Jac Herman
University of Arkansas, Fayetteville

An Experimental and Computational Evaluation of the Importance of Molecular Diffusion in Gas Gravity Currents

An Experimental and Computational Evaluation of the
Importance of Molecular Diffusion in Gas Gravity Currents

A dissertation submitted in partial fulfillment
of the requirements for the degree of
Doctor of Philosophy in Chemical Engineering

by

Jeremy J. Herman
The University of Toledo
Bachelor of Science in Chemical Engineering, 2008

December 2013
University of Arkansas

This dissertation is approved for recommendation to the Graduate Council.

_____
Dr. Jerry Havens
Dissertation Director

_____
Dr. Robert Beitle
Committee Member

_____
Dr. Edgar Clausen
Committee Member

_____
Dr. Rick Couvillion
Committee Member

_____
Dr. Tom Spicer
Committee Member

ABSTRACT

The accidental release of hazardous, denser-than-air gases during their transport or manufacture is a vital area of study for process safety researchers. This project examines the importance of molecular diffusion on the developing concentration field of a gas gravity current released into a calm environment. Questions which arose from the unexpectedly severe explosion in 2005 at Buncefield, England were of particular interest. The accidental overfilling of a large tank with gasoline on a completely calm morning led to a massive open air explosion. Forensic evidence showed that at the time of ignition, a vapor cloud, most of which now appears to have been within the flammability limits, covered approximately 120,000 m^2. Neither the severity of the explosion, nor the size of the vapor cloud would have been anticipated.

Experiments were conducted in which carbon dioxide was released from a sunken source into a one meter wide channel devoid of any wind. These experiments were designed in such a way as to mitigate the formation of a raised head at the front of the gravity current which would have resulted in turbulent entrainment of air. This was done to create a flow in which molecular diffusion was the controlling form of mixing between the carbon dioxide and air. Concentration measurements were taken using flame ionization detection at varying depths and down channel locations.

A model of the experiments was developed using COMSOL Multiphysics. The only form of mixing allowed between carbon dioxide and air in the model was molecular diffusion. In this manner the accuracy of the assertion that molecular diffusion was controlling in our experiments was checked and verified.

Experimental measurements showed a large variation of gas concentration with depth of the gravity current at the very beginning of the channel where the gas emerged up from the sunken source and began flowing down channel. Due to this variation, molecular diffusion caused the vertical concentration profile to get more uniform as the gravity current flowed down the channel. A COMSOL model was developed which showed an overall increase in the depth of the flammable region of a cloud with increasing time, due to this effect.

ACKNOWLEDGEMENTS

I would like to thank the many people who helped make the completion of this dissertation possible. First and foremost I would like to thank my advisor, Dr. Jerry Havens, for allowing me to work for him at a time when he didn't have any intention to take on any graduate students. I benefited greatly from his experience and wisdom.

I would also like to thank George Fordyce and Harold Watson. This project does not get off the ground without their expertise. I am grateful.

My fellow graduate student, Jeff Martinez was a huge source of assistance and support.

I received amazing support from the entire Chemical Engineering department, but I want to single out Dr. Rick Ulrich and Dr. Bob Beitle who as my first contacts in the department were vital in my ending up at this university.

Special mention goes to my sisters, Deanna Buckley and Christine Volk, along with my brothers in law, Terry Buckley and Leon Volk. Their support during this process was vital to my success.

Last but not least, I want to thank my mentor and friend, Dr. Heather Walker. She and the rest of her family, Doug, Abigail, Audrey, and the incomparable Annie, have become like a second family to me.

DEDICATION

To my parents, without whom I wouldn't be the person I am today.

Donna J. Herman
December 9, 1941- June 3, 2010

Jack H. Herman
December 4, 1939 - November 1, 2000

TABLE OF CONTENTS

LIST OF TABLES

LIST OF FIGURES

LIST OF SYMBOLS

a	constant
B_H	Hall's buoyancy flux parameter
b	constant
C	gas concentration (mole %)
c	constant
d	constant
E_S	saturation vapor pressure of water (N/m^2)
e	natural base
Fr	Froude number
h	depth of gas cloud (m)
g'	reduced gravity (m/s^2)
g'_{BF}	reduced gravity at Buncefield (m/s^2)
La	layering number
M_{CO2}	molecular weight of carbon dioxide (kg/mol)
M_D	molecular weight of dry air (kg/mol)
M_W	molecular weight of water (kg/mol)
P_D	partial pressure of dry air (N/m^2)
P_V	partial pressure of water vapor (N/m^2)
P_T	total pressure (N/m^2)
Q_0	volumetric flow rate (m^3/s)
q_0	volumetric flow rate per unit width (m^2/s)
R	universal gas constant (m^3 Pa/K mol)

Re	Reynolds number
RH	relative humidity
Ri_P	overall plume Richardson number
T	temperature (K)
t	time (seconds)
U	mean velocity (m/s)
u_*	friction velocity (m/s)
W	width of source or temperature related parameter in saturation vapor pressure of water equation (K)
x_{CO2}	mass fraction of carbon dioxide
x_{DA}	mass fraction of dry air
ρ	density (kg/m^3)
ρ_{CO2}	density of carbon dioxide (kg/m^3)
ρ_{DA}	density of dry air (kg/m^3)
ρ_T	density of air in the wind tunnel during experiments (kg/m^3)
ν	kinematic viscosity (m^2/s)

CHAPTER 1

INTRODUCTION

1.1 Natural and Accidental Releases of Hazardous, Denser-Than-Air Gases

On August 21, 1986, at Lake Nyos in the African country of Cameroon, a sudden release of up to one cubic kilometer of carbon dioxide [26] caused 1746 people, and about 8500 livestock to die of asphyxiation [20]. Lake Nyos is a crater lake which sits near the top of an inactive volcano, so most of the adjacent land is below the lake. This caused the released carbon dioxide to flow down valleys flanking the volcano, killing everything in its path. Of the 800 inhabitants of the nearby village of Nyos, only 6 survived [20]. Fatalities occurred as far away as *16 miles* [20]. The concentration of carbon dioxide required to cause these speedy deaths is about 100,000 ppm, which is 300 times the normal background levels. To have this concentration so far from the source was a stunning mystery, a mystery that remains over 25 years later.

The key to the lethality of this tragedy is the fact that carbon dioxide is denser than air, and therefore it clung to the ground as it flowed down hill. Given this, it was not surprising that there were fatalities, but for the carbon dioxide to have this high a concentration after travelling so far was shocking. In the absence of wind, a denser-than-air-gas flows only under the action of gravity, just as a river would if a dam suddenly gave way. Because of this, these flows are called gravity currents. Even in calm conditions, it would have been expected that enough turbulent mixing would have taken place between the carbon dioxide and air to bring the concentration down below lethal levels long before it flowed for 16 miles.

Lake Nyos is a dramatic (and exceedingly rare) example of a naturally occuring release of a hazardous, denser-than-air-gas. With the rise of industry has come the danger of *accidental* releases of hazardous, denser-than-air gases. Commonly, these gases pose a risk of fire and explosion along with often being toxic. Assessing the risks associated with these releases is a important area of academic research. For obvious reasons, much process safety research focuses on lessening the likelihood of an accidental release of these chemicals during manufacture and transport. However, accidents of this type have continued, and will continue to occur. It is important for researchers to examine how dense gases disperse into the atmosphere (and are thus diluted) in order to assess the danger to lives and property. This project focuses on releases into a completely calm (no wind) atmosphere.

1.2 The Buncefield Accident

An industrial accident of direct interest in this project occurred early on the morning of December 11, 2005 in central England. A series of explosions, and a massive fire rocked the Buncefield oil depot after a large tank on the site was mistakenly overfilled with gasoline. Various media accounts described both the main explosion and fire as the largest in the history of peacetime Europe. It was also reported that the main explosion measured 2.4 on the Richter scale, broke windows over 50 miles away, and was felt as far away as Belgium [2, 17]. There were forty injuries and no fatalities. That there were no deaths is almost certainly only due to the accident taking place early on a Sunday morning. The British Government's final report on the incident estimated a total economic cost exceeding £ 1,000,000,000.

Figure 1.1 Photograph of the Buncefield site [4] in the immediate aftermath of the explosions. The nearly straight fire line is the western wall of the dike which contained the overfilled tank. Between this dike and the smoldering structure is the parking lot where the largest explosion took place. The fuel depot was surrounded by an office park. If the accident had taken place during normal working hours it is likely that there would have been fatalities.

Gasoline escaped the full tank through vents near the roof and then poured down the side of the tank into a one meter tall dike meant to capture any spilled fuel. This went on for 41 minutes before the initial blast. The gasoline pooling inside the dike immediately began to evaporate forming a dense cloud of gasoline vapor inside the dike. The vapor was visible to surveillance cameras on the grounds presumably because the heat of vaporization caused ice crystals to form in the cold, humid air. Approximately 18 minutes after the tank began to overflow, vapor emerged from the northwest corner of the dike and began flowing west over the parking lot. The western wall of the dike is visible as the straight line of fire in Figure 1.1. This wall ran north-south, with the left side being north in the above photograph. The main explosion took place in

the parking lot between the dike and the building seen smoldering in Figure 1.1. Investigators were initially baffled by the size of the explosion since it took place in an unconfined setting. The specific nature of the explosion mechanism is outside the scope of this work, but some possible explanations for this have come from tests showing that the trees on the site may have created turbulence within the cloud which speeded up the flame front, and resulted in overpressures.

Another mystery which *is* of relevance in this project is the size of the cloud which was within the flammability region at the time of the accident. The footprint of the burned area of the site suggested that the vapor cloud stayed within the upper and lower flammability limits even while the gas was pouring over the dike walls, and flowing radially, for 23 minutes. It would have been anticipated that much of the vapor cloud would have been sufficiently diluted through mixing with air so as to render it incombustible. The fact that there was no wind at the time of the accident clearly contributed to the lack of mixing with air, but classical gravity current theory would still suggest significant mixing (and therefore dilution) at the front of the gravity current. As will be described in detail later this work focuses on the potential effects of molecular diffusion on these flows.

1.3 Gravity Currents

Gravity intrusion fluid flows occur when a mass of heavy fluid displaces a mass of lighter fluid. Such flows can be beneficial - stored water distribution systems (the water towers that dot the countryside) enable us to obtain irrigation water or drinking water at the flick of a wrist – or they

can cause catastrophic damage – dam breaks and tsunamis are much in the news today. In dam breaks or tsunamis, the two fluids (water and air, usually) do not mix. Instead, the water simply displaces the air – pushing it out of the way. The mixing of water and air in a gravity driven flow such as a tsunami wave is of very minor importance because of the great difference in density and the limited miscibility of the two fluids - about 1000 kg/m^3 for water compared with about 1.2 kg/m^3 for air at ambient temperature and pressure, with limited solubility of air in water. In a water-intrusion-into-air the water is positioned below the air (by gravity) and the air and water can mix only by a process of molecular diffusion. The dynamics of such flows, where mixing of the two fluids can be neglected, are reasonably described by a simplified application of energy conversion of the water during its movement. The potential energy of the water (say behind a dam which breaks) is converted to kinetic energy - as the water flows laterally while diminishing in depth.

Gravity driven flows also occur as a result of the displacement of fluids by others of slightly different densities – weather report “cold fronts” consisting of higher density regions of (cold) air displacing lower density air masses, and thunderstorm outflows (“microbursts”) are two examples.

In such atmospheric flows the density differences may be only a few percentage points, in direct contrast to liquid/gas intrusions such as following dam breaks. Although mixing can still occur by molecular diffusion, the mixing is characterized by velocities much smaller than the frontal movement (intrusion) velocities and has generally been dismissed, but (large) cold front movements due to density differences of a few percentage points can result in frontal velocities of order 10 m/s. For such large scale flows, with velocity scales of order 10 m/s and (intruding) fluid depths of order 100 meters, these gravity intrusion flows exhibit large Reynolds number

(turbulent) flow patterns resulting in substantial mixing of the high/low density fluids. The Reynolds number (*Re*) is defined as

$$Re = \frac{Uh}{\nu} \qquad (1.1)$$

where U is the characteristic velocity, h is the characteristic height, and ν is the kinematic viscosity.

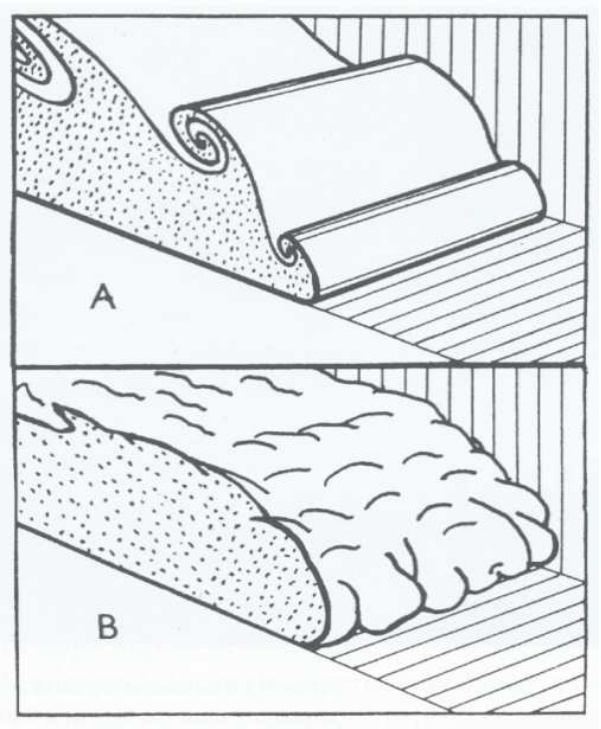

Figure 1.2 Two forms of mixing in the head of a gravity current: (A) billows (ambient fluid gets drawn into the head), (B) lobes and clefts (caused by current over running ambient fluid near the ground) [36].

Academic studies of gravity currents have focused on two primary forms of mixing, both of which occur at the frontal region (head) of the flow. Figure 1.2 shows an illustration of these two forms. Ambient fluid is drawn into the gravity current just behind the head by billows (called Kelvin-Helmholtz billows) formed due to shear instability. The other form of mixing is ambient fluid getting trapped between the ground and the gravity current as it flows across a surface. This is believed to have a much smaller net effect on the concentration in a cloud than the billows do, but this effect is responsible for the lobe and cleft structure commonly observed at the front of a gravity current. This is because overrun fluid immediately begins to rise within the cloud. This is an unstable and transient process which results in the lobe and cleft feature. Experiments have been conducted in which the floor is moved at the same speed, and in the same direction, as the flow caused the lobes and clefts to dissappear, proving that this feature is caused by the no-slip boundary condition and the resulting overrunning of fluid [36].

A third form of mixing, molecular diffusion, (generally neglected in comparison with turbulent mixing) has been little discussed in the literature. The impact of molecular diffusion on gravity currents is the focus of this project. The motivations for this are discussed in the following chapter.

CHAPTER 2

LITERATURE REVIEW

2.1 Classical Gravity Current Studies

Gravity current flow was first characterized qualitatively by Schmidt in 1911 [29, 31]. While studying thunderstorm outflows he created gravity currents at varying *Re* through temperature induced density differences and produced the shadowgraphs seen in Figure 2.1. When the flow profile stopped changing as *Re* was increased (the profile staying like that of part f in Figure 2.1) he proposed that there was an upper limit of *Re* beyond which turbulent mixing remained unchanged. This is the first mention of such *Re* independence in the literature. Additionally, these shadowgraphs show some of the key physical characteristics of a fully turbulent gravity current, the deeper frontal region (head) with a leading edge raised above the surface (nose), and the turbulent waves trailing behind the top of the head region.

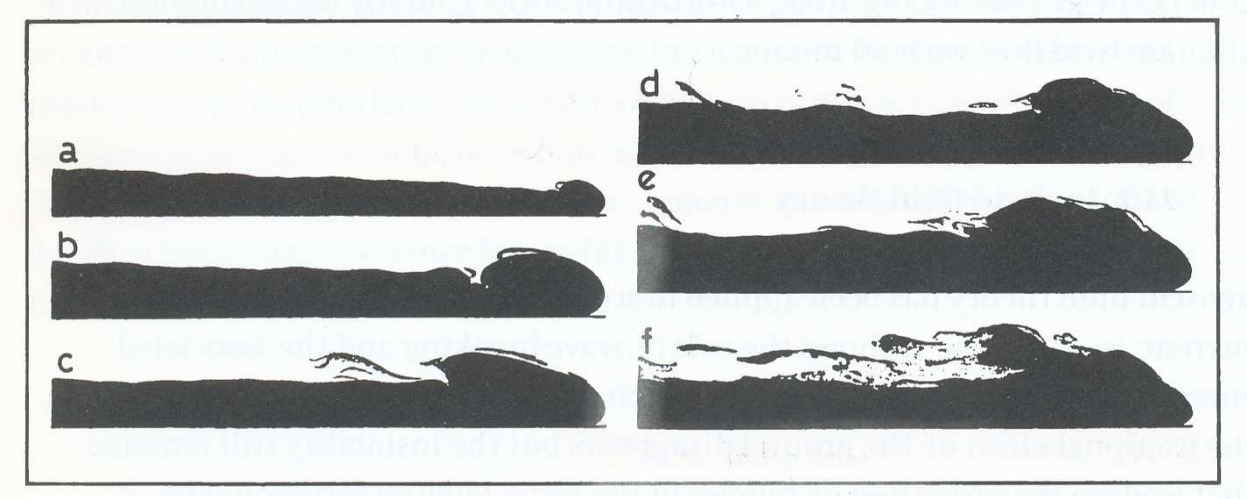

Figure 2.1 Profile view of gravity currents showing distinctive head. The Re increases from less than 10 in (a) to greater than 1000 in (f). The final view (f) shows a profile that is independent of Re (Schmidt, 1911: Taken from Simpson, 1997) [36].

The first quantitative treatment of gravity currents was done by Theodore von Karman in 1940 [41]. As shown in Figure 2.2, he treated the problem as if one were moving with the gravity current so that the gravity current is motionless and the (infinitely deep) ambient fluid is flowing past. This is valid analytically, but it is noted that the profile in Figure 2.2 does not assume a no-slip boundary condition and therefore does not have the raised "nose" of the profiles in Figure 2.1. Assuming inviscid flow, and an infinitely deep ambient fluid, he applied Bernoulli's theorem along the interface between the two fluids, thus developing the following non-dimensionalized expression for velocity of advance of the gravity current,

$$\frac{U^2}{g'h} = \sqrt{2} \tag{2.1}$$

where g' is the reduced gravity;

$$g' = g(\frac{\rho_1 - \rho_2}{\rho_2}) \tag{2.2}$$

where ρ_1 is the heavier fluid. The expression on the left-side of Equation (2.1) is equivalent to the densimetric Froude number (*Fr*), a dimensionless number which gives the ratio of inertial forces

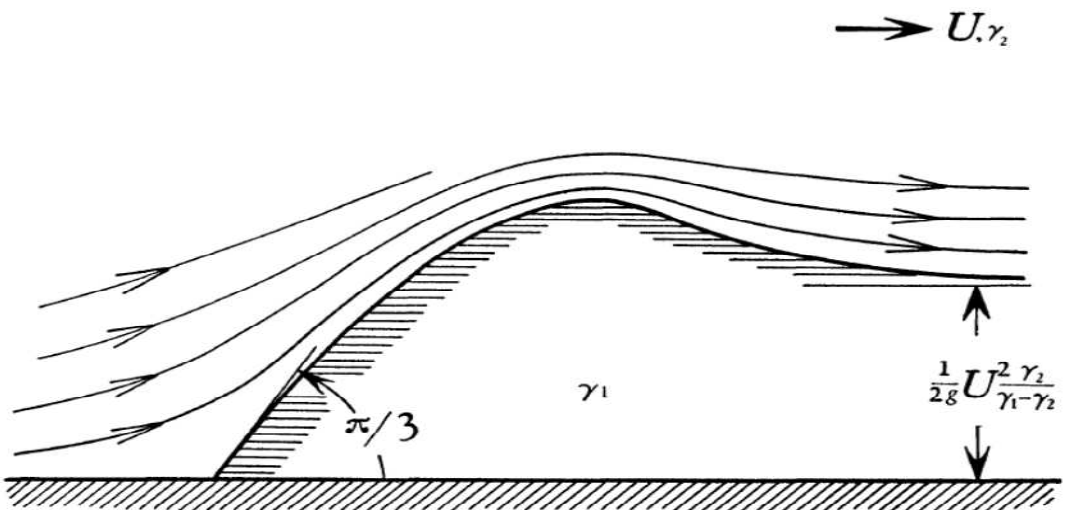

Figure 2.2 von Karman's idealized picture of a gravity current head. There is no assumption of a no-slip boundary condition and therefore no raised nose. The expression on the right is equivalent to Equation (2.1) [42].

to buoyancy forces.

In the years since von Karman's work there have been numerous analytic, numerical, and experimental studies of gravity currents [7,14,18,20-24,29,30,32,36] Most of these works have focused on characterizing the head region, and on issues like *Re* independence and the value of the *Fr*. This, along with the fact that most of the experimental work has been done with liquids (saline-water) in very short running experiments, has meant that studies of the effect of molecular diffusion on pure gravity current flow has largely been neglected. It is molecular diffusion that will be the focus of this work, but before getting to that, there will be a slight digression to make a point about the potential impact of diffusion on the concept of *Re* independence.

Re independence has been a vital tool in the study of gravity currents at laboratory scales. Applying conclusions drawn from small scale experiments to large scale dense gas releases requires similarity between the two flows. The formal requirement for similarity is geometric similarity, and the equivalence of all relevant dimensionless numbers [36]. In the case of gravity current flow, these are *Re* and *Fr*. Achieving *Re* equivalent to those in large scale flows is generally not possible in the laboratory because the length and velocity scales cannot be reproduced, nor can the kinematic viscosity be lowered enough to make up for this fact. Because of this, it has been necessary at laboratory scales to fall back on the concept of *Re* independence.

A seminal work on gravity currents by Simpson [36], describes *Re* independence thusly, "…when the *Re* is greater than about 1000 the flow patterns are independent of its value." This statement is not cited in the text. Based on the given value of 1000 and the similarity in language to Schmidt regarding unchanging flow patterns, it seems that the source of this assertion by

Simpson is figure 2.1. This judgment is helped by a familiarity with Simpson's work on gravity currents which included extensive experimental studies using salt water geared toward understanding the nature of the head of a gravity current. These experiments included photographic studies similar to Schmidt's shadowgraphs and an extensive set of experiments where the geometry of the head was detailed by measuring the heights of various locations within, and around, the head. In stating that the flow appears "dynamically similar" [31,36], Schmidt and Simpson are stating that the *appearance* of the head of the gravity current stops changing above *Re* 1000 and therefore the conclusion is drawn that the turbulence is fully developed. This allows investigators to do laboratory scale experiments and still extrapolate their findings to Buncefield sized releases as long as the *Fr* is the same in both flows, since it is also argued that the flow is fully characterized by *Re* and *Fr* alone [36].

The original experimental plan for this project started with the above argument. If we could create a flow with a *Re* safely above the threshold for independence, there was the potential for finding some answers to the mysterious questions raised by the Buncefield event. We would check for independence (by collecting concentration data at different *Re* and assuming that dynamically similar flows would have a statistically equivalent, non-dimensionalized, concentration profile), but there was no interest in it other than as a tool to allow us to scale a Buncefield type release in the wind tunnel. In this early planning stage there was much consideration given to the vagueness surrounding the arguments for Re independence, but no real questioning of its validity. Also, there was no consideration given to molecular diffusion having an important role in our experiments. Intuitively, this makes perfect sense. Even if out of due diligence one considered the implications of diffusion on these releases, the thought would pass quickly. It seemed more than safe to assume that the turbulent entrainment of ambient fluid into

the head of a gravity current (figure 1.1, top illustration) would dwarf any entrainment due to diffusion. At this thought molecular diffusion was dismissed as an important consideration. However, this thinking began to change when the potential importance of molecular diffusion on our experiments began to emerge during our attempts to fill our reservoir full of pure carbon dioxide (discussed at length in Chapter 3, Section 3.2).

2.2 Laminarization Criteria

At this point, molecular diffusion became the focal point of the project and it became desirable to revisit the idea of fully developed flow which emerges out of the ideas of *Re* independence and *Fr* constancy in the literature. While the literature does make a convincing argument that fully developed turbulence is achieved in the head, the trailing flow is neglected. Is there turbulence at the interface between the two fluids in the region behind the head?

Investigating this question meant moving slightly away from the study of classical gravity currents (where the ambient fluid is generally treated as motionless), to the related field of dense gas dispersion, which is the study of what happens to a dense gas when it is released into a turbulent boundary layer (the atmosphere near the ground, in the presence of wind). In studying this type of release there is less emphasis on the leading edge of the flow and more on the rate of vertical mixing (dilution) at the interface between the two fluids. The conditions under which turbulent mixing, or conversely, molecular diffusion are controlling has been studied extensively in wind tunnels. Long noted in these studies is the phenomenon of laminarization. The vertical density gradients present when a denser-than-air gas is released inhibit vertical motion and can

cause turbulence to be damped [6,38]. When this occurs the flow is said to have been laminarized and the dominant form of mixing in such a flow is molecular diffusion.

There have been several laminarization correlations developed by investigators over the years. These are dimensionless quantities which when matched with experimental observation give ranges over which flows are laminarized. Four of them were used in this work, and they are introduced below. First, however, a table is displayed which introduces the variables used to calculate values of the correlations, along with the values of these quantities for both the Buncefield event, and our wind tunnel experiments. After each correlation is introduced, their calculated values for both Buncefield and our experiments will be given.

Table 2.1 Variable values used in laminarization correlations

Quantity	Symbol	Units	Buncefield Values [17]	Experimental Values
Reduced gravity	g’	m/s^2	1.37	1.37
Bulk flow velocity	u	m/s	0.6	0.1
Volumetric flow rate	Q_0	m^3/s	100	0.0033
Flow rate per unit width	q_0	m^2/s	0.4	0.0033
Width of source	W	m	270	1

Hall & Waters (1989) [17] $$B_H = \frac{g'\sqrt{Q_0}}{u_*^{2.5}} \quad (2.3)$$

u_* is the friction (or shear) velocity. Localized velocities were not calculated in the experiments conducted for this project, so u_* was calculated by using a general rule which states that $u_* = \frac{1}{20}u$, where u is the mean (bulk) flow velocity [38].

Hall & Waters gives the following criteria for their correlation:

0 – 10	passive dispersion (flow unaffected by density effects)
10-1000	mixed
> 1000	laminarized buoyancy flow

Buncefield

B_H = 88,000

Experiments

B_H = 45,000

McQuaid (1976) [27]

$$La = \frac{u}{(q_0 * g')^{\frac{1}{3}}} \tag{2.4}$$

McQuaid reported a transition from passive to nonpassive flow as the layering number (La) fell below 3.23. This isn't as descriptive as the criteria used by Hall & Waters and could indicate a "mixed" flow pattern at values below, but near 3.23. Because of this confidence that a flow is fully laminarized may only be achieved for $La \ll 3.23$.

Buncefield

La = 0.73

Experiments

La = 0.60

Britter (1989) [13]

$$B_B = \frac{g' Q_0}{u^3 W} \tag{2.5}$$

Britter gives the following criteria for his correlation:

0 – 0.005	passive dispersion (flow unaffected by density effects)
0.005 – 0.1	mixed
> 0.1	laminarized buoyancy flow

Buncefield

B_B = 2.3

Experiments

B_B = 4.6

Stretch (1986) [38] $$Ri_p = \frac{q_o g_0'}{u^3} \quad (2.6)$$

Stretch states that a flow is laminarized for any values above 0.005.

Buncefield

Ri_p = 2.5

Experiments

Ri_p = 4.6

Upon examination it can be seen that all of these correlations are all very similar (with the last three being essentially identical). Four of them were used because they all drew conclusions about the transition to laminarized flow based on empirical data.

The calculated values all show that both Buncefield and our experiments are strongly in the laminarized regime. This may not seem surprising given how these correlations were used to ascertain whether the dense flow damped out turbulence caused by wind, and neither our experiments, nor Buncefield occurred in the presence of wind. Surprising or not however, these calculations did change our thinking about the meaning of *Re* independence. Instead of a flow with fully developed turbulence throughout, you have a flow which can be thought of as having two distinct regions: a head region with (possibly) fully developed turbulence, and the trailing region where molecular diffusion is the only mechanism for the entrainment of ambient fluid. The ramifications of this is that it is possible to have the type of flow similarity in the head

reported by von Karman and Simpson at *Re* above 1000 *and still not have Re independence*, since molecular diffusion does not scale. Given this, it is not reasonable to assume at the outset that molecular diffusion does not impact the concentration profile within a gravity current, be it a small scale one created in a laboratory, or a large scale one resulting from an accidental release.

This project does not set out to compare the relative amount of dilution caused by molecular diffusion and turbulent entrainment. Instead, we will seek to look at the effect of diffusion alone by attempting to eliminate turbulent entrainment altogether. Evidence being found that diffusion plays an important role in how the concentration field develops in a dense gas release does not necessarily eliminate the possibility of doing scaled down experiments, but it would mean that *Fr* would not characterize the flow alone at *Re* above 1000 (the current implications of *Re* independence).

CHAPTER 3

EXPERIMENTAL PLAN

3.1 Equipment

3.1.1 Facility

The experimental work was conducted within the ultra-low-wind-speed tunnel located at the University of Arkansas' Chemical Hazards Research Center. This tunnel was specifically designed to study the atmospheric dispersion of dense gases at low wind speeds (< 2.0 m/s). Since the experiments here were done in still air, the fans were not utilized, but the interior of the tunnel housed the instrumentation and provided the controlled environment needed to conduct these experiments. All of the instrumentation utilized on this project is operated from a control room which is isolated from the wind tunnel.

3.1.2 Source Box

The gas source box is 1 meter long, 1 meter wide, and 0.325 meters in depth and is constructed out of 3/8 in. aluminum with 5 inch wide polycarbonate strips running down the center of two of the sides to serve as windows. The top of the box is flush with the floor of the wind tunnel which serves as the channel, down which the gas flows once it emerges from the source box.

The gas is expelled from the box by a piston-like moving floor. The floor is bolted to four threaded posts (see Figure 3.1) around which is wrapped a chain (see Figure 3.2) attached to an electric motor. When the shaft of the electric motor spins, the chain spins and therefore the floor moves up (or down).

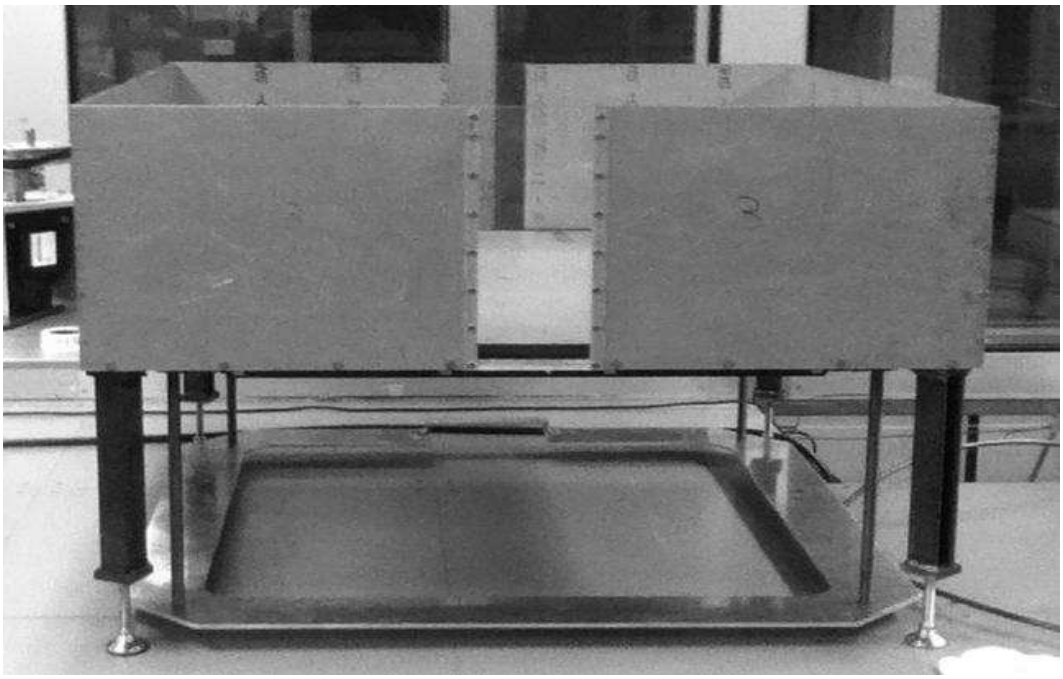

Figure 3.1 The box before it was lowered into place. The (moving) floor is all the way at the bottom of the box. Note the four posts. If the floor were at the top, the posts would be in the interior of the box and be invisible in this photo. (Photograph by author)

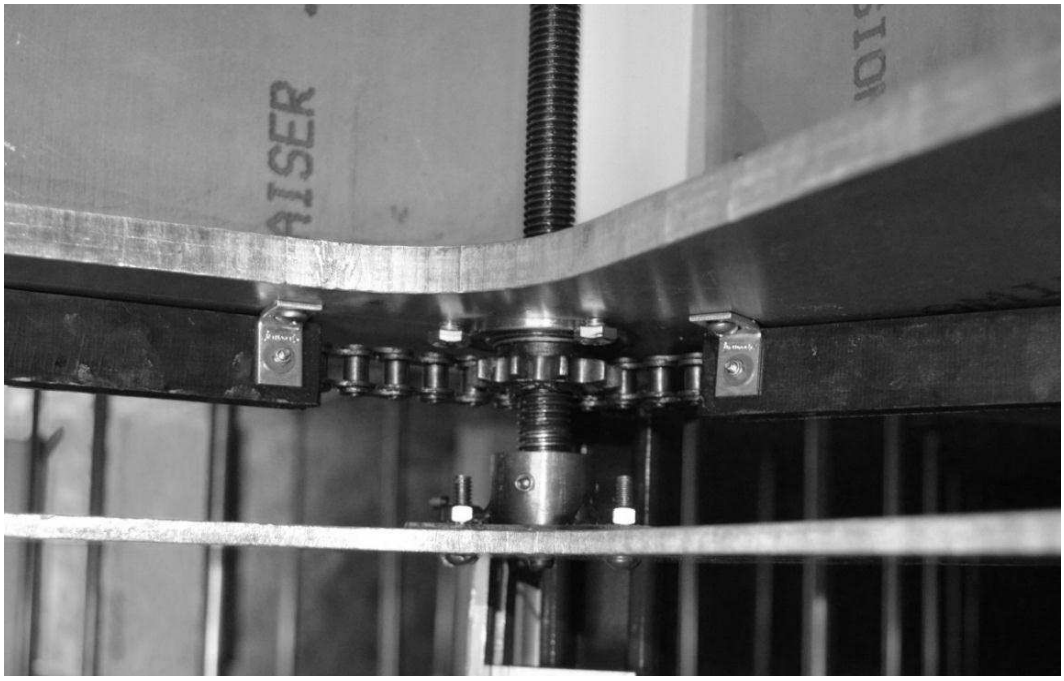

Figure 3.2 A view of the chain attached to a gear which is attached to the post. In this photo the moving floor is all the way at the top. The plate just above the gear is stationary and provides stability to the box. When the moving floor is at the bottom position (seen in figure 3.1) it is 5 mm. above this plate. (Photograph by author)

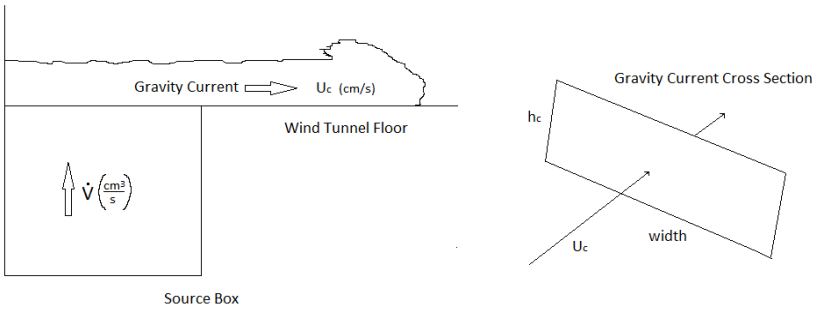

Figure 3.3 Drawing showing the basic design of the experiments. h_c and U_c are characteristic height and characteristic velocity respectively. Both are zero at time equals zero, and both eventually reach steady-state values (Figures 5.3 and 5.4).

The holes in the floor were drilled bigger than the body of the bolts attaching it to the posts and rubber grommets were used to fill the gap. In this way the floor could be securely fashioned to the posts, but it was able to move a little laterally. The floor was than able to seat itself in the best location to ride up and down. This design eliminated the need for a perfect fit between the floor and the side walls all along the depth of the box.

The moving floor design means that the total depth of the box can only be half the distance between the raised wind tunnel floor and the lab floor beneath it because the moving floor needs that travel distance below the box. Because of this the stationary walls of the box rest on four welded steel legs with adjustable feet screwed into them. A seal between the walls of the source box and the moving floor is provided by a closed cell EPDM rubber seal (Figure 3.3). The seal consists of two main parts: a serrated rectangular edge which is used to lock the seal into place and the open, circular bulb with two protruding edges which provides the seal. A groove was cut

into the sides of the moving floor to allow the serrated edge to be pushed in, locking it into place in the side of the floor. A piece of 7/16 inch outside diameter tygon tubing was threaded into the open space of the seal to give it some rigidity. The interior corners of the box and the corners of the moving floor are rounded. When the box was first built the corners were sharp, but it proved impossible do get a good seal (discussed further in Section 3.2). Vegetable oil was periodically sprayed onto the walls of the box to reduce friction between the walls and the seal. Vegetable oil was used because all common silicone or oil based lubricants dissolved the seal.

Figure 3.4 EPDM rubber seal (Source: McMaster-Carr)

The movement of the floor was achieved by using a 1000 Watt AC servo motor and accompanying control system from Automation Direct. The most important feature of the motor for this application was the capability of very fast acceleration/deceleration times. We used a value of 30 milliseconds for both in this project which justifies defining the experiments as having a single, continuous volumetric flow rate.

The control system allowed for precise positioning of the floor and simple programming of rpm rates while travelling between vertical positions. An experiment was defined by its volumetric flow rate and we only had direct control over rpm so an experiment was set up to collect rpm vs. floor velocity data which of course is easy to translate into rpm vs. volumetric flow rate.

Three floor positions were programmed: bottom (full), top (empty), and filling. The filling position will be discussed further in Section 3.2. As referenced the bottom position is 32.5 cm below the top of the box and the channel and top is flush with the tunnel.

A video camera was placed under the floor of the wind tunnel and pointed at one of the windows of the source box. The camera was connected to a television in the control room. The moving floor, chain and pulley (Figure 3.2), and smoke inside the box were made visible by the video feed.

3.1.3 Lid

A lid for the box was fashioned out of ¾ inch medium density fiberboard. The motivations for installing this lid will be discussed further in Section 3.2. As can be seen in Figure 3.4 there is a rope which pulls the lid off behind the box. There is a channel around the box which is flush with

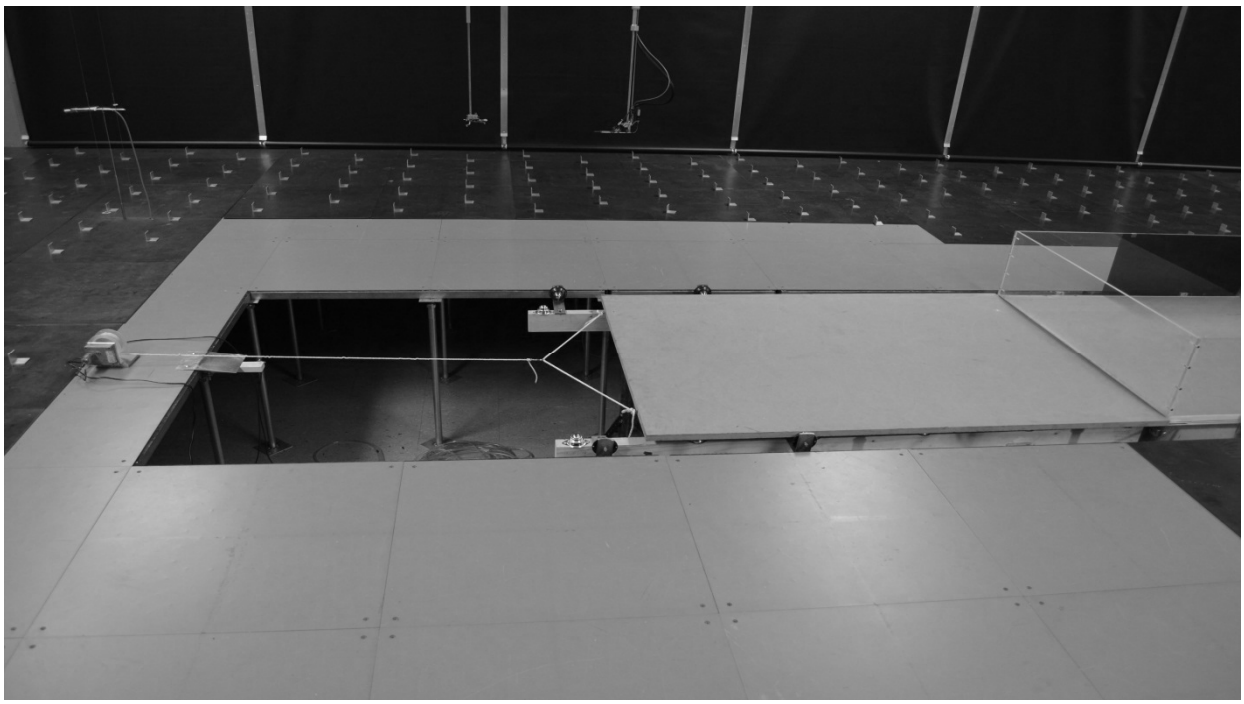

Figure 3.5 Lid shown along with supports (2x4's with rollers on top), rope, and motor (far left). The lid is covering the box (far right) in this photo. The small fan written about in Section 3.1.4 is not in this photo, but when in place it sat atop the lid immediately behind the back panel of the channel. (Photograph by author)

the sides so the only point of contact between the box and lid while the lid is being pulled off is the back wall. Because of this the lid was made 8 feet long. This extra length prevents the lid from falling down into the box once it clears the front edge while moving back. Metal stands topped with ball bearing rollers were used to support the lid and reduce friction. A strip of ¼ inch polyethylene foam was attached to the sides of the lid to serve as a low friction contact point between the lid and the channel. A 0.68 volt motor was used to pull the lid back. This motor has a plastic spool attached to its shaft which was sized in such a way that it takes one minute to pull the lid off the box. As will be discussed further later, pulling off the lid is the final step before releasing the dense gas into the channel so the box is full while the lid is being pulled off. Having the lid move one meter in a minute was determined to be a slow enough as to not create

significant a disturbance of the gas within the box. The motor is operated from within the control room. The flipping of a switch causes the lid to roll off of the box. A limit switch was installed to stop the motor at the moment the lid completely fully clears the box opening. The motor only operates in one direction so when ready for a new run the lid must be pushed manually back over the box.

3.1.4 Flow Channel

The basic design consists of a simplified version of a section of the Buncefield release. The burn pattern at Buncefield is approximately circular, implying a radial release. This fits the overall shape of the dike fairly well, but the east and west sides of the dike consist of long straight walls. Because it is where most of the explosions took place, the area to the west of the dike is of particular interest and that straight western wall means that approximating this section of the release with a planar, 2-dimensional channel is reasonable. The 1 meter tall dike at Buncefield is eliminated in the experimental design and replaced with a sunken source (the source box). The channel was constructed out of plexiglass and from the front of the box to the end it is 11.2 meters long though this entire length was never utilized. The pieces of plexiglass wrapped around the box are 3/8 inch thick while the remaining down channel pieces are 3/16 inch thick. The pieces around the box needed to be made thicker because extra strength and rigidity were needed and also they needed to be screwed both together and to the box and the extra thickness made this easier. The panel sitting atop the back of the source box is raised to allow the lid to slide underneath it. The bottom of this panel has ¼ inch polyethylene foam attached to it just like the sides of the box to reduce friction and maintain a gas seal.

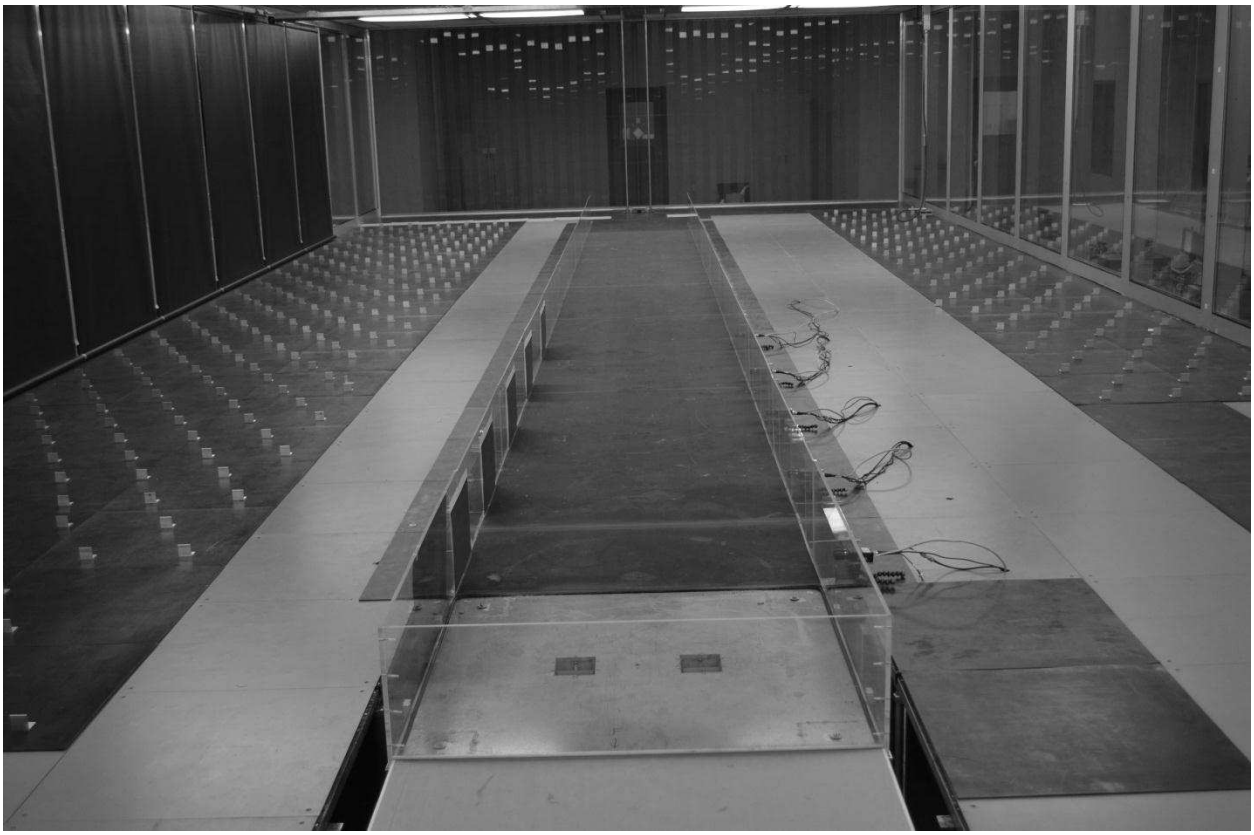

Figure 3.6 A view looking down the channel from behind the box. Note that in this photo the lid is not covering the box (as opposed to Figure 3.4) and the moving floor is at the top position. (Photograph by author)

A four inch diameter fan was placed on top of the lid and pointed down channel. The fan could be turned on and off from within the control room. During the filling of the source box (Section 3.2) excess gas would get into the channel and a thin layer of it would remain during the release and be detected by the FID (flame ionization detector). This was especially true for experiments done at low elevations and close to the source box. This small fan helped mitigate this issue. Testing was done to determine how long before the release the fan needed to be shut off so that lingering currents would not affect the release.

3.1.5 Gas Metering System

Three gases were used in the experiments: propane, carbon dioxide, and air. A mixture of carbon dioxide and air was needed to achieve the reduced gravity at Buncefield and propane was needed as a tracer for the flame ionization detector (FID) (Section 3.1.6). A detailed sketch of the system is provided by figure 3.6 on the following page. In this sketch you can see the three gases along with their respective flow meters. A fourth flow meter is needed for the gas being sent to calibrate the FID. All of the flow meters and the flow controller were manufactured by MKS Instruments. The model number of the controller and the capacities of the meters are shown in Figure 3.6.

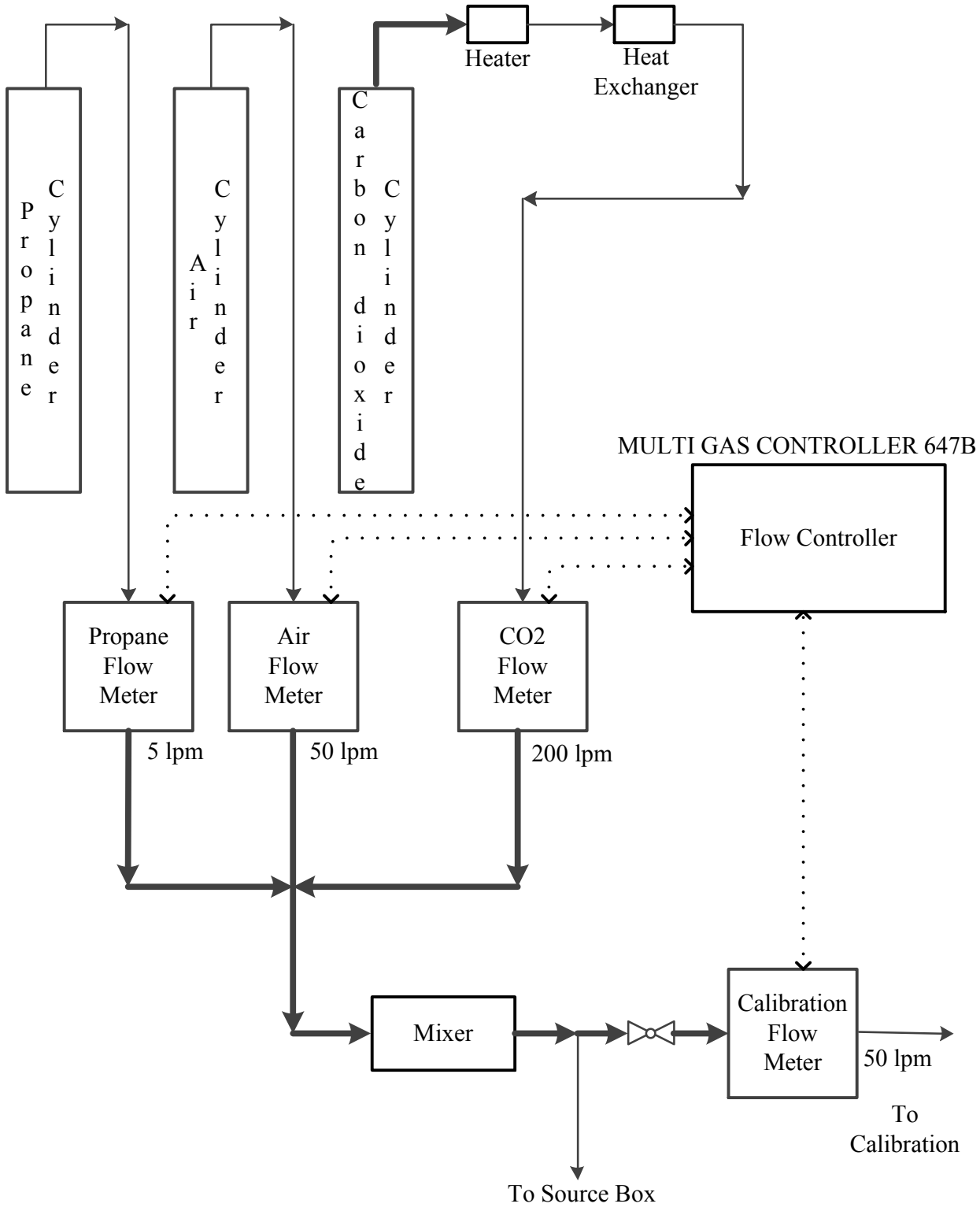

Figure 3.7 Gas metering system schematic.

The thin lines on the schematic are 3/8 inch gas tubing. The dashed line connections shown between the flow meters and the flow controller are electronic connections. The thick lines shown exiting the flow meters are 3/8 inch copper tubing. The heater for the carbon dioxide connects directly to the cylinder. It is a Profax brand 1000 Watt in-line heater. The heat exchanger is custom made and consists of 20 feet of copper tubing coiled up inside a 10 inch plastic cylinder with a fan installed inside of it to blow air past the tubing. The gas was consistently close to ambient temperature when it exited this heat exchanger. After the three gases came together they went through a mixer which was just a foot long piece of 2 inch pipe.

There are two modes of operation for this system: filling and calibration. After going through the mixer the flow splits with one line going to the source box (filling) and another going to the calibration flow meter (calibration). The reason for a separate flow meter dedicated to calibration is that the flow rate used to fill the source box (50 liters/min.) is much too high for calibration. The choice of 50 liters/min. for filling and the calibration procedure will be discussed in more detail in subsequent sections, but it will be said here that a flow rate of 6 liters/min. was used for calibration. A valve placed in front of the calibration flow meter is closed when in filling mode so the front end of the closed flow meter will not be pressurized. When in calibration mode this valve was opened and 6 liters/min was diverted to the calibration rig (seen in Figure 3.8). The remaining 44 liters/min. was still going out to the source box. This did not affect the calibration or the subsequent box filling.

3.1.6 Concentration Data

Flame Ionization Detectioon

Concentration data was collected using flame ionization detection. This technique utilizes the fact that during the combustion of hydrocarbons, ions are produced in proportion to the number of carbon atoms “burnt” in hydrocarbon form. Through creation and collection of these ions, a Flame Ionization Detector (FID) produces a voltage signal. The CO_2/air gas streams used in this project were seeded with 3 mole% propane to facilitate the use of the FID.

The FID used on this project is an HFR400 High Frequency Response system manufactured by Cambustion Ltd. The main components of the FID are the sampling tube, the Hydrocarbon Sampling Module (HSM), and a gas handling and electronics subsystem called the Main Control Unit (MCU). The sampling tube and the HSM are visible in Figure 3.7 at the top of the following page. Also visible in the photo is the vertical arm installed inside the wind tunnel. The movement of this arm is controlled remotely from the control room. The HSM is the metallic rectangle extending behind the arm with several tubes and wires emerging from it. These tubes and wires are connected to the MCU. Inside the HSM is a combustion chamber with a flame lit by a regulated supply of air and hydrogen. A tube from a vacuum pump is attached to the HSM to allow the combustion chamber to be operated at less than atmospheric pressure. This vacuum is what draws the sample from the tube into the chamber. In our experiments the vacuum was 300 mm Hg. The tube length and inside diameter were 5 feet and 0.005 inches respectively. Run with this tube and vacuum setting the FID had a frequency response of 17 Hz and a velocity at the inlet of the sampling tube of 60 cm/sec.

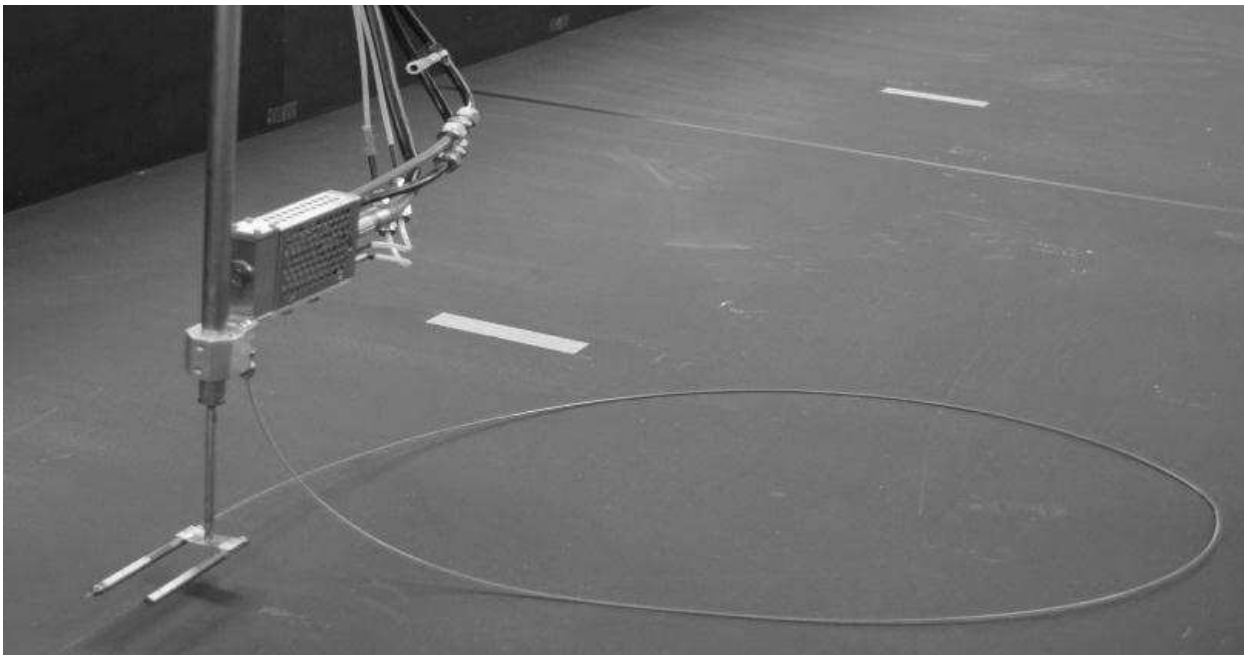

Figure 3.8 Photograph of the sampling tube, HSM, and measurement arm. (Photograph by author)

ThermalPro

The voltage signal produced in the MCU of the FID was run through an analog-to-digital (A/D) converter which was in turn connected to a desktop computer in the control room. A software package designed by TSI, Inc. called ThermalPro (version 5.00.10) was installed on this desktop and used to collect and store the data. The FID was also calibrated using this software. Data collection was initiated by the click of a mouse. In these experiments data collection and the start of the experiment (the moment the moving floor started up to release the gas into the channel) were synchronized. ThermalPro allows the data collection rate to be specified. All of the experiments discussed in this work had a collection rate of 100 Hz. The data was cataloged and stored on the hard drive of the computer and backed up on a removable storage device. The data was imported into Microsoft Excel for analysis.

Calibration (Flow Meter and Tube)

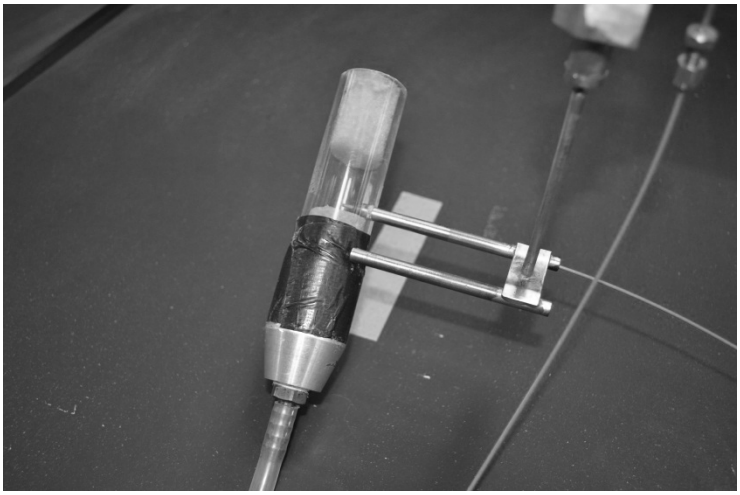

Figure 3.9 The calibration rig fitted over the FID inlet tube. (Photograph by author)

As seen in figure 3.6 (and briefly discussed in Section 3.1.5) there is a separate flow meter for calibration. This didn't necessarily need to be the case. In the early work on this project there was a valve which would divert the flow entirely to the source box or entirely to the calibration tube. When it was determined that 50 liters/min. was the optimal (the reasons for this will be discussed in detail in Section 3.2) flow rate to fill the box, a separate calibration flow meter became necessary. This was because at a flow rate of 50 liters/min. accurate calibration became impossible due to the fact that the voltage would not steady out.

Figure 3.8 shows the polycarbonate cylinder used for calibration. It is 5 inches long and has an inside diameter of 1 inch. Halfway down the length a hole is drilled so the cylinder can be placed snugly onto the horizontal metal tube which holds the FID tube. Above and below this hole, foam is placed inside the cylinder to help dampen turbulence. At 50 liters/min. the velocity in this tube is 1.95 m/s and the *Re* is 4100. Under these conditions the voltage would fail to steady out. This changing voltage implies that the concentration of the gas inside the tube is bouncing around chaotically. It isn't obvious why this would be so (even in a turbulent flow) since it would require air to get into the tube, but nonetheless it happens. So the flows were split and a dedicated flow meter was used for the calibration line. There were two issues at hand when it came to choosing a flow rate for calibration, 1) a flow rate low enough was needed to eliminate

the oscillations and 2) the flow rate needed to be high enough to be in the accurate operational region of the flow meter. It was found that 6 liters/min. worked well on both fronts.

Calibration Procedure

Using ThermalPro, a 10 second data file was taken at 100 Hz with no gas present around the FID tube. The software would report the arithmetic mean of the 1000 points taken and this would set the baseline voltage (or 0% point) of the FID. This would then be repeated and the values averaged. Next the calibration tube was placed over the FID tube (as in Figure 3.8) and two more points were taken with "pure" gas flowing over the FID at 6 liters/min. These were averaged to get the 100% point. Even though they were averaged, two points were taken mainly as a precaution. When things were working correctly there would be very little separation between the values. Using these averaged values a linear calibration file would be created within ThermalPro using the 0 and 100% points. This linear calibration would be applied by ThermalPro to any data subsequently collected until another calibration was done. It was found that data could be collected for up to 4 hours before another calibration was required.

3.1.7 Velocity Data

The two dimensions of interest in this set of experiments are cloud thickness (denoted z-direction) and the down channel extent of the cloud (denoted x-direction). The instant the moving floor starts up and gas gets ejected into the tunnel there is a bulk velocity profile which develops in both these dimensions. The velocities were a function of ejection flow rate from the box. The higher the flow rate the thicker the cloud would grow and the faster it would travel

down channel. The bulk velocities were measured using flow visualization and cameras. Visualization was used only in experiments where velocity was being measured. Once collected, the velocity data was transferred to Matlab and regressed. The velocity curves created in Matlab served as part of the input for a computational model (Chapter 5).

Flow visualization

White smoke was used for visualization. This smoke was generated using pellets manufactured by Arctic Products. The pellets, made out of potassium chlorate and sugar, weigh 13 grams and are 1 inch diameter by 1 inch tall cylinders, but only a half a pellet was used in each run. The pellets require ignition and burn for about 20 seconds. The ignition system consisted of rectangular wells built into the floor of the box. Two wells with two ignition compartments each were built (they are clearly visible in Figure 3.5). An ignition compartment consists of two nichrome wires about 1cm apart pulled taut between electrical terminals. Two wires were used because it makes a convenient stand for the pellets to rest on. Wiring runs under the floor of the box and into the control room where a toggle switch is used to provide power and ignite the pellets. During these runs, ignition of the smoke was the last step before pulling the lid back and releasing the gas. After the 20 second burn time elapsed another 30 seconds was allowed to elapse before starting the lid to allow the turbulence generated by the smoke production to subside.

Down channel velocity of the cloud

Five video cameras from Teledyne DALSA (Model# Genie M1280) were used to make measurements of the average bulk velocity of the cloud in the x-direction. These cameras have a resolution of 1280x960 pixels, and take video at a rate of 24 frames per second. Each camera

was directly linked to a computer with a software package installed (StreamPix5) which allowed the cameras to be triggered from the computer. In addition, the videos were stored, accessed, and analyzed via this software. A basic setup of these cameras can be seen to the right of the channel in Figure 3.5. The cameras themselves cannot be made out clearly, but what is apparent is that they were placed essentially right up against the outside of the channel. The wiring for each can also be seen to disappear under the tunnel where it runs into the control room and connects to the computer. The cameras were wired in series and when the mouse on the computer was clicked to trigger the cameras this triggered camera 1 which then triggered camera 2 and so on. This happened so quickly so as not to cause any computational issues.

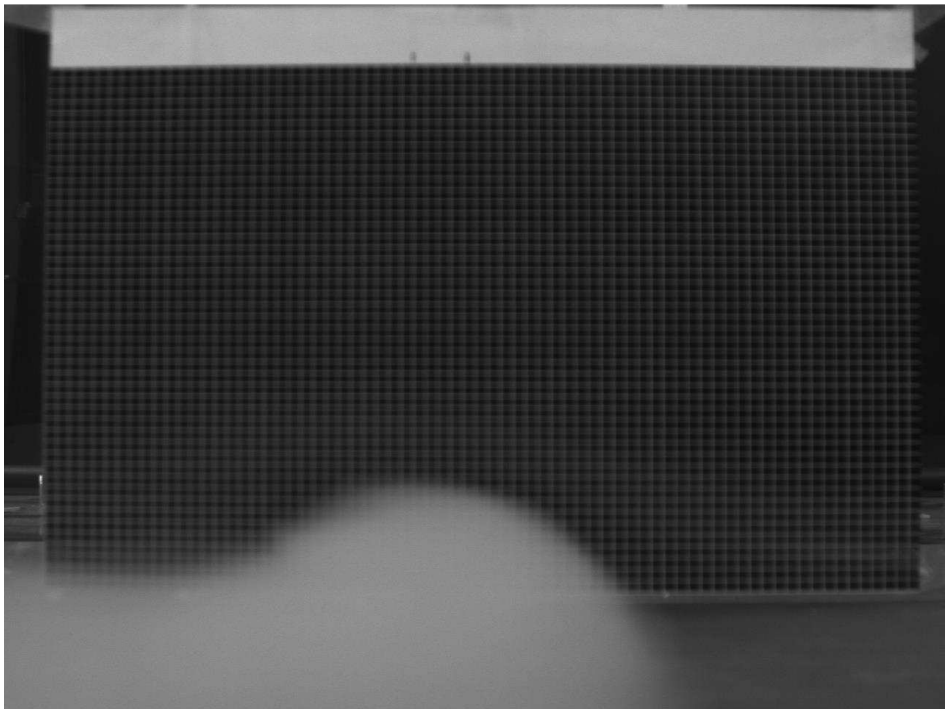

Figure 3.10 A screen capture from video taken with one of the Teledyne DALSA cameras. This video was of an experiment with a much higher flow rate than the experiments discussed in this work, but this higher flow rate and resulting raised head make the cloud very distinguishable. (Photograph by author)

Velocities were measured by simply calculating the time of travel of the front of the cloud between each of the cameras, which were placed a known distance apart from one another. For instance, if camera 1 was placed 1 meter down channel, camera 2 was placed 2 meters down channel and it took 10 seconds to travel between these two cameras the *instantaneous velocity* at 2 meters was regarded as 10 cm/sec. This is of course, very much an approximation, but the experiments were repeated with the cameras in varying positions. Doing this was akin to measuring the area under a curve by using narrower and narrower rectangles. We never approached a true limiting value, but confidence in this method was secured because it showed repeatability and it could be checked by comparing arrival times with the FID measurements. Obviously there was a spike on the FID when the cloud arrived and this data correlated well with the video data. In addition, this process was helped by the fact that the velocity steadied. This meant that most of the challenges presented by this method were only present in the range where the cloud was accelerating and so data collection could be focused on this area.

Vertical velocity of the cloud

What was being measured here is the rate at which the cloud thickness grew during a run. This was done by taking video from the side with a Nikon D5100 digital camera and a Nikon AF-S NIKKOR 18-55 mm 1:3.5-5.6G lens. A screenshot from one of the videos is shown in Figure 3.10.

At the release rate discussed in this work, the cloud height would steady out before the end of the experiment. In other words, the vertical velocity would go to zero. To come up with a function that would accurately predict the final height of the cloud it is necessary to *know* the final height

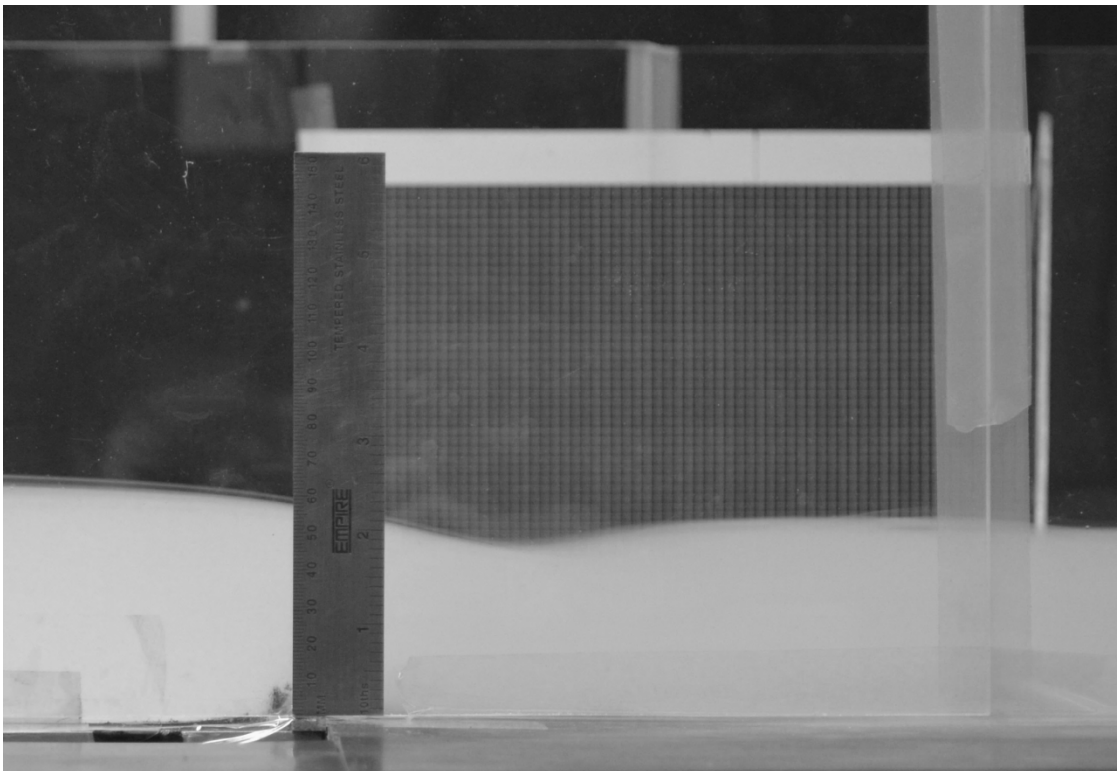

Figure 3.11 Photograph taken with the Nikon 5100 from the side of the channel. The left side of the ruler coincides with the front of the channel. The wave formation seen only persisted at the front and was more pronounced for greater flow rates. (Photograph by author)

of the cloud. Because of this, preliminary runs were done in order to determine this final height. Then the camera would be positioned in such a way that it was focused on this location. Video taken subsequent to this would then be uploaded to a computer and analyzed with the software package that came with the purchase of the camera. The camera could not be remotely controlled so it was not possible to synchronize the start of the experiment with the beginning of the video. Because of this the video was started several minutes before the start of the experiment. The first thing that would be determined while viewing the video is the time the experiment started. This was easily determined by detecting the motion of the smoke upward. This was recorded as time

zero. The video would be paused at every full second after time zero and the height of the cloud would be recorded by observing where the smoke lined up next to the ruler.

3.2 Box Filling Study

The first two design tasks of the project were 1) designing a two dimensional Buncefield type release in the wind tunnel (discussed in detail in Sections 3.1.2-3.1.4) and 2) Developing a procedure for filling the source box with 100% (or very close to it) dense gas throughout the depth of the box. The gas being used to fill the source box was a CO_2-air mixture with the same reduced gravity as the gas which poured over the dyke at Buncefield. This mixture being only 11% denser than air added to the challenge of filling the box.

Beyond the basic design of a sunken source and the two dimensional channel these two design problems become intertwined because many of the details of the source box design and the existence of the lid were predicated on what was learned while conducting box filling experiments. Adding to the challenge was the fact that a box filling study could not be accomplished without a source box, but a source box couldn't be designed without a filling study. This problem was solved by using a rudimentary box, one with no moving parts, to start the filling study. The initial box was 117.5 cm long, 43.5 cm wide, 29.8 cm deep and constructed out of plexiglass. Just like the final box design it had a hole in the center of the bottom panel where the 3/8 inch gas tubing was connected. Before the filling experiments began with this box the basic design of the permanent box was worked out and construction was begun. There was some risk in this, but time constraints dictated this decision.

The filling study is described in some detail in this section because what was learned dictated so much of the final design of the source box and, even more importantly, it greatly impacted the focus of the project because it was during this time that the potential impact of molecular diffusion became apparent. Data will be provided in this section where it is deemed necessary, but the emphasis will be qualitative rather than quantitative.

Step 1: Test Initial Hypothesis

The study began with the idea that filling the box with a dense gas was only a more complicated version of filling a vessel from the bottom with a liquid. At this point it was assumed that the only major complicating factor was the potential for mixing. With this in mind a flow rate with the following competing characteristics was sought; 1) low enough that the flow was laminar inside the 3/8 inch tubing and wouldn't jet upon entrance to the box, but 2) high enough that the box would fill in a practical amount of time ($\leq$ 4 hours). Under these criteria, 2.0 liters/min was chosen and the study was begun. At this flow rate the concentrations in the box steadied out after 1.5 hours at 76% near the bottom, 52% in the middle, and 13% near the top. The experiment was run for another 2.5 hours with no change. Repeats conducted over the next two days elicited the same results. At this point 1 liter/min. was tried and the concentrations went down, contradicting the idea that lower flow rates would result in higher concentrations due to less mixing and jetting. Next, 3 liters/min. was attempted and the concentrations went up slightly, but the gas was now jetting slightly into the box instead of placidly filling. Again another contradiction from the initial hypothesis: the jetting increased mixing, yet the concentration went up, albeit only slightly.

Step 2: Test New Box, Try Distributing Flow

At this point the permanent box had been completed (still no lid though) and all further filling experiments were conducted with it. The run at 2.0 liters/min. was redone in the new box and the concentration near bottom steadied out at only 33% and it took 90 minutes to steady out even though the sensor was 1 cm. above the bottom. The flow was switched to 1 liter/min. and the concentration at the bottom dropped to 21%. Again these results proved to be repeatable.

So the new, permanent box performed much worse. The search for the reason(s) began with identifying the differences between the two boxes. The relevant differences were: the new box had about twice as much cross-sectional area and the presence of the seal between the moving floor and the side walls introduced a greater potential for leaks. The greater area meant that the vertical velocity of the gas filling the box was lowered to about 1 mm/min. per liter/min. of filling. If there were significant leaks this would be lower still. It was speculated at this point that diffusion may be partly, or even wholly, responsible for the low concentrations.

Testing this idea meant going up in flow rate, which introduced the problem of jetting. To help with this a 1 foot diameter,1 inch thick, radial distributor was built which took the vertical flow in and divided it in eight horizontal tubes so the inlet flow to the box was now running parallel to the floor. Tests were conducted with this configuration at 8 liter/min., and the concentrations were still very low.

The next idea was to lay a permeable material over the distributor. The idea was to create some back pressure so that the gas would fill the space under the permeable layer, and then begin moving up through the layer into the box above, throughout the whole cross section. Several types of foam and insulation were tried, but there was no improvement in filling percentage.

Step 3: Experiments with a Small Cylinder

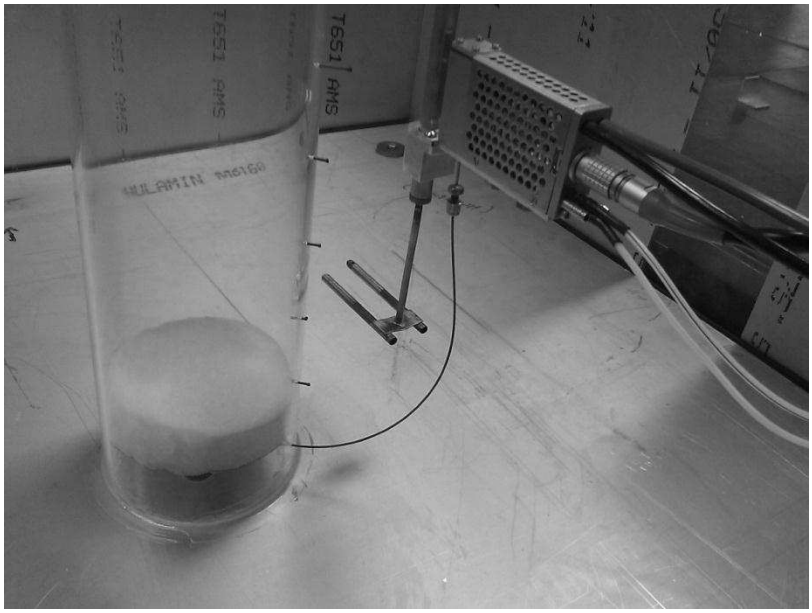

Figure 3.12 The cylinder sitting inside the source box. The plugged holes and the vacuum grease around the bottom are visible. (Photograph by author)

The geometry of the box next came into question. The square corners were coming under greater scrutiny as potential locations for leaks and it was questioned whether having a radial inlet flowing into a square box could set up complex circulation patterns and prevent air from escaping. With this in mind a series of tests were conducted with a 2 foot long, 4 5/8 inch diameter polycarbonate tube. This tube was centered over the opening in the box and a seal was created using vacuum grease so no gas could escape under the cylinder. A series of 1/16 inch holes were drilled in the side which allowed the FID tubing to be fit snugly inside the cylinder. Holes not in use were plugged.

In the first experiment, show in Figure 3.11, the concentration went to 100% in about five residence times regardless of flow rate. This result was consistent both with and without the foam. After this result a series of tests were conducted with the cylinder. The variables were vertical location, flow rate (1-3 liters/min.), and the presence or absence of the foam. As the sensor was moved up in the cylinder 100% was still consistently achieved with or without the foam. At 1 cm below the top of the cylinder, 3 liters/min. and the foam was required to get to 100%.

The experiments with the cylinder led to the suspicion that two effects speculated about earlier were possibly controlling the efforts to fill the box. These two effects were leaks and diffusion.

Obviously, the fact that we were able to fill a cylinder known to not be leaking does not *prove* that leaks are a significant contribution to our inability to fill the source box. However, achieving 100% throughout so much of the length of the cylinder after not being able to get even 80% *at the bottom* of the box was a dramatic result. It was not a surprise that it was proving difficult to fill the box, this was anticipated. The inability to get 100% even at the bottom after trying several ideas was surprising. This along with the fact that maintaining the basic integrity of the seal in the corners of the box, was a constant struggle led to the conclusion that leaks were important.

Besides not leaking, the other major difference between the box and the cylinder is the geometry. It is a much smaller space, of course, but in the absence of leaks and diffusion smaller does not mean easier to fill. It only means it will take less time. (As noted before, a third possibility is complex flow patterns trapping air. By the end of the filling study, this was eliminated as a major effect.) Specifically, the geometrical differences are the circular vs. square geometry (not believed to be a factor), the smaller cross-sectional area, and the much smaller ratio between cross-sectional area and height. The last two differences have a major impact on the effects of diffusion. A smaller cross-sectional area mitigates diffusion by increasing the upward velocity of the gas. Having greater depth with respect to the cross-sectional area helps in this situation where the inlet to the box is relatively small. It was stated earlier that jetting out of the 3/8 inch inlet was first detected at 3 liters/min. At this flow rate the velocity in the inlet to the source box is 70 cm/s, but the upward velocity within the 1 meter square box is 3 mm/min. In order to get this velocity to even 1 mm/s, the velocity in the inlet needs to be 14 m/s. At this velocity the gas would definitely not stay in the 32.5 cm deep box.

At this point the argument that diffusion was making it harder to fill the box was mostly qualitative, but it was decided that higher flow rates would be tried and that meant using a lid. At the same time this was decided, a redesign of the box was being worked out which would round off the corners. Since this would be a major time consuming step, experiments with different lids were undertaken first.

Step 4: Testing Permeable Lids

The first lids tried were a rigid, 3 inch thick, upholstery foam, and a ¼ inch thick sheet of peg board with ¼ inch holes. These were chosen because they would provide a barrier to the open air, but would not create a seal. A lid was desirable, but anything that prevents gas from escaping, and therefore pressurized the box, was not.

Thus far, the problem being written about has been described as a filling problem. How do we fill the source box with our mixture of carbon dioxide and air? However, it was stated in the beginning of this section that the major complicating factor was the potential for mixing. That is for mixing with the air already present in the box. So the problem can be thought of as one of replacing one gas with another, heavier, one. With this in mind and a lid now being used, it made a lot of sense to begin filling with the moving floor at the top instead of at the bottom because there would be so little air to replace. If you position the floor all the way up so it was touching the underside of the lid there would be no air to vacate. This wasn't possible because of the bolt heads sticking up out of the top of the floor, but the floor could be positioned 1.5 cm below the bottom of the lid. This is referred to as the "filling position" of the floor. At filling position there are 15 liters of air to replace instead of 325 liters with the floor all the way at the bottom. The hope was that the 15 liter space could be filled to 100% and then, with the gas still on, the floor

could be lowered. As long as the flow rate of gas is greater than the rate at which the volume inside the box is increased, there is a positive pressure inside the box so no air can get in.

Several experiments of this nature were undertaken with both the foam and pegboard lids at flow rates from 1-6 liter/min. The FID rig could not be dropped into the box with a lid on it, so the FID tube was threaded vertically through a hole equidistant from a side wall and the center of the box, and placed 1 cm below the bottom of the lid (and therefore 0.5 cm above the floor while at filling position). The FID tube being used at this time was much shorter than the 5 foot long one eventually used so there was no ability to get much deeper into the box once the floor moved down and out of the way.

Gas was sent to the box with the floor at filling position until the concentration steadied out and then the floor was lowered at a rate 20% lower than the filling rate. The results of these tests were both promising and confusing. The concentrations before the floor was lowered would steady out around 85% and then drop 10% while the floor was being lowered. After the floor reached the bottom, the gas was left on, but there was never any rebound in concentration no matter how long the gas was left on. These results were consistent for both the foam and the pegboard lids.

On the one hand, the results were very encouraging in that concentrations in the seventy percent range were reached at the top of the box as opposed to those in the teens without a lid. The best explanation for this improvement was that the effects of diffusion were eliminated (or at least greatly diminished) by the addition of a lid.

On the other hand, the results posed several questions:

Why was only 85% reached in the 15 liter space?

It was discussed whether leaks could explain this result. It didn't seem possible for it to be the only explanation. If gas were input at a higher rate than the leaks, eventually a 100% concentration would be reached. If gas were input at a lower rate than the leaks, it's hard to envision 85% being reached. Perhaps, some diffusion remained and higher flow rates were needed to overcome it. The use of higher flow rates with the permeable lids was problematic because the much of the gas would be blown through the lid instead of remaining inside the box. With this in mind it was decided to try an impermeable lid.

Why was there a 10% drop by the time the floor reached the bottom?

Leaks did seem to be a good explanation for this. While the floor was moving down the effective flow rate into the box was greatly diminished and the effect of any leaks were be enhanced. This idea would be tested by lowering the floor at a slower rate relative to the gas input. If leaks were to blame, the effect should be mitigated by slowing the floor.

Once the bottom was reached, why was there never any rebound in concentration no matter how long the gas was left on?

Explanations for this were difficult to come up with. It was possible that a vertical distribution was developing inside the box while the floor was being lowered and that the concentration was 85% (or higher) at the bottom. This possibility had ramifications for the previous question as well. However, even if this was the case it seemed as if the concentration distribution should go away in time. Ideas of how to measure concentrations deeper inside the box were developed, but it was decided to first test an impermeable lid.

Step 6: Test Impermeable Lid

The material chosen was ¾ inch medium density fiberboard. This is the same material used in the final design, except the board initially tested was cut to the outside dimensions of the box meaning it could not be moved off of the box. A small hole was drilled for the FID sensor (again equidistant from a side wall and the center) to allow it to be placed vertically 1 cm down into the box. The lid weighed about 30 pounds and there were concerns as to whether allowing it to lie upon the box would create enough of a seal to pressurize the box during filling. Experiments were conducted both with it lying on the box and with thin shims being placed in between. Flow rates were varied between 3-12 liter/min., with this being the first set of experiments where a flow rate over 8 liter/min. was used.

The results indicated that both the impermeable lid and a higher flow rate (12 liter/min.) independently helped, but they worked best in combination. The lid worked best without shims to create a gap for gas to escape. Experiments were conducted with a manometer which showed no measurable pressure increase inside the box.

At 12 liter/min. filling rate the 15 liter space steadied out at 93% (up from 85%). After the concentration steadied, the floor was lowered at 10 liter/min. until it reached the bottom. At this point the concentration 1 cm below the top was 87% (up from 75%). As before, there was no rebound in this concentration no matter how long the gas was left on.

So all the concentrations went up with the new lid and higher flow rate, but qualitatively, the picture did not change. There was still a decrease in concentration while the floor moved down, and no subsequent rebound after it reached the bottom. At this point it was decided to go ahead with alterations to the box and seal which would decrease the amount of leaking around the seal.

The alterations undertaken were the rounding off of the four corners, a small decrease in the gap between the moving floor and the walls to “tighten” the seal, and the addition of Tygon tubing to the interior of the seal as outlined in Section 3.1.2. This work took several weeks so, with the source box out of commission, attention turned to further studying the impact of diffusion.

Step 7: Experimental and Computational Filling Study of an Open Topped Cylinder

A filling study was undertaken using a much larger cylinder than the one pictured in Figure 3.10. The larger cylinder is 88.2 cm in diameter by 87.7 cm tall and it has 3/8 inch gas tubing fitting on the center of the bottom plate just like the source box. By this time it was certain that a lid would be used on the source box yet all of these runs were done with the top of the cylinder open to the air. So in that sense these experiments were a complete departure from where the box filling procedure was headed, but this was an opportunity to study the diffusional effects which were such a surprise.

The size of this cylinder was ideal for extending the experiments done with the small cylinder. The greater height allowed for a wider array of flow rates into the cylinder without having to be concerned with jetting of gas out of the cylinder. Flow rates of 3-20 liters/min. were used during this batch of experiments. This is a much smaller effective flow rate than the 1-3 liters/min. used with the small cylinder because of the disparity in volume between the two cylinders (600 liters vs. 7 liters). This smaller effective flow rate in, along with the much higher cross-sectional area of the big cylinder, meant that diffusion would have a greater impact during filling.

In addition to the experiments, a one-dimensional computational model was built using COMSOL. This simple model had a gas with the properties our carbon dioxide-air mixture

flowing in from the bottom and a flux boundary condition at the top allowing for diffusion at the interface. The concentration data collected by the FID was compared with output of this model.

Just like every other type of filling experiment run, the concentration would eventually reach a steady value. The value reached and the time taken to get there was a function of flow rate and elevation. Two types of experiments were run: one where the FID would be kept stationary and the run up to a steady concentration would be recorded, and another where once steady state was reached, the FID would be moved vertically to determine the steady state, vertical, concentration distribution within the cylinder.

The agreement between the COMSOL model and the data was very good, thus justifying that diffusion was a major impediment to filling an open topped vessel with a denser than air gas. This may not be a major surprise to some, but the initial assumptions were that rate of diffusion would be too slow to have a major impact. It was thought that whatever layer at the top had been diluted through diffusion could be removed simply by over filling the box until this layer was gone. In actuality, the rate of diffusion was so much higher than the initial assumption that 100% could not be reached even at the bottom of the vessel, at the flow rates tested. In truth the problem of diffusion was coupled with the problem of turbulence. At a high enough flow rate diffusion would theoretically cease to be an issue, regardless of the cross-sectional area of the vessel, but in reality the turbulence and jetting created by this high flow rate would make filling the vessel impossible unless it was very deep.

A lot of time has been spent in this section laying out the research and design challenges associated with filling the box. Many of these challenges had nothing at all to do with diffusion, for instance, designing an effective moving seal was particularly difficult. However, as was

stated in the beginning, the main motivation for this section was to convey that what was learned about the impact of molecular diffusion on box filling greatly impacted the focus of the overall project. The work with the large cylinder was a culmination of efforts to understand the role of diffusion on the box filling process, and so in a sense it served as an ending. In another sense it was foundational. The final product of this project is, just like the cylinder work, a set of concentration data compared to a COMSOL model where the only form of entrainment is molecular diffusion.

Step 8: Test the Effectiveness of the "New" Source Box

In conclusion, there was one more step in the filling study. The source box with the rounded corners and altered seal was installed and tested. In addition the filling flow rate was raised to 50 lpm and this is where it stayed during the main experimental program. As was consistent with other iterations, the concentrations increased, but the qualitative picture did not change. The small space with the floor in filling position still didn't get to 100% (It reached 98%). There was still a drop in concentration while the floor moved down to the bottom (in this case to 95%), and there was not any rebound no matter how long the gas was left on. The vertical concentration distribution which became a mystery once the lid was deployed was checked by drilling a series of 1/16 inch holes into the side of the box and threading the FID tube through these holes. These experiments showed no variation of concentration by height within the box. In over 40 times that the filling concentration was checked during this final step of the filling study, the concentration inside the box was always inside the range of 95% +/- 1%. This was deemed both an acceptably high concentration, and an acceptably high level of consistency, and the filling study was ended. The filling concentration was also checked often during the main data collection process and it remained consistent throughout, never deviating from the 95% +/- 1% range.

3.3 Experimental Procedure

As has been noted there were two types of experiments; those without visualization where concentration was measured using an FID, and those with visualization (smoke) where velocity was measured using video cameras. The procedure for the FID runs was more involved and it will be written out in detail. Anywhere that the procedure for the video runs differed will be noted parenthetically.

The first step was to light the FID (omitted for video runs). The FID needed to be lit at least an hour before it could be calibrated. During this hour the following would be done; the HVAC system inside the wind tunnel room would be turned off to eliminate any air currents, the side walls of the source box would be lubricated with vegetable oil if necessary, the lid would be moved over the box and the rope would be attached, the moving floor would be moved into the filling position using the keypad on the motor controller, the video camera under the tunnel would be turned on, the tank pressures of the gas cylinders would be checked, and the laboratory notebook would be prepared to record the days experiments.

After passage of the hour, the FID would be calibrated (omitted for video runs). The first step in this process was move the FID into position. Generally the FID would be calibrated in the location of the first test of the day. The only exception to this was when the FID was too low to get the calibration tube onto it. When this was the case the FID would be raised. The gas which would contaminate the channel during calibration was not an issue because of the subsequent use of the fan during box filling. The next step was to open the valve on the gas metering system which allowed for flow through the calibration flow meter.

The relative flow rates of air and carbon dioxide necessary to create a gravity current with the equivalent reduced gravity of that at Buncefield is a function of ambient temperature, pressure, and relative humidity. The values of temperature and relative humidity are continuously transmitted by instruments within the tunnel to a digital readout in the control room. The pressure would be obtained from an online weather service. With these values a series of calculations would next be done to determine the flow rates needed for that days runs. (These calculations will be discussed in detail in Chapter 4). The flow rates did not vary wildly from day to day because of the relatively controlled conditions within the tunnel, but there was small variation occasionally. As has already been stated, the total fill rate was 50 liters/min. 1.5 liters/min. of this was automatically propane (for concentration runs only). The calculations done in Chapter 4 did not account for the propane. They would give values of carbon dioxide and air totaling 50 liters/min., but since carbon dioxide and propane have such similar molecular weights they were treated like they contributed equally to the density. For instance if it was calculated that 13.1 liters/min. of carbon dioxide and 36.9 liters/min. of air was needed, then the values programmed into the flow controller would be 1.5 liters/min. of propane, 11.6 liters/min. of carbon dioxide, and 36.9 liters/min. of air. Sometimes as many as 12 experiments would be run under the same calibration, but the needed flow rates would be checked before every experiment and if they changed from one to the next a new calibration would be performed.

With the needed flow rates typed into the flow controller the calibration procedure would be performed as outlined in Section 3.1.6. Once this was complete the calibration tube would be taken off of the FID and taken out side of the channel and the valve to the calibration flow meter would be closed.

The next step would be to fill the source box. The steps of this process were precisely timed based on what was learned during the box filling experiments. First, all three gases would be turned on along with the fan which pointed down the channel. After they ran for two minutes the floor would be started down at a rate of 42 liters per minute. Like all movements of the floor, this action would be initiated at the keypad of the motor controller inside the control room. It would take approximately seven and a half minutes for the floor to travel the 31 centimeters to the bottom of the box. Once the bottom was reached the floor would stop automatically because a preset number of rotations were programmed into the motor controller. The gas would be run for another two minutes with the floor stationary at the bottom. 45 seconds before the gas was shut off, the fan would be shut off to allow the air in the channel to become calm before the release. After these two minutes were up the gas would be shut off. Five seconds after this the motor controlling the lid removal would be started. It would take one minute for the lid to move off of the source box. The moment the lid cleared the box the floor would be started up and the FID data collection would be initiated with ThermalPro. This would be done simultaneously so time zero would be easily discernible in the FID data. (In the video runs, x-velocity data collection (Teledyne DALSA) would be synched to the start of the experiment while the z-velocity data collection (Nikon) would usually be started before the experiment even began because it could only be initiated within the tunnel.)

It would take 96 seconds for the floor to move all the way to the top and eject all of the gas into the channel. When the run was completed the floor would be moved to filling position, the FID would be moved into position for the next experiment, the lid would be moved back over the source box, and the flow controller would be rezeroed. In total it would take about 20 minutes

from the beginning of one run to the next. At this pace 12 experiments could be run in four hours. This was the maximum time allowed to elapse between calibrations.

After the last experiment of the day, the FID would be shutdown, the gas cylinders would be bled, and the tunnel would be flushed of excess carbon dioxide with an exhaust fan.

3.4 Location of Experimental Runs

The FID could only collect concentration data at one location per experimental run. This meant that a set of testing locations within the cloud needed to be strategically mapped out in order to fully characterize the time varying concentration distribution. As has been stated there were two dimensions of interest, down channel (x), and height (z). The lateral (y) dimension within the one meter wide channel was disregarded in the data collection, but only after verifying that the concentrations did not vary significantly in this dimension. All of the data reported in this work was collected in the center of the channel.

The down channel distance travelled by the cloud, within the experimental window, was determined first. This process is discussed in detail in the next section, but it will be stated here that the usable section of the cloud extended four meters down channel. With this in mind, it was decided that it would be sufficient to collect data at 1, 2, 3, and 4 meters down channel.

The transient nature of these experiments made it necessary to do preliminary testing to discern where to collect vertical data at each down channel location. The elevations chosen were 0.1 cm, 1.0 cm, 2.0 cm, 3.0 cm, 3.5 cm, 4.0 cm, 4.5 cm, 5.0 cm, 6.0 cm, 7.0 cm, 7.5 cm, and 8.0 cm above the floor of the channel. More testing was done at the middle elevations because it was the

area of greatest concentration gradient. More testing was done at the top elevations in order to carefully define the top boundary of the cloud. It will be noticed in Chapter 6 that not all of these elevations are displayed on the concentration vs. time graphs. Doing so was not necessary or helpful to display the results effectively.

Chapter 4

THEORETICAL DISCUSSION OF THE PHYSICAL EXPERIMENTS

4.1 Buncefield Calculations

This section lays out the calculations which went into creating a gravity current in the wind tunnel with the same relevant flow characteristics as that at Buncefield. Eschewing any concerns with regards to scaling, this comes down only to equating the reduced gravity. To do this it is necessary to know the densities of the hydrocarbon vapor cloud and the air. The meteorological conditions at the time of the event are known so the density of the air is easy enough to calculate. The initial density of the vapor cloud is much more problematic, of course. The Health and Safety Executive of Great Britain has done extensive experimental and computational work in regards to the Buncefield event, including work on the formation of the vapor cloud within the dyke [2,3,4,5]. Their reported value of the initial density of the vapor cloud was used in this analysis. The product of these calculations is the flow rates of propane, carbon dioxide, and air needed to produce a vapor with the same reduced gravity as that at Buncefield.

Calculate the Density of Tunnel Air

In calculating the density of the air in the wind tunnel, the contribution of the water vapor is taken into consideration even though its contribution is small. The relative humidity within the wind tunnel room can vary from a low of around 15% in the winter to a high of around 50% in the summer. Over this range the density of the air will change a little less than 1%, but the change this causes in needed flow rate of carbon dioxide is about 5%. It can be argued that this is still small enough to ignore, in fact there is probably more than 5% uncertainty in the density

value reported for Buncefield. However, accounting for it was not difficult so it was decided to do so.

For an ideal gas the law of partial pressures gives

$$P_T = P_D + P_V \tag{4.1}$$

where P_T is the total pressure inside the tunnel, P_D is the partial pressure due to dry air, and P_V is the partial pressure of the water vapor. P_T is assumed to be equal to atmospheric pressure. The equation

$$P_V = RH \times E_S \tag{4.2}$$

where RH is the relative humidity, and E_S is the saturation vapor pressure of water, can be used to calculate P_V. The saturation vapor pressure is calculated by the following formula developed at the Navy Weather Research Facility

$$E_S = \frac{6.1078}{W^8} \tag{4.3}$$

where

$$W = (c_0 + T \times (c_1 + T \times (c_2 + T \times (c_3 + T \times (c_4 + T \times (c_5 + T \times (c_6 + T \times (c_7 + T \times (c_8 + T \times (c_9)))))))))) \tag{4.4}$$

where T is the temperature in degrees Celsius and c_0-c_9 are coefficients. With these last three equations, P_V becomes a function of relative humidity and temperature, both of which are known quantities. Since P_T is also known, equation 4.1 can be used to calculate P_D. The ideal gas law can now be used to calculate the density of the air inside the wind tunnel.

$$\rho_T = \frac{P_D M_D}{RT} + \frac{P_V M_W}{RT} \quad (4.5)$$

In the above equation, ρ_T is the density of air in the wind tunnel, M_D is the molecular weight of dry air, M_W is the molecular weight of water, and R is the universal gas constant.

Calculate the Density of Gas Mixture Required

This step is accomplished using the reduced gravity equation

$$g'_{BF} = (\frac{\rho_M - \rho_T}{\rho_T}) \times 9.81 \quad (4.6)$$

In the above equation, g'_{BF} is the reduced gravity at Buncefield. 9.81 is the gravitational constant, and ρ_M is the density of the mixture required to create a gravity current with an equivalent reduced gravity to that at Buncefield. ρ_M can be solved for simply since it is the only unknown in the equation.

Calculate the Mass Fractions of CO_2 and Air Necessary to Form Mixture

The first step in this process is to again appeal to the ideal gas law, this time to calculate the densities of the carbon dioxide and air coming from the gas cylinders. The cylinder air is assumed to be dry.

$$\rho_{CO2} = \frac{P_T M_{CO2}}{RT} \quad (4.7)$$

$$\rho_{DA} = \frac{P_T M_{DA}}{RT} \quad (4.8)$$

Using the above values for density of carbon dioxide and air, and the fact that the mass fractions of carbon dioxide and air sum to one, the following equation can be used to solve for the mass fractions.

$$\frac{1}{\rho_M} = \frac{x_{CO_2}}{\rho_{CO_2}} + \frac{x_{DA}}{\rho_{DA}} \tag{4.9}$$

x_{CO2} is the mass fraction of carbon dioxide and x_{DA} is the mass fraction of cylinder air. The next step is to convert the mass fractions to mole fractions. With the mole fractions calculated, the process is almost complete. The necessary flow rate is obtained by multiplying the mole fractions times the overall flow rate into the box (50 liters/min.). There is one intermediate step, however. As was discussed in the last chapter, the filling percentage for the source box is 95% carbon dioxide. The remaining is dilution by air, so the calculated mole fraction of carbon dioxide is divided by 0.95 to raise it up to make up for the fact that 100% concentration isn't reached in the source box. This corrected mole fraction subtracted from one gives the corrected air mole fraction.

In these calculations there is no mention of propane. The flow rate of propane (a constant 3% and therefore a constant 1.5 liters/min.) was simply subtracted from the flow rate of carbon dioxide. Because of the nearly equivalent molecular weights of carbon dioxide and propane, this has no effect on the density of the gas mixture.

4.2 Creating a Gravity Current Controlled by Diffusion

All, or virtually all, of the previous studies on mixing in gravity currents have focused on the entrainment of ambient fluid which takes place at the front of the gravity current due to shear instability. This instability causes convective transport of ambient fluid into the region immediately behind the raised head. Behind this region, it is argued in the literature review and the previous section, is a laminar region where no turbulent entrainment is likely to exist. Therefore, the only mode of transport of ambient fluid into this region of the cloud is through molecular diffusion.

The stated purpose of this project was to focus on evaluating the effects of molecular diffusion, and the above paragraph states that analytically at least, a gravity current can be divided into two distinct regions. Focusing on only one of these regions experimentally is challenging however, because there is no way to distinguish between the two forms of dilution when observing a batch of concentration data. This problem was dealt with in this project by attempting to eliminate the turbulent head altogether.

The development of the raised head is only a function of the *Re* and *Fr* number. It was stated previously that at *Re* above about 1000, the properties of the head do not change and therefore the flows are *Re* independent [7,36]. If you think about the *Re* as a ratio of inertial force to viscous force, the above sentence can be thought of as stating that inertial effects are fully controlling the properties of the flow at *Re* above 1000. The other end of the spectrum is also spoken of in the literature. Experiments have been done on so called ‘viscous gravity currents’, which have concluded that below a *Re* of 10, there is *no head* and the gravity current flows as a smooth wedge [36]. This can be thought of as a state where viscous effects are fully controlling

the flow, and furthermore, the implication would be that the only possible form of entrainment in such a gravity current would be via molecular diffusion. In truth, gravity current theory does state that a small amount of ambient fluid is entrained between the raised nose of the current and the ground due to the no slip boundary condition, and the resulting velocity profile. This entrainment is believed to be very small (especially so in such a low *Re* flow) and will be ignored in this analysis.

If an experiment could be designed with a *Re* less than 10, we would be fully justified in moving forward without any concerns with regards to turbulent entrainment. The truth is however, that such a small *Re* was not practical. The flow would be so thin and so slow that data collection would be impossible, and also, somewhat ironically, it is possible such a flow would diffuse away so fast as to be practically non-existent. However, this rigid standard did not need to be met. Through a combination of video and FID runs, a volumetric flow rate was found where there was little to no head formation, yet the cloud was thick enough to facilitate measurement. The volumetric flow rate was used as the variable in this search because attaching a single *Re* to a release was problematic with the transient development of velocity and height, and the varying vertical concentration profile. The length scale (layer depth), and bulk velocity do steady out in the volumetric flow rate which was eventually chosen, to values of 0.07 meters and 0.1 m/s respectively. Using these values along with a kinematic viscosity of 1E-05 (a one significant digit value for pure carbon dioxide at room temperature) results in a *Re* of

$$Re = \frac{Uh}{\nu} = \frac{(0.1)(0.07)}{0.00001} = 700$$

in our experiments.

Manipulating the flow rate from the source box had the same practical effect of adjusting the *Re* because lowering the flow rate, resulted in lower cloud velocity and height. Video runs were supplemented with FID runs because they were not completely conclusive on their own. These experiments started at 400 liters/min. and went down 50 liters/min. at a time until it was judged that turbulent entrainment was minimal. This was not at all easy to determine at these low flow rates. Though there was an easily discernible difference from high flow rate releases in which a classic raised head would develop, the flows never looked like a smooth wedge. The smoke was very wispy and thin and not well defined. Careful, slow motion observation, and repeated runs helped this, but FID runs were a useful tool when making a final decision as to whether a particular flow rate met the criteria. When a head existed a small peak would appear in the data as the head flowed past the FID.

The FID helped not only distinguish the proper flow rate to use, but also the down channel extent which could be used at a given flow rate. It was found that as the currents travelled down the channel they would eventually develop a head, even at very low flow rates. For instance, at the flow rate that was chosen (200 liters/min.), the cloud would travel 10 meters down channel before the box was emptied, but only the first four meters of this experiment were viable for data collection.

Chapter 5

THE COMPUTATIONAL MODEL

5.1 Overview

A computational model was created using COMSOL, a finite element, partial differential equation solution engine. The model was created for purposes of comparison with the concentration data collected in the wind tunnel experiments. As the only form of entrainment in the model is molecular diffusion, the relative level of agreement between the experiments and the model help discern the accuracy of the argument that dilution in our experiments was controlled by diffusion.

5.2 The Domain

The model started with the creation of a five meter long, and one meter tall domain as a two-dimensional representation of the channel. A horizontal boundary was placed into this domain at a height of two millimeters (see Figure 5.2). Before this internal boundary was added, the model would not allow the gravity current to flow through the domain. In a sense, this boundary represents an initial cloud height of two millimeters throughout the length of the domain, but it does not contain any dense gas at time zero. The entire rectangular domain, both above and below, is defined as containing 99.9% air and 0.1% of the dense, Buncefield gas. Similarly to the addition of the internal boundary, this was done because the model would not run when it was attempted to introduce dense gas into a domain containing pure air. Once the gravity current

begins flowing through the domain, the internal boundary becomes the interface between the gravity current and the air above it; therefore this boundary is defined as having a flux boundary condition, allowing for molecular diffusion across it. This is the only form of mixing between the two fluids allowed by the model.

The top boundary of the overall domain was fixed as being pure air. This is why the domain was made one meter tall even though (as will be seen) the gravity current does not ever reach 10 centimeters in depth. Having a boundary fixed as pure air near this interface could potentially increase the driving force for diffusion between the two fluids. To avoid this, the domain was made much taller than the gravity current.

The bottom boundary was fixed as a slip, no flux boundary condition. The input and outlet boundaries, (that is the boundaries whose cross-sectional areas are perpendicular to the flow) allow flux. The bottom and inlet boundary will be described in more detail in the following section.

Figures 5.1 and 5.2 on the following page show the initial gridding of the domain. It can be seen the resolution increases towards the bottom of the domain. In actuality, the mesh is getting finer in response to the addition of the internal boundary. When the gravity current begins flowing through the domain, this boundary moves up vertically as the current gets thicker. As this occurs, the fine meshing moves up automatically with the boundary.

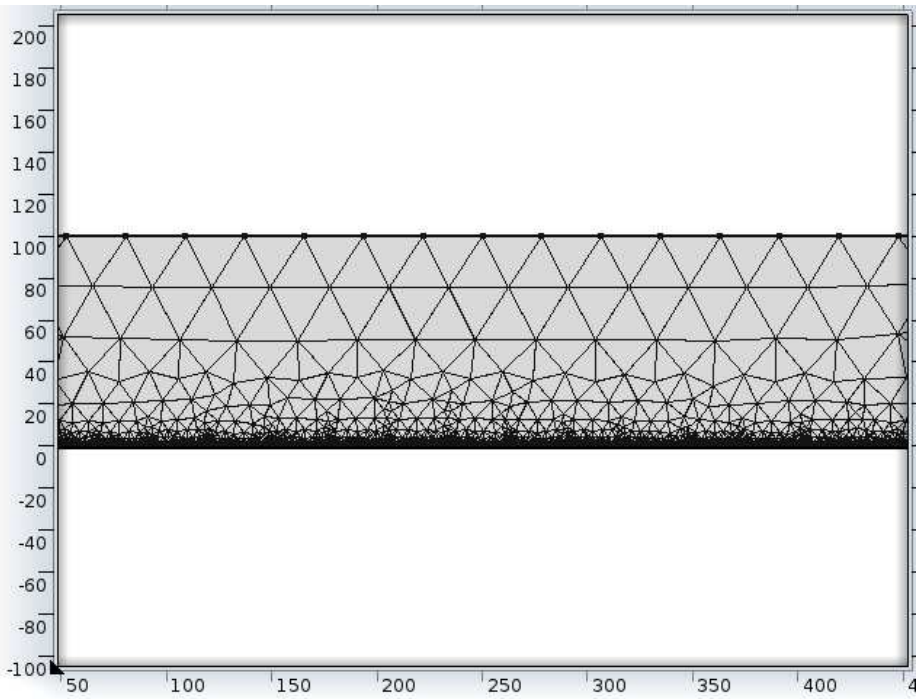

Figure 5.1 The initial gridding of the domain. The gridding becomes finer and finer towards the boundary initially set at two millimeters. The units for both axes are centimeters.

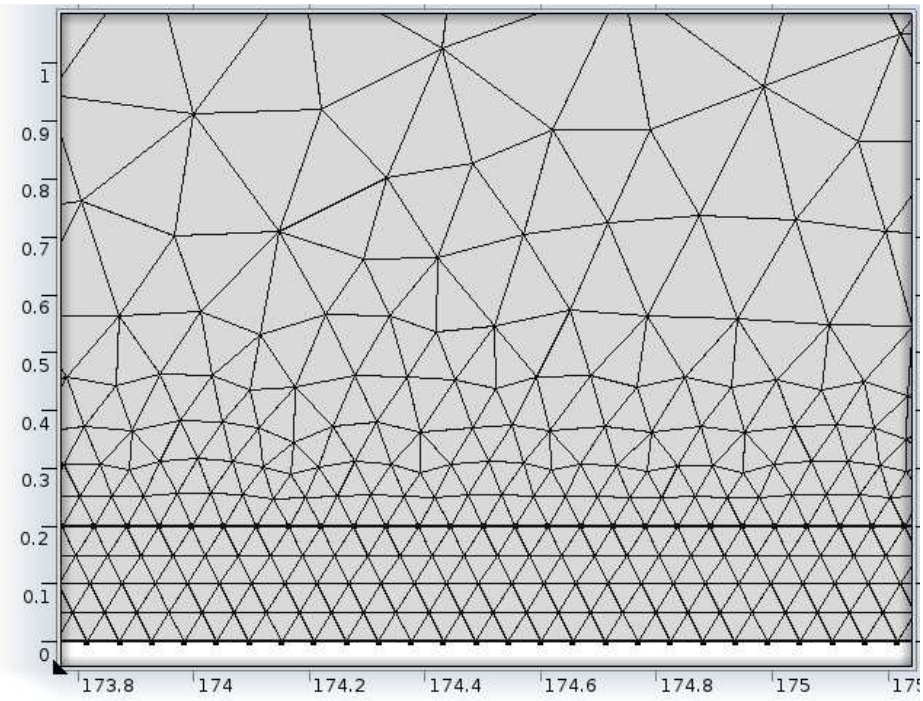

Figure 5.2 A blown up picture showing the bottom one centimeter of the domain. The internal boundary located two millimeters above the ground is plainly visible, as is the 0.5 millimeter height of the smallest element.

5.3 Modeling the Flow

With the domain in place the stage is set to input the flow of the gravity current through the domain. At time zero there is, of course, no vertical or horizontal velocity. The initial height of the gravity current is 2 millimeters, but with an initial concentration of only 0.1%. In order for the model to have comparative value with the physical experiments, the input conditions need to be based on what happens during the physical experiments. The original attempts to provide accurate inputs for the model were focused on modeling the source box in addition to the channel. Good results were not achieved with this methodology. Replicating the moving floor and having the gas turn a sharp 90° corner from the source box into the channel were particularly troublesome issues. It was with this in mind that the domain outlined in the previous section was devised. In this simplified representation of the channel, the far left side of the domain is the beginning of the channel and the source box is omitted. Thus, the accurate input for the model is for the flow to be introduced through this boundary of the domain in the exact same manner it flows through this cross-section in the actual experiments. The manner in which this input data was collected and integrated into the model will be discussed later in this section, but first there will be a slight digression to discuss the bottom boundary condition and the flow properties of the model.

Flow Properties of the Model

The Navier-Stokes equations were not used in the model. Instead, the flow was generated simply by inputting the down channel and vertical velocities calculated during the smoke/video experiments (Section 3.1.7). Figures 5.3 and 5.4 on the next page show these velocities. The

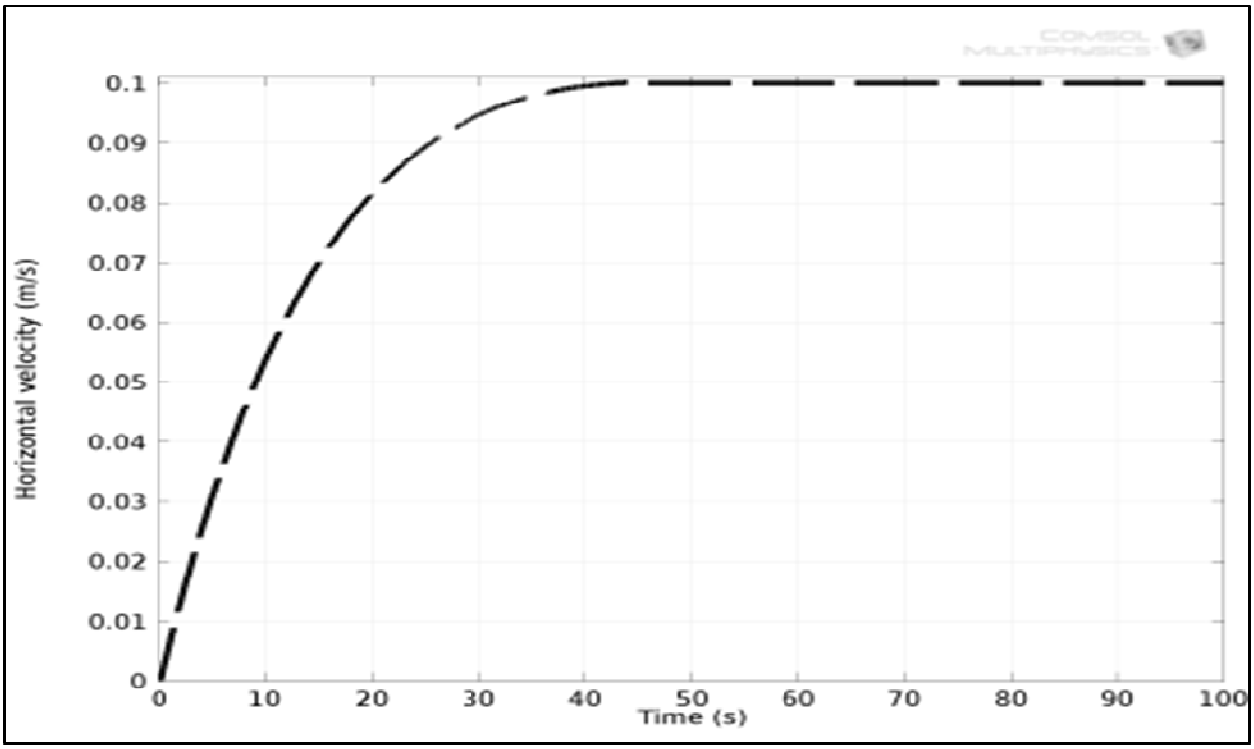

Figure 5.3 The regressed horizontal velocity vs. time curve used as input into the model and used in the regression of the concentration data in Figure 5.6

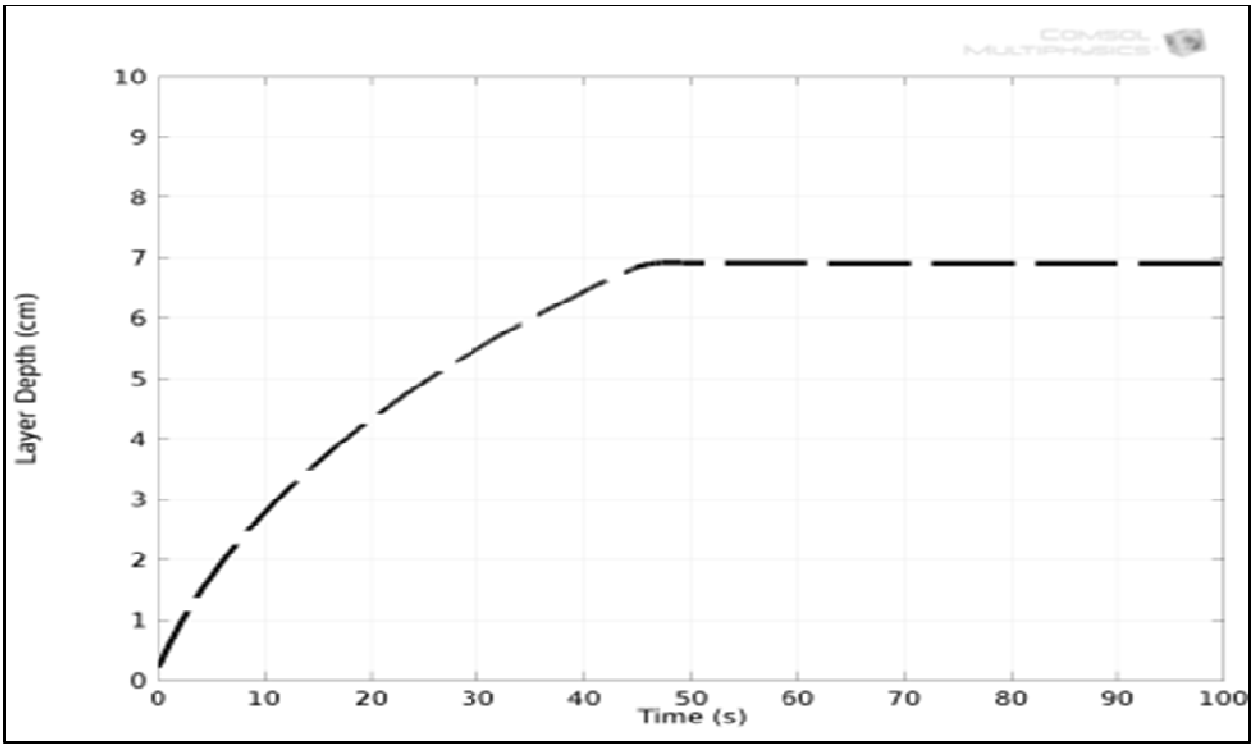

Figure 5.4 The regressed vertical velocity. Note that the graph does not go through the origin. At time zero the cloud height is 2 millimeters as discussed on the previous page.

vertical velocity was translated into layer depth vs. time data because it was easier to input into the model this way. Figure 5.3 is a simple regression of the raw velocity data collected in the manner outlined in Section 3.1.7. It shows that the down channel velocity is transient for the first 40-45 seconds before steadying out at 10 cm/s. Setting up the model this way means that there is a slip boundary condition given to the bottom boundary, so there is no vertical velocity gradient and the flow in the model has a flat front. This simplification is not believed to have introduced significant error. This belief is supported by the agreement between the model and the experiments shown in the next chapter.

Figure 5.4 shows a similar transient beginning, but is more complex then Figure 5.3 in that its creation required interpretation of the raw data and a judgment on how to define the boundary of the cloud. Interpretation was necessary because the smoke did not define the boundary of the cloud very accurately in the vertical dimension even though there was a very clear interface between the smoke and the gas above (see Figure 3.10). For instance, the smoke only reached four centimeters in height for the 200 lpm run. FID experiments showed that at four centimeters the concentration in the cloud was approximately 50%. Testing done at various flow rates (and therefore different cloud thicknesses) showed that the smoke interface occurring near the 50% concentration point was consistent. The above begs the following question: How do you define the boundary of the cloud? Deeming everything below 50% concentration to be outside the cloud did not seem defensible, which meant that the smoke runs did not show the cloud in its entirety. (Interestingly, this was not the case down channel (Figure 5.3). In this dimension, the smoke defined the cloud boundary very well).

At this point, the next thing to decide was the best way to define the edge of the cloud. It was decided that anything less the 10% concentration was not a part of the cloud. FID runs showed

that at an elevation of seven centimeters, the concentration steadied out at very slightly above 10%, so the cloud was defined as being seven centimeters thick. Since the smoke only went to four centimeters for this run, the depth vs. time data could not be directly translated into Figure 5.4. Instead, the video data was used to map out the acceleration rate and the elapsed time before the depth steadied out. This was then translated into a curve which steadied out at seven centimeters. This disconnect between the smoke and the FID concentration data means that Figure 5.4 is an approximation, but the agreement seen between the model and experiments vindicates the process used to create this curve.

Input Into the Input Boundary

An experimental program was undertaken with the FID at one centimeter down channel (zero centimeters down channel could not be achieved because the lid was in the way). Six runs each were performed at 10 different elevations. The elevations chosen were 0.1 cm, 1.0 cm, 2.0 cm, 3.0 cm, 3.5 cm, 4.0 cm, 4.5 cm, 5.0 cm, 6.0 cm, and 7.0 cm. More data was taken at the intermediate elevations because this is where the greatest variation in concentration occurred. The raw data from this experimental program is shown in Figure 5.5 on the following page. The curves have been normalized such that the filling percentage (95%) reflects a 100% concentration. Each curve represents the arithmetic mean of the six runs done at that elevation. Since the data collection was done at 100 Hz, there are 9620 data points per curve for the 96.2 second long experiment.

The first thing that stands out when viewing this graph is just how transient the concentration field is in this experiment. Early on, during the design phase of this project, it was assumed that

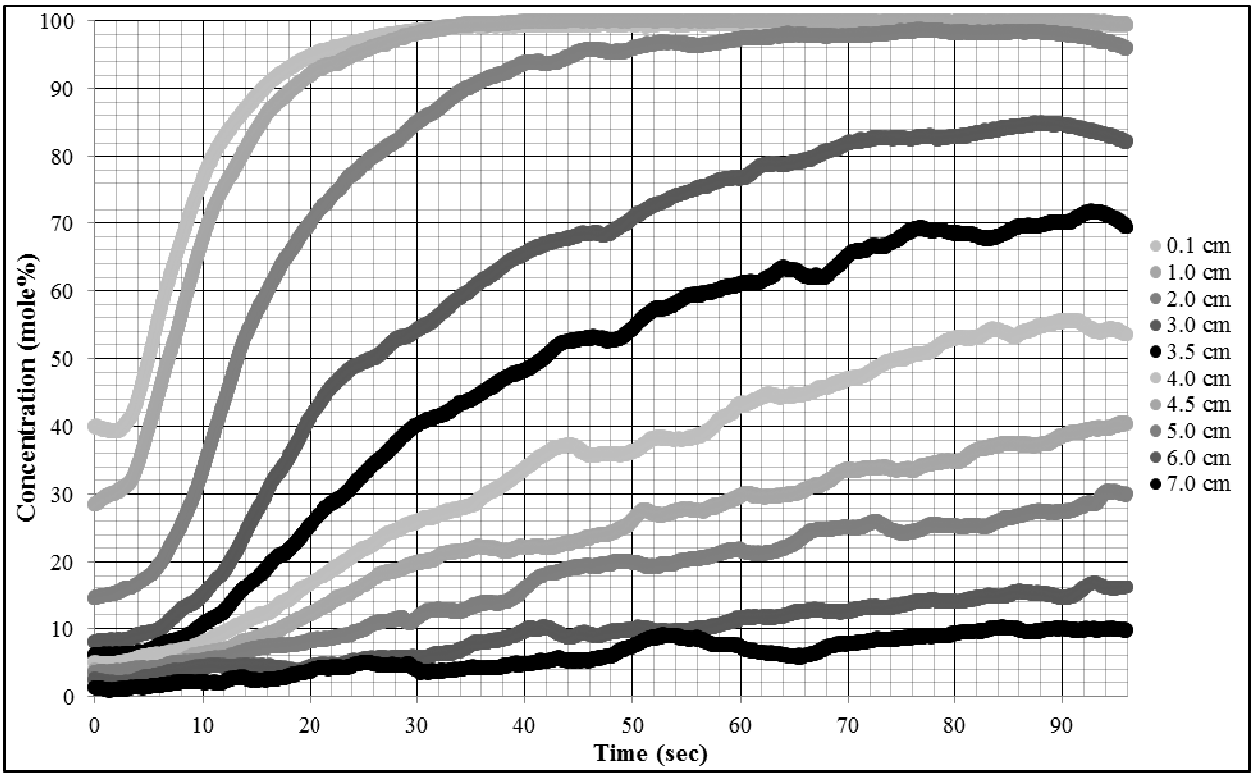

Figure 5.5 Raw concentration vs. time data at one cm down channel for various elevations.

the down channel curves would look approximately like step changes. In other words the concentration would be near zero before the cloud arrived and then the concentration would jump to some value as the cloud flowed by. With the data in Figure 5.5 serving as the "beginning" of the experiment, there is obviously no potential for any subsequent down channel concentrations to behave like a step change. The fact that they are nothing like step changes has a dramatic impact on how the cloud develops and the importance of diffusion on this development. This will be discussed in detail in the following chapter.

Another interesting feature of this graph is how only at 0.1, 1.0 and 2.0 centimeters depth does the concentration approach 100%, even at the beginning of the experiment. It does not seem likely that molecular diffusion is the sole reason for this result, even if its impact is greater than intuitively expected. One potential explanation put forward is the fact that by the time the floor is

started up some dilution has taken place within the box. It was stated near the end of Section 3.2 that a concentration of 95% +/- 1% was achieved throughout the box. This is true, but during the minute it took for the lid to slide off the box air was entrained lowering this concentration near the top and resulting in a concentration profile within the box. Tests showed that at one centimeter below the top of the box the concentration was 60%, at five centimeters below the top of the box the concentration was 90% and at 10 centimeters below the top of the box the concentration was 100% (values normalized). This dilution was caused by a combination of leaks, and the small disturbance caused by the moving lid. Neither of these issues could be eliminated entirely. Moving the lid faster would have reduced the time available for gas to leak, but it would have increased the turbulence caused by the lid. The one meter per minute velocity for the lid chosen worked best to minimize both effects.

As described in Section 3.1.4, a small fan was pointed down channel to help clear out the gas which leaked into the tunnel during the filling of the box. Since almost all of the curves start out above zero concentration at time zero, it's clear that the fan did not work perfectly. This is because the fan had to be turned off before the end of the filling process in order to ensure that the channel was calm before the release. It can be seen in the graph that this leakage has a larger impact near the floor of the channel. This contamination of gas meant that Figure 5.5 could not be directly input into the left hand boundary of the domain. The model would not have run properly (or at all) since the data in Figure 5.5 had to be incorporated with Figure 5.4 to get the model to work. As an example, Figure 5.4 shows that the cloud does not reach a depth of four centimeters until about 18 seconds have passed, while Figure 5.5 shows an *initial* concentration of 5% at four centimeters and a concentration of about 13% at the 18 second mark. This all meant that the graphs had to be manipulated to synchronize the initial rise in concentration with

the arrival time of the cloud as shown in Figure 5.4. This was done by first chopping all of the data to the left of the arrival time for each elevation (i.e., 0 seconds for 0.1 cm, 18 seconds for 4 cm, and 25 seconds for 5 cm). At this point judgment was used to further cut data to allow the curve to smoothly go to zero. The higher the elevation, the more additional data had to be cut. For instance at 0.1 centimeters, only about 3 seconds had to be cut out, while at seven centimeters 45 seconds had to be cut to allow for the arrival time and an additional 13 seconds were cut to allow for the graph to smoothly approach zero concentration from the right.

In addition to this, the last 6.2 seconds were cut from the data. This was done because the there was a transient effect at the end of the experiment as the moving floor approached the height of the channel. In the smoke runs this transient effect would be seen as a slight lowering of the cloud in the last few seconds of the run. In Figure 5.5 this transient effect can be seen in the downturn of the concentrations at 1.0, 2.0, 3.0, and 3.5 centimeters over the last six seconds. This downturn did not seem to reflect anything other than the approach of the floor so this data was cut out.

With these sections removed from the data set, some form of regression was needed to fill in the gaps. One option was to attach regressed sections to the experimental data thus creating a piecewise function for each curve, but this idea was abandoned in favor of using the regression tool in Matlab to replace the entire curve for each elevation. For all of the curves except 3.0 cm and 7.0 cm functions of the form

(5.1)

were used. For 3.0 and 7.0 cm, functions of the form

(5.2)

were used. In both equations, C is concentration (mole percent), t is time (seconds), e is the exponential function, and a,b,c, and d, are constants. The curves are shown in Figure 5.6.

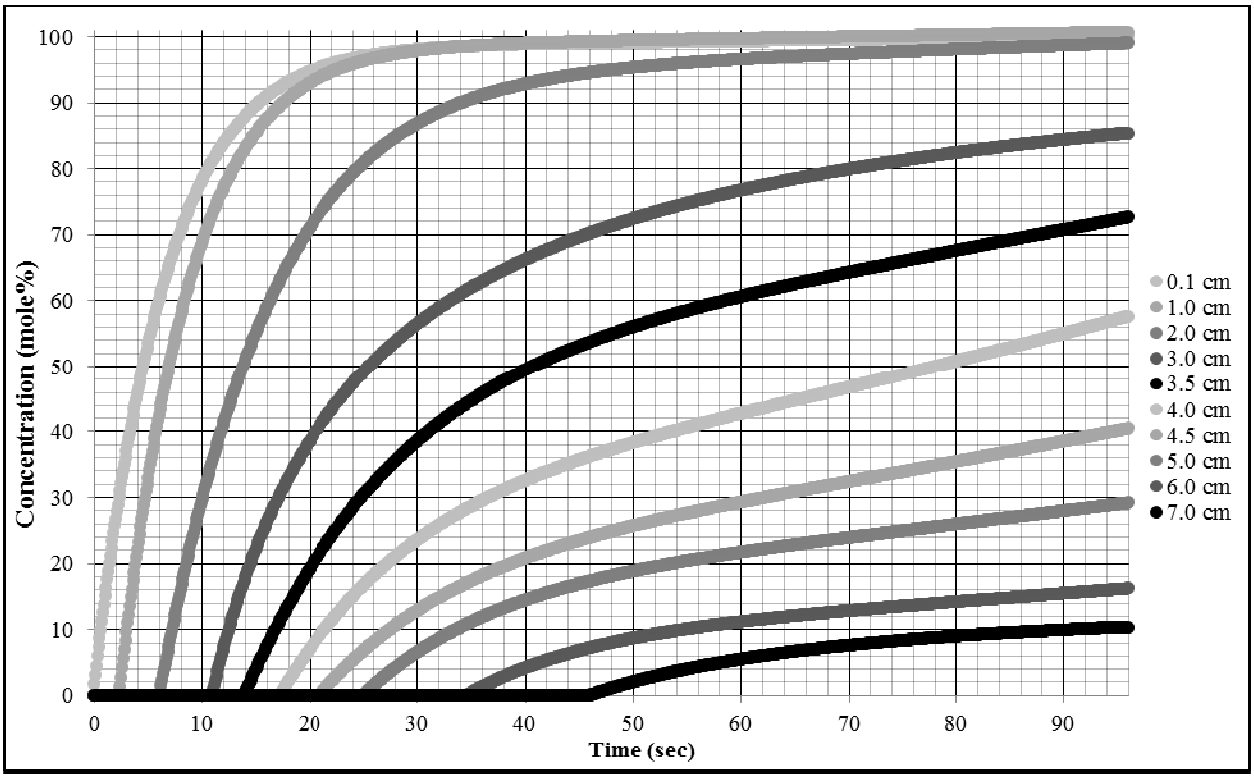

Figure 5.6 Regressed concentration vs. time data at one cm down channel. This data served as the input into the left hand side of the model.

Chapter 6

RESULTS AND DISCUSSION

The FID was used to collect down channel concentrations in the developing cloud. The FID was placed at 100, 200, 300, and 400 cm down channel. At each of these locations, data was collected at the following heights above the channel floor: 0.1 cm, 1.0 cm, 2.0 cm, 3.0 cm, 3.5 cm, 4.0 cm, 4.5 cm, 5.0 cm, 6.0 cm, 7.0 cm, and 8.0 cm. These are the same heights which were selected in the experiments conducted at the front of the channel (Figure 5.5), except in the down channel locations 8.0 cm was added to the experimental program. This was done because the concentrations at the top of the cloud were deemed particularly important due to the interest in molecular diffusion. Only data collected at 0.1 cm, 2.0 cm, 4.0 cm, 6.0 cm, and 8.0 cm is plotted on the graphs in this section in order to keep the graphs uncluttered.

Data was also generated with the COMSOL model at the same locations listed above. As stated previously the model was made for purposes of comparison with the experimental data. Since molecular diffusion was the only form of entrainment in the model, agreement between the experimental results and the model would imply that diffusion was controlling in our experimental releases.

On the following four pages is a series of graphs where the data is grouped by down channel location. To facilitate an analysis of the level of agreement between the experimental data and the model each page has two concentration vs. time graphs: one showing experimental data, and one showing model results, each at the same down channel location. Each curve on the experimental data graphs is the arithmetic mean of two runs.

100 cm down channel

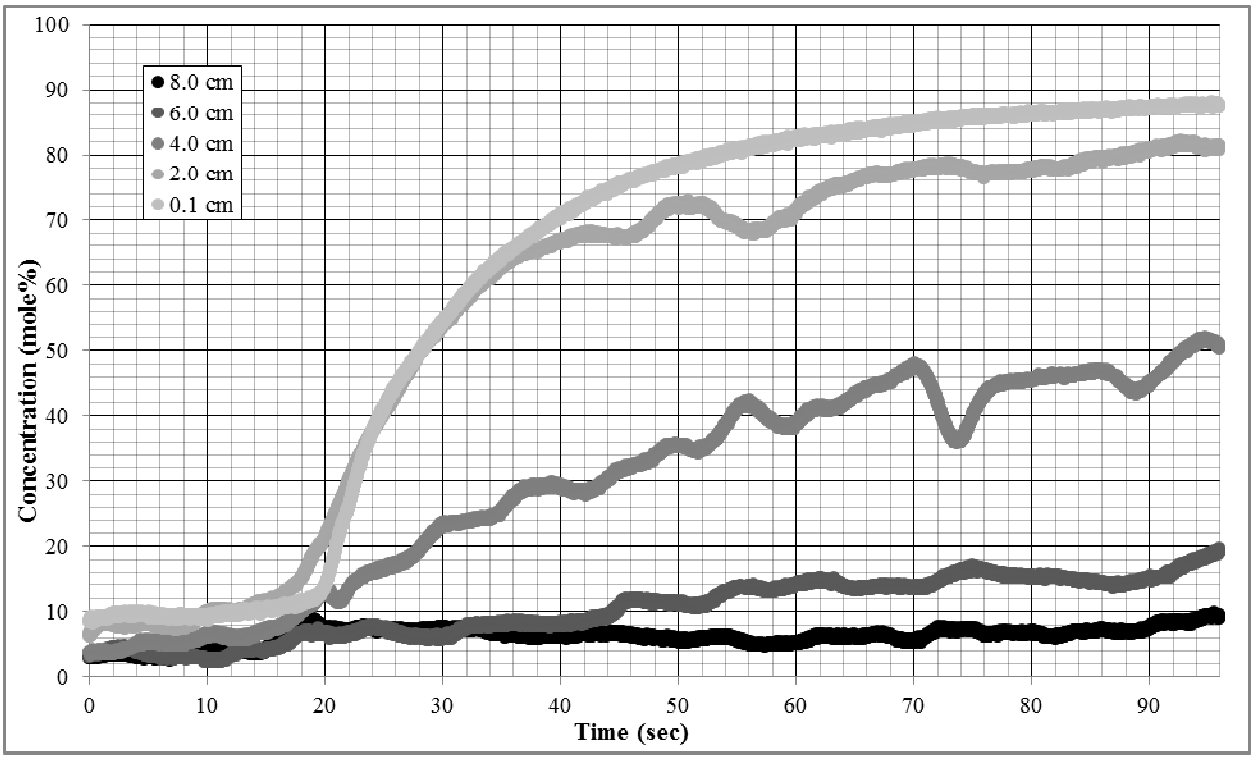

Figure 6.1 Experimental data at 100 cm down channel

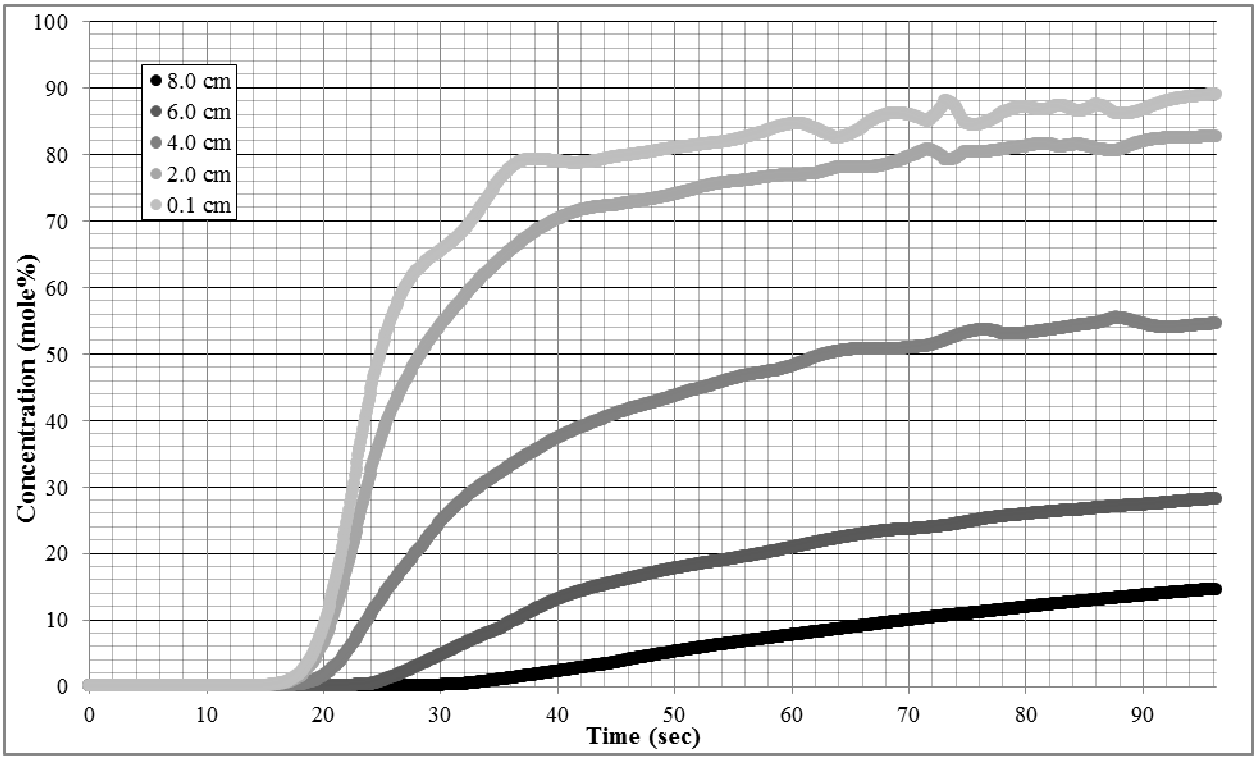

Figure 6.2 COMSOL model results at 100 cm down channel

200 cm down channel

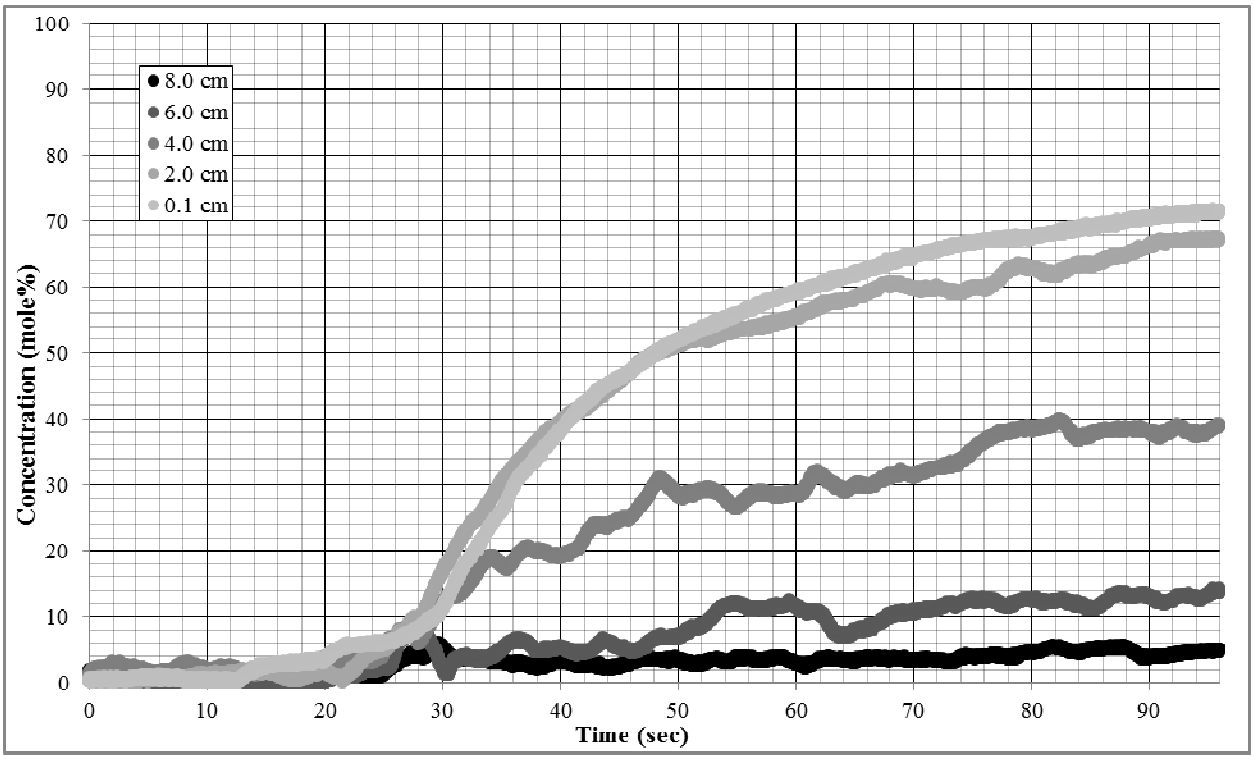

Figure 6.3 Experimental data at 200 cm down channel

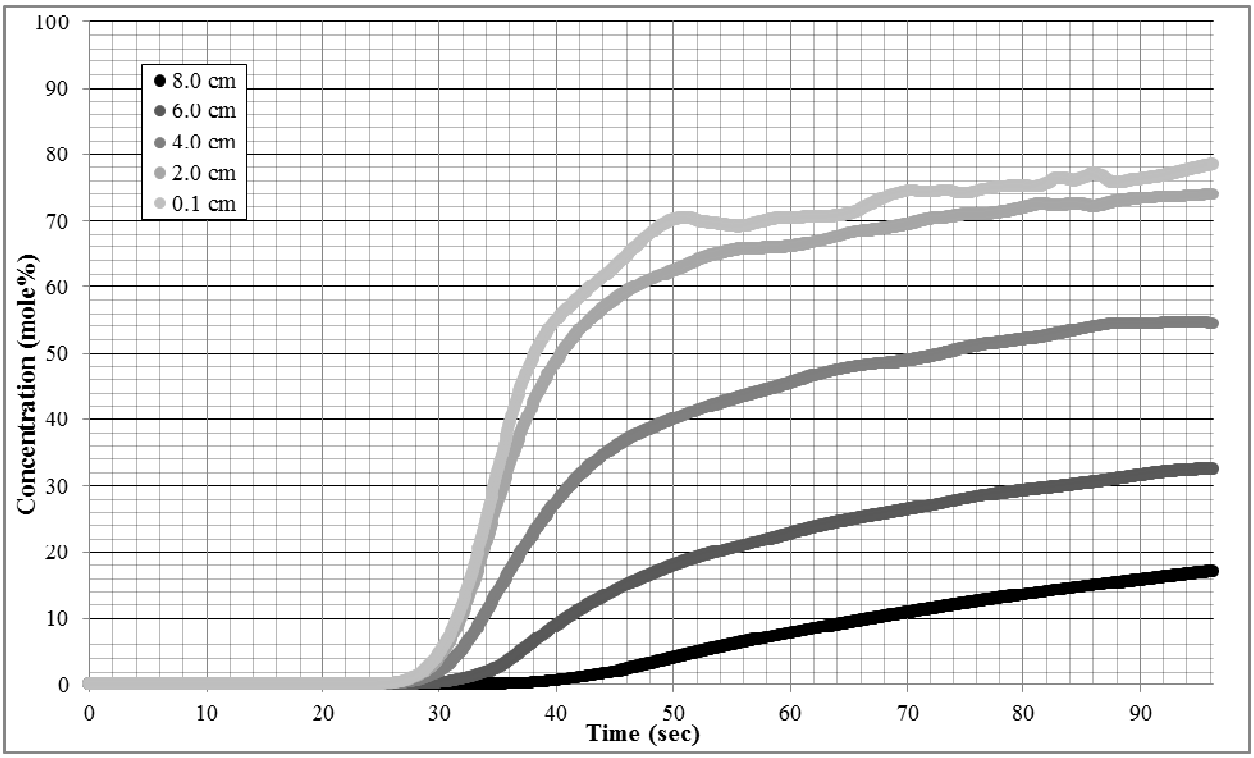

Figure 6.4 COMSOL model results at 200 cm down channel

300 cm down channel

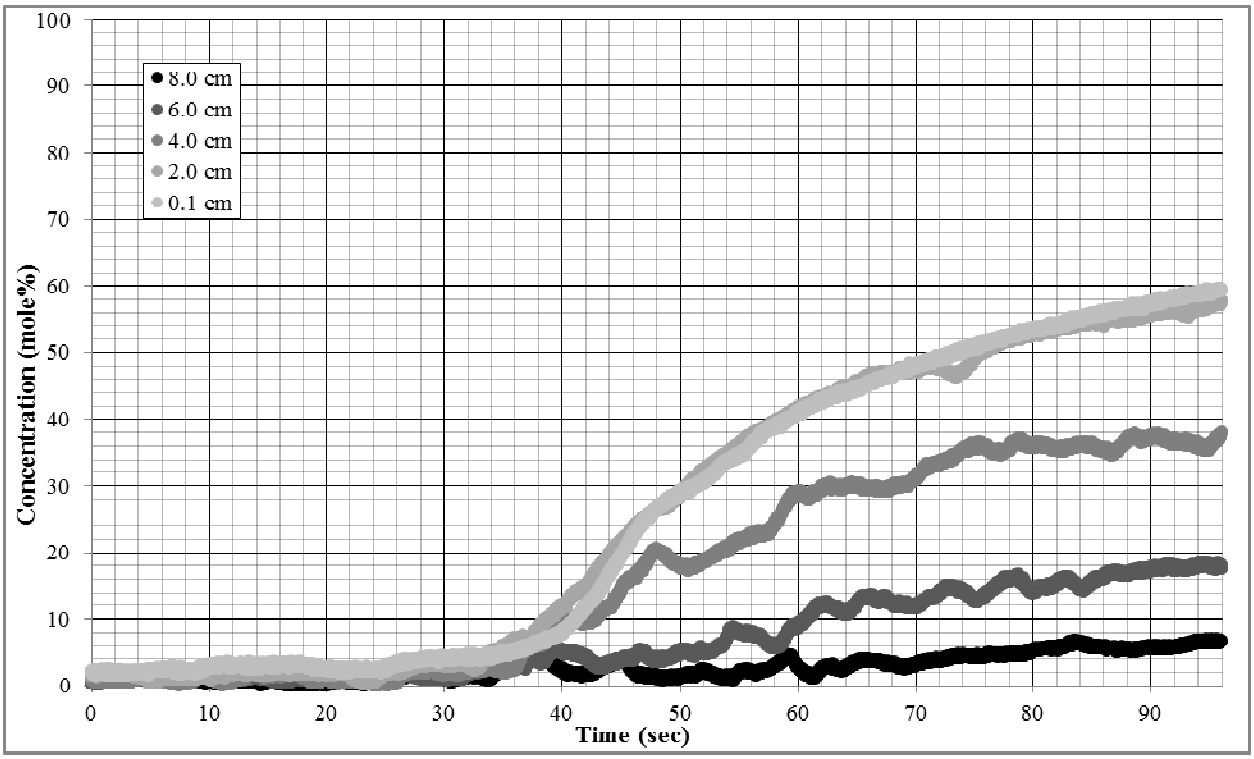

Figure 6.5 Experimental data at 300 cm down channel

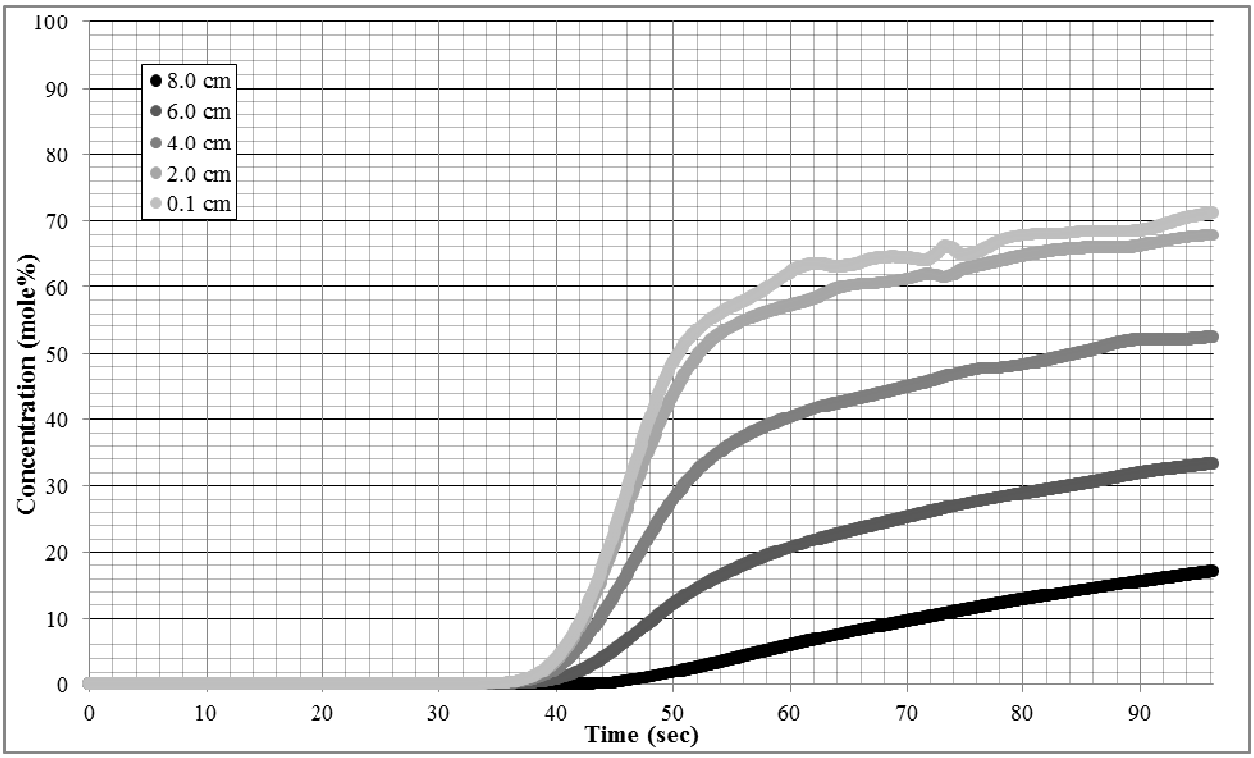

Figure 6.6 COMSOL model results at 300 cm down channel

400 cm down channel

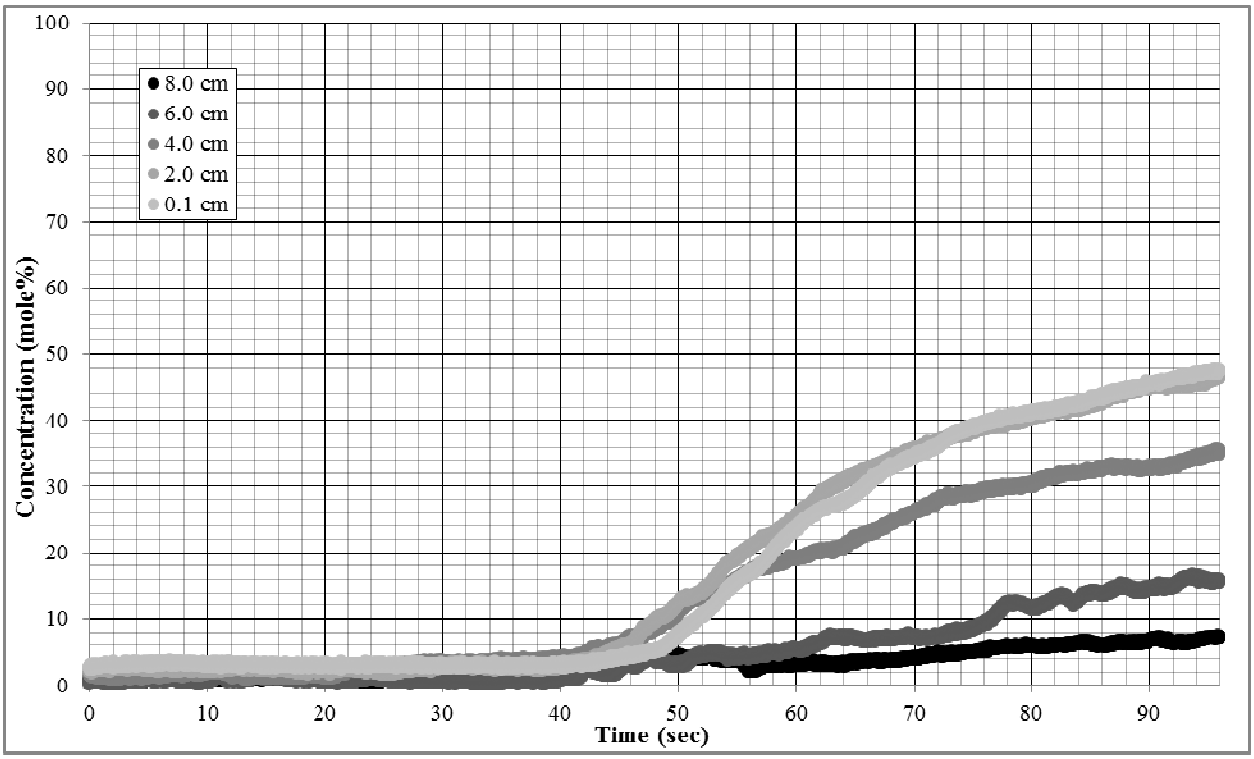

Figure 6.7 Experimental data at 400 cm down channel

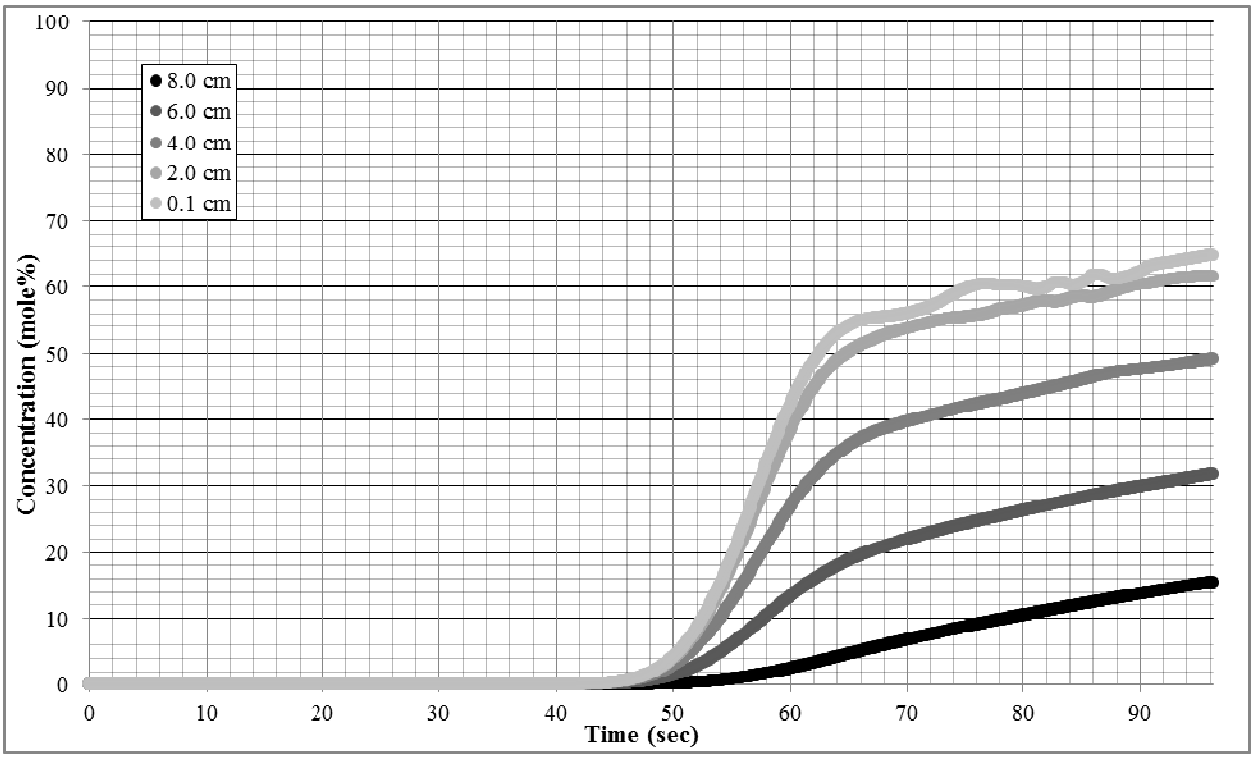

Figure 6.8 COMSOL model results at 400 cm down channel

To prevent the graphs from getting cluttered, only five elevations were graphed. It is clear that the transient “beginning” of the experiment shown in Figure 5.5 is highly influential in the shape of the concentration vs. time graphs down channel. The analysis of the trends in the data, and the level of agreement between the experimental data and the model will be broken down by grouping 0.1 cm and 2.0 cm together as “low” elevations, grouping 6.0 cm and 8.0 cm together as “high” elevations, and keeping 4.0 cm alone as a “medium elevation.

Low Elevations (0.1 cm and 2.0 cm)

The concentrations at these elevations drop much more than the higher elevations do as the current moves down the channel. Recall that these were the only elevations where 100% concentration was reached by the end of the experiment at the front of the channel. At 100 cm down channel, concentrations had already dropped below 90% for both the experimental data and the model. In the experimental data, the concentrations continued to drop between 10 and 16 percent per down channel location, resulting in concentrations just below 50% at 400 cm down channel. This trend is the same for the model, except the reductions in concentration are not as large from station to station. At 400 cm the model reports concentrations under 65%. The gap between the experiments and the model gets larger as the current moves down channel, but the approximately 15% difference at the conclusion of the experiment still represents excellent agreement between the model and the experiments. The conclusions drawn from this level of agreement will be discussed in more detail in the next chapter. So in summation, at 0.1 and 2.0 cm, there is a significant drop in concentration down channel. In the experiments, the drop is from 100% to approximately 50%, while in the model the drop is from 100% to 60-65%.

Middle Elevation (4.0 cm)

Figure 5.5 shows that at 4.0 cm elevation at the front of the channel, the concentration reaches a value in the mid-fifties before falling slightly near the end of the experiment. As mentioned earlier, it is believed that this downturn is due to the approaching floor so the ending value of about 58% shown in the regressed curve in Figure 5.6 is more indicative of the value at this height. For the experiments, the down channel graphs show a progression of 50% at 100 cm, 39% at 200 cm, 38% at 300 cm, and 36% at 400 cm. These values represent a large drop from 1 to 100 cm, and 100 to 200 cm, but after that very little change. The model results show very little change throughout, only dropping from 58% at 1 cm to 50% at 400 cm. As was seen at the lower elevations, the gap in concentrations between the model and the experiments widened as the current traveled down channel, but in this case it was only in the first 200 cm. From 200 to 400 cm they both showed small drops. Overall, the expected trend of decreasing concentration as the current travels down channel is seen at 4.0 cm, but the drop isn't as large (either in absolute value or percentage of starting value) as that seen in 0.1 and 2.0 cm.

High Elevations (6.0 and 8.0 cm)

In the experimental data, the concentration at 6.0 cm bounces around some between stations, but in the end, basically remains unchanged. Figures 5.5 and 6.7 both show a final value of around 17%. The concentration at 6.0 cm in the model nearly doubles from 1 cm to 400 cm. It goes from 17% to about 32%, but interestingly most of this increase comes as the cloud goes from 1 to 100 cm. So it is at 6.0 cm that we see our first reversal of the trend of decreasing concentrations as the cloud travels down channel with the experimental data showing a steady value and the model showing a significant increase.

At a height of 8.0 cm the story is similar to that at 6.0 cm. No data was collected above 7.0 cm at 1 cm down channel because the 10% concentration reached at this height was deemed to be the boundary of the cloud, so the only thing which can be said is that the concentration was not more than 10% at 8.0 cm elevation and 1 cm down channel. The experimental values drop slightly from 100-400 down channel, going from 10% to about 7%, while the model shows an increase in concentration at 8.0 cm from what the value had to be at 1 cm down channel since it gives a value of about 15% at both 100 cm and 400 cm own channel. From this, the conclusion can be drawn that the greatest increase at 8.0 cm came as the cloud travelled from 1 to 100 cm, just as at 6.0 cm.

It is also instructive to view the data grouped by elevation instead of down channel location. The data is displayed in this manner on the following five pages. This alternate view helps further highlight the trends discussed earlier in this section and it also highlights the time lag between the data collection stations. This analysis is helped by the inclusion of the data collected at 1 cm down channel on these graphs, with the exception of those at 8.0 cm elevation since, as has been noted, no data was collected for this elevation at 1 cm down channel. This discussion will be picked up after the graphs.

8.0 cm elevation

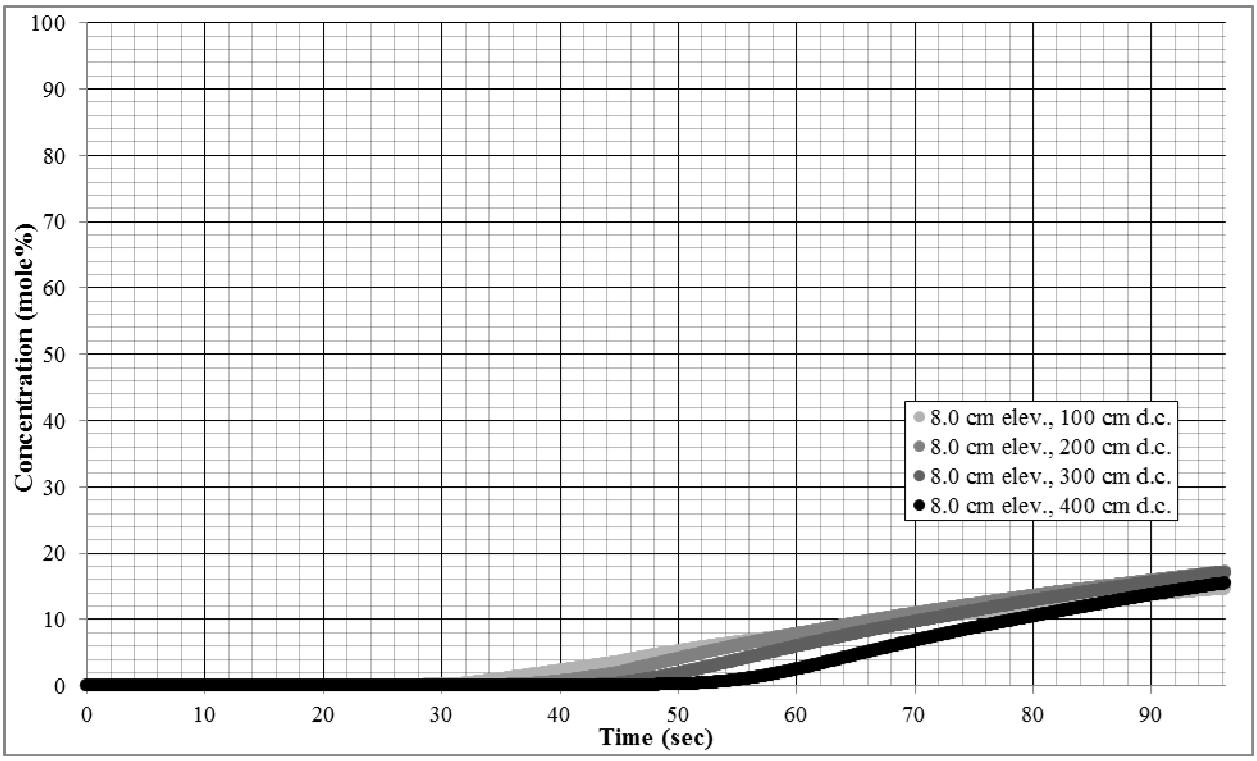

Figure 6.9 COMSOL model results at 8.0 cm height above channel floor

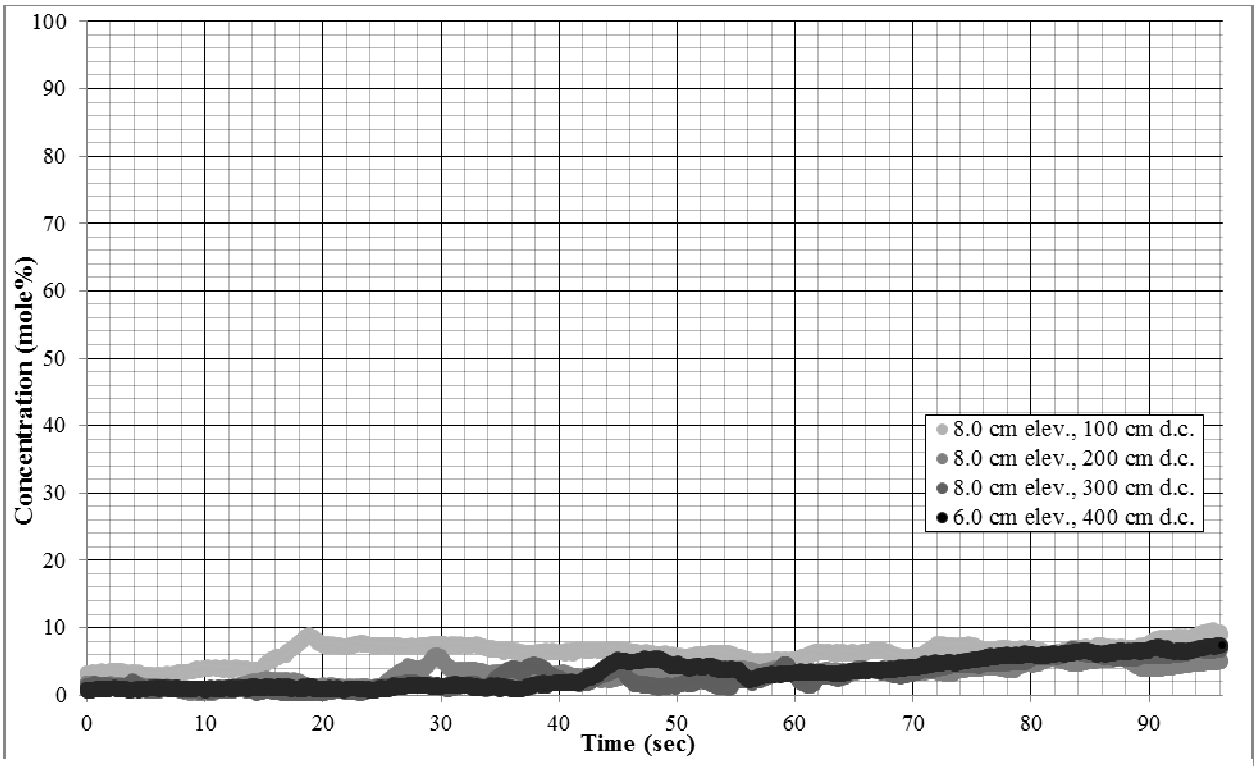

Figure 6.10 Experimental results at 8.0 cm height above channel floor

6.0 cm elevation

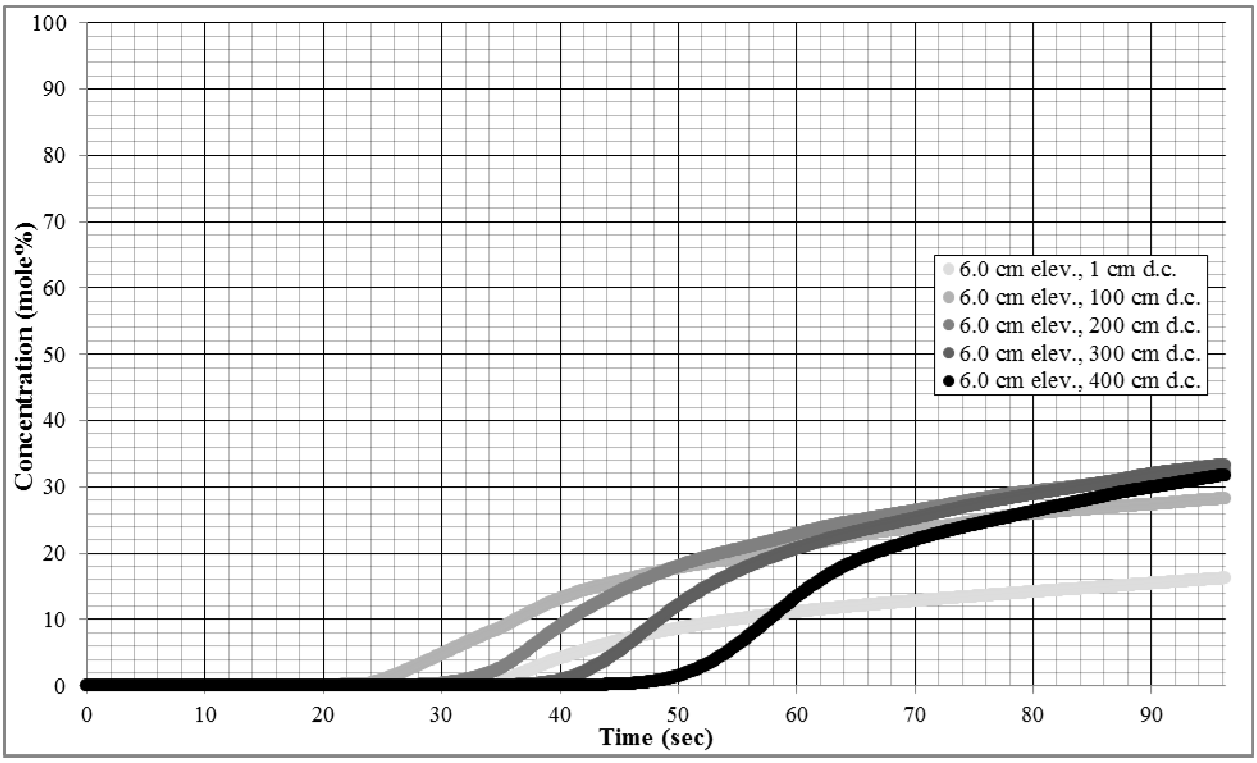

Figure 6.11 COMSOL model results at 6.0 cm height above channel floor

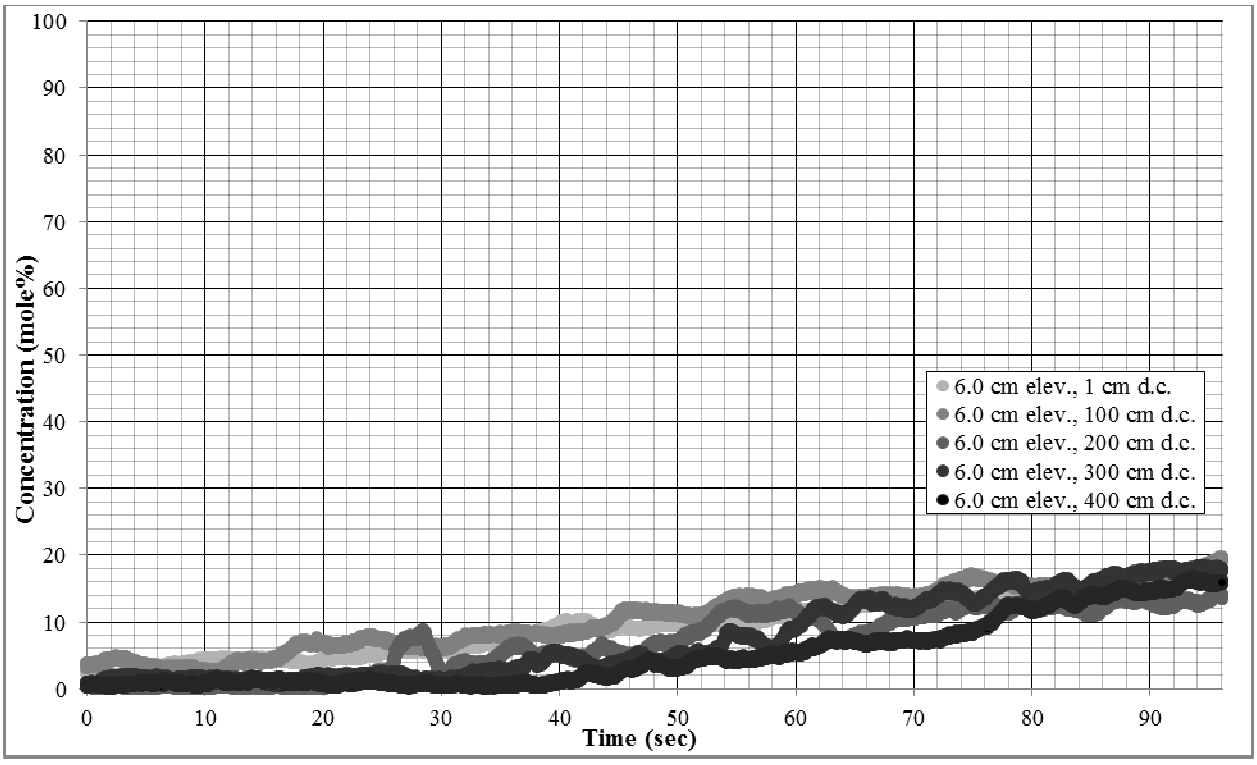

Figure 6.12 Experimental results at 6.0 cm height above channel floor

4.0 cm elevation

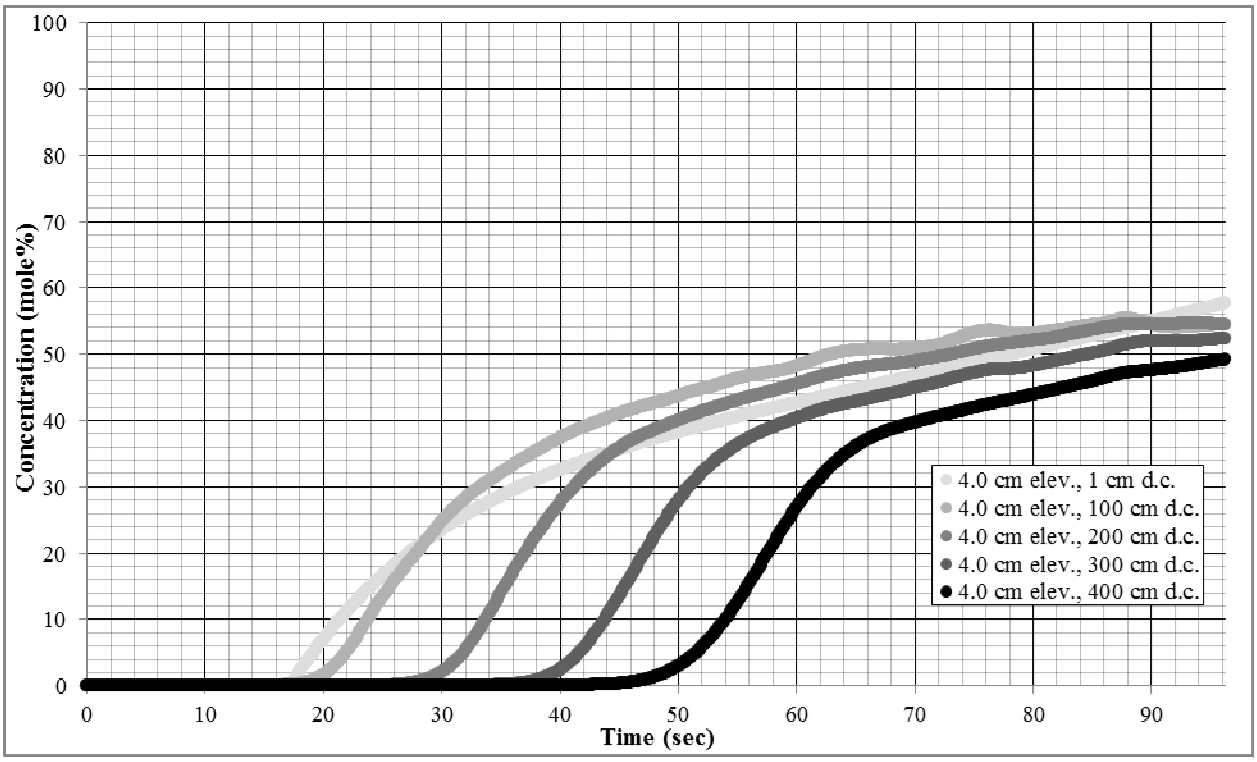

Figure 6.13 COMSOL model results at 4.0 cm height above channel floor

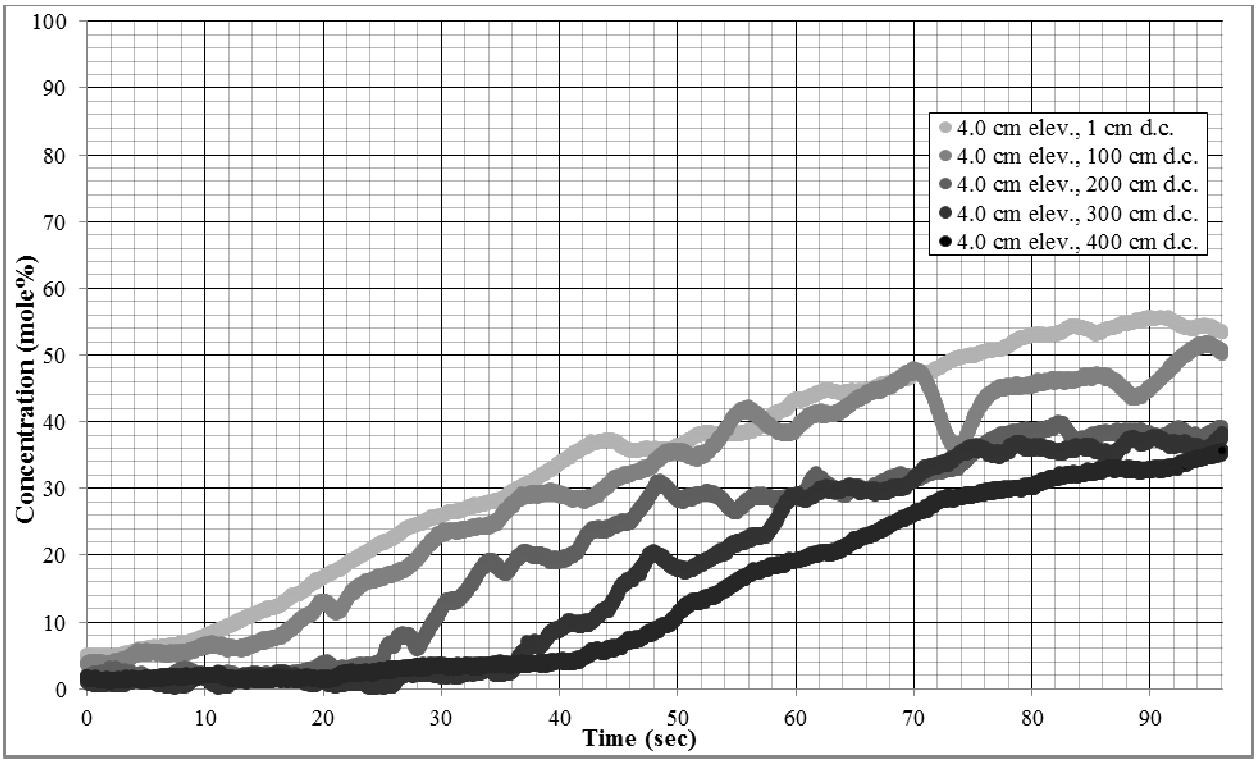

Figure 6.14 Experimental results at 4.0 cm height above channel floor

2.0 cm elevation

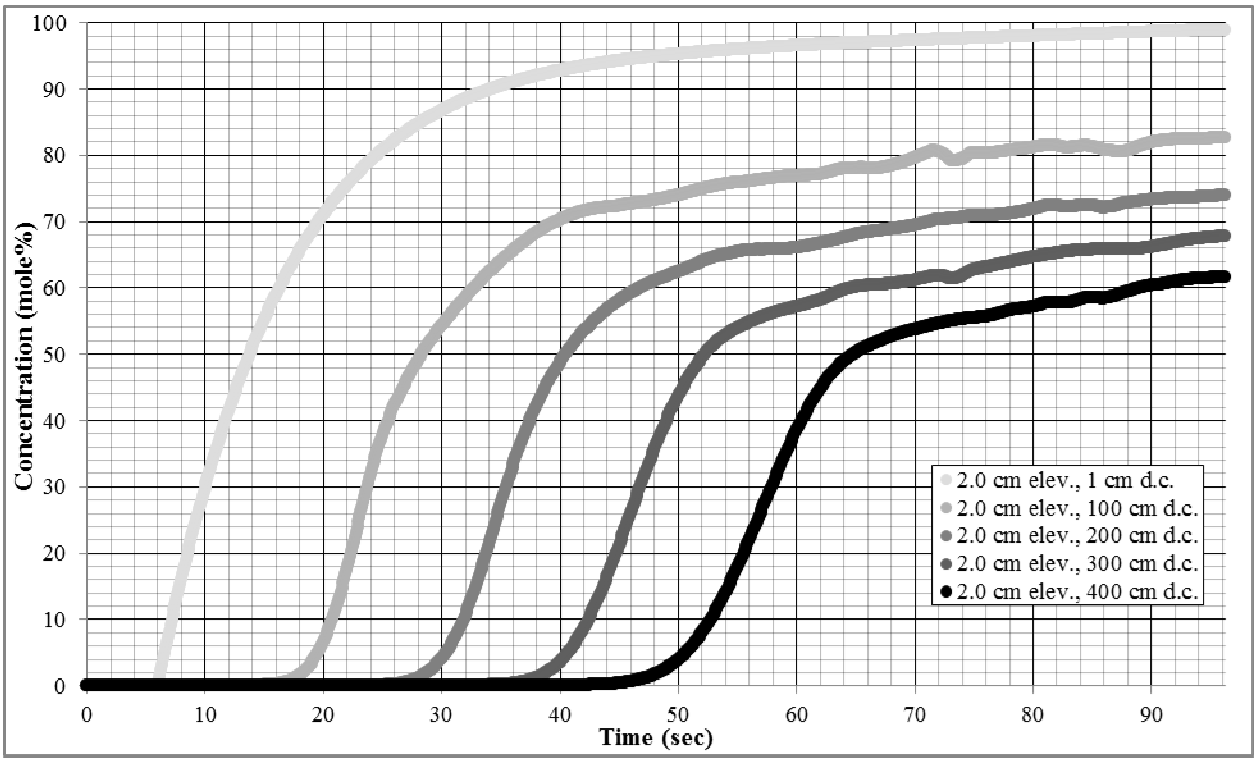

Figure 6.15 COMSOL model results at 2.0 cm height above channel floor

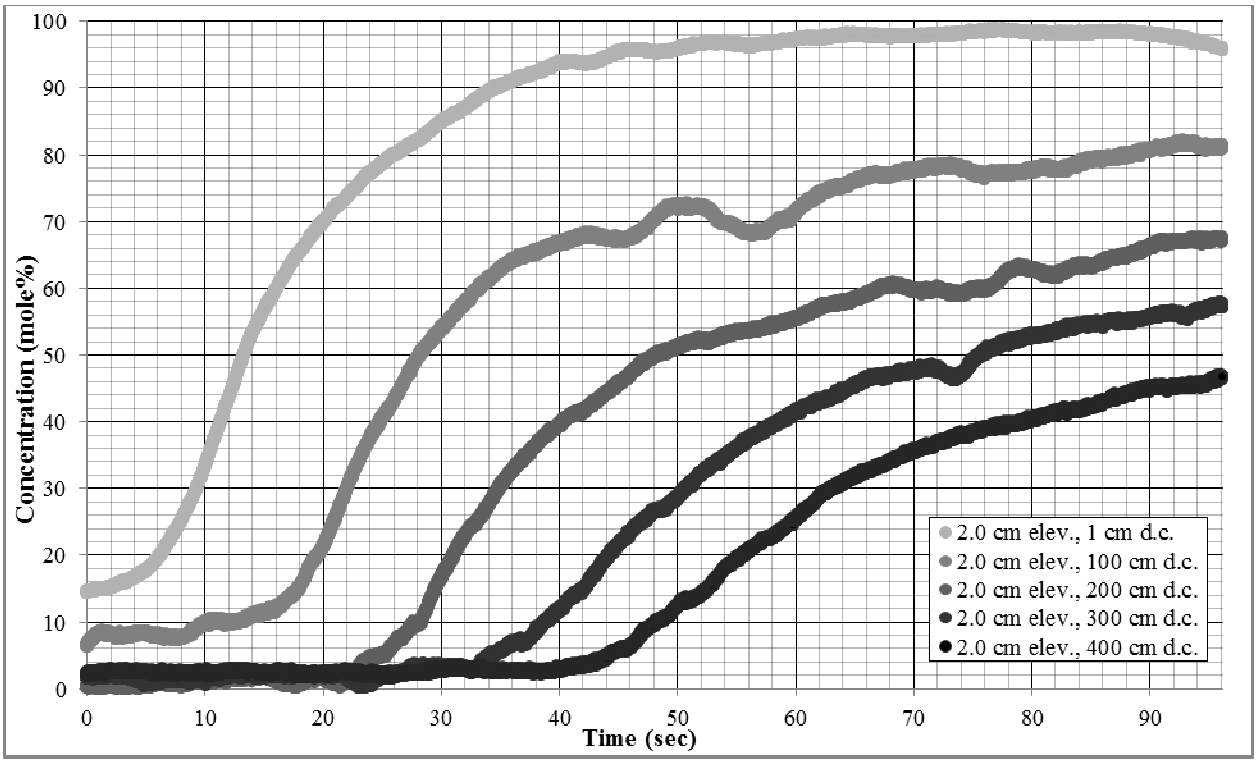

Figure 6.16 Experimental results at 2.0 cm height above channel floor

0.1 cm elevation

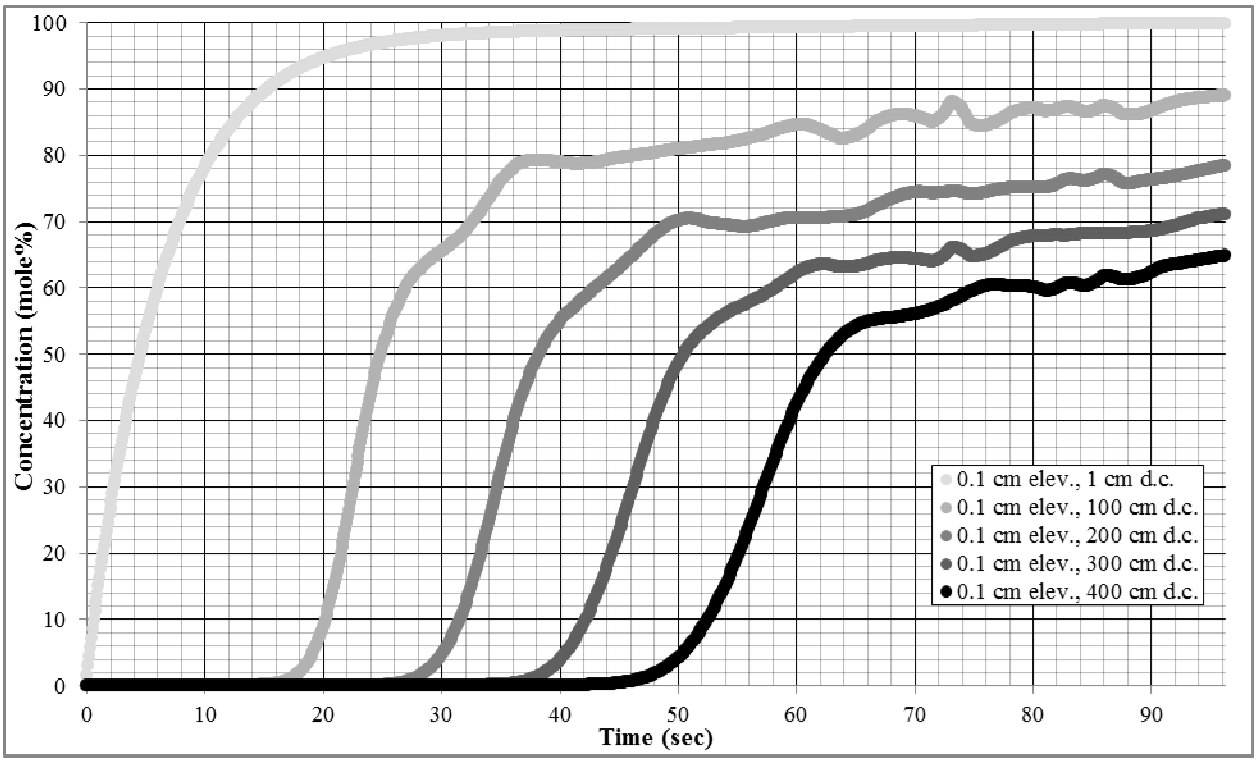

Figure 6.17 COMSOL model results at 0.1 cm height above channel floor

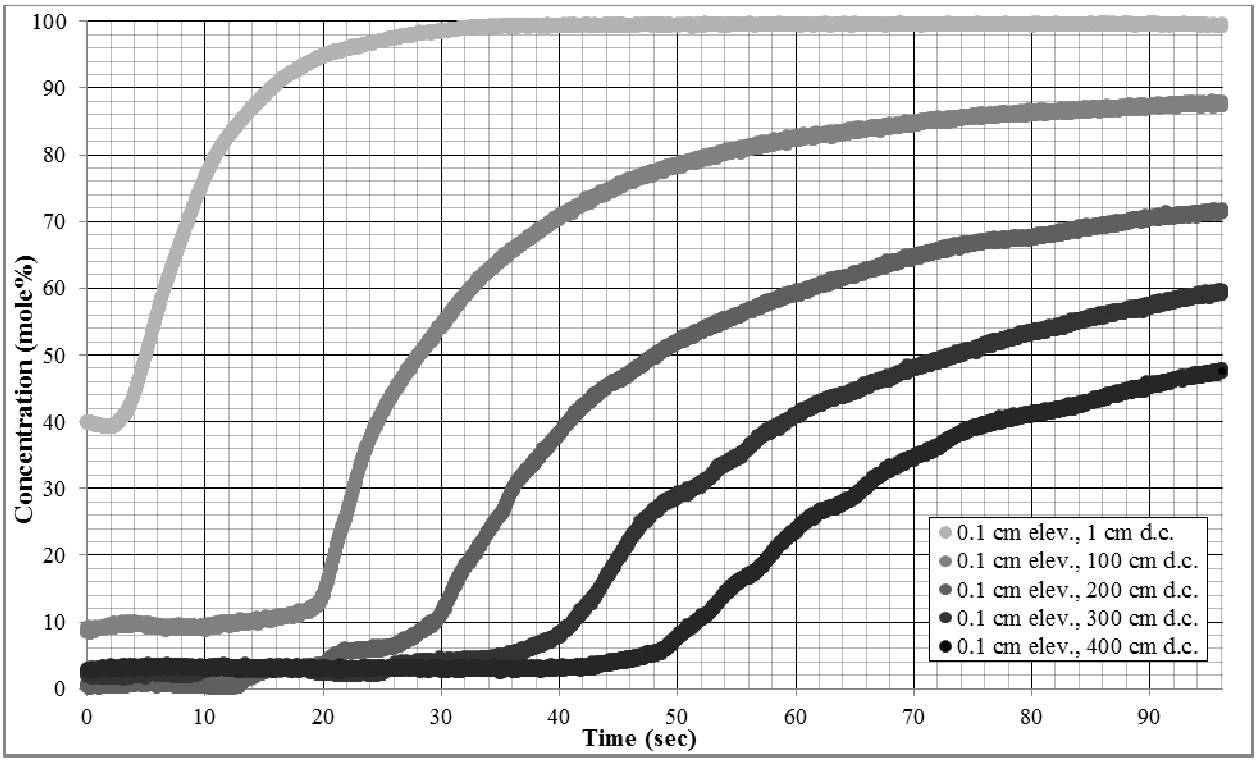

Figure 6.18 Experimental results at 0.1 cm height above channel floor

In figure 6.9 (8.0 cm, COMSOL model), the lag in the arrival of the cloud at each station does not stand out as much as it does for the rest of the elevations due to the very small slopes of the curves, but it is apparent upon close observation. It is interesting to note that in spite of the lag, all the curves are converging to the same concentration as the experiment ends. Figure 6.11 (6.0 cm, COMSOL model) starkly shows the big increase between 1cm and 100 cm, in fact the 1 cm curve looks out of place compared to the other curves on this plot.

CHAPTER 7

CONCLUSIONS

Conclusion #1 The experimental runs are diffusion controlled.

The support for this conclusion is given in the previous chapter. In that chapter, there are 18 concentration vs. time graphs displayed, nine each of the experimental data and COMSOL model. A central question when comparing these two sets of data was whether we were successful in designing an experiment which was molecular diffusion controlled. There is indeed a growing separation in concentration values between the two data sets as the current travels down channel, and as logic would dictate the experimental concentrations are lower than those predicted by the model. This is logical because it stands to reason that we could not completely eliminate all forms of mixing other than molecular diffusion. However, given that the difference in concentration never reaches a gross value of even 20% for any height, and that qualitative picture told by both data sets is completely consistent, it seems defensible to conclude that our experimental runs were indeed diffusion controlled.

Conclusion #2 The transient development of the cloud impacts the effect of molecular diffusion.

As seen in Figures 5.3-5.4, the cloud thickness and spreading velocity both start out at zero at time equals zero and they both eventually reach a constant value. In addition, as seen in Figure 5.5, the concentration field at the front of the channel is variable in both time and vertical location. These three facts (especially the last) all impact the manner, and degree to which molecular diffusion affects the developing, down channel, concentration field.

Cloud Thickness and Spreading Velocity

If you were to expose two pools of pure carbon dioxide with the same cross-sectional area, but differing depths to air for the same amount of time, the rate of diffusion would be the same in both. Of course, this is true only for the amount of time it takes for the first molecule of air to reach the bottom of the shallower pool so let's say that we end the experiment before this time. If we do this and examine the vertical concentration profile in both pools we would find that though the rate of diffusion was the same in both, the net effect on the shallower pool was greater because a larger percentage of the mass in the shallow cloud will have been replaced by air.

In our experiments, we are starting from zero depth and working up to 7 cm at the front in about 45 seconds. Contrast this with an alternative way to do the experiment in which a seven cm cloud of pure carbon dioxide is set up behind a gate and the experiment is initiated by the removal of the gate. (Making this cloud pure carbon dioxide throughout the whole 7 cm would be extremely difficult to accomplish, making this more of a thought experiment than an alternative release method). In this experiment the net depth over the length of the experiment would be greater and thus diffusion would have less impact on the cloud.

I will note here that this isn't the only thing that would change between these two alternative methods of initiating a gravity flow down a channel. The spreading velocity and concentration profile would both certainly be different than that shown in Figure 5.3 and 5.5 respectively. This is what was meant when it was stated earlier that it is not strictly valid to treat these three effects as independent from one another. In fact, it can be asked whether the impact of diffusion during the transient growth of the cloud is to some extent the reason for the unexpected shapes of the curves in Figure 5.5. The importance of the answer to this question depends on yet another

question which arises from doing a thought experiment about this alternative release method, and that question is this: Which method of initiating the flow more closely resembles the release at Buncefield? This question will come up again later in this chapter when the issue of applying our results to the Buncefield incident is considered.

Developing Concentration Field

Looking at the oft referred to Figure 5.5 (or the regressed curves in Figure 5.6) you see the highly transient ramping up of the concentrations (especially the low elevations), but you also see that each elevation appears to be approaching a steady value. The values being approached are setting up a highly stratified cloud, one going from pure carbon dioxide at the bottom 2 cm to 10 percent carbon dioxide at seven cm. This creates a large driving force for the diffusion of carbon dioxide up through the cloud, which provides a very good explanation for the trends seen in the data in Chapter 6. In those graphs you see a very steep drop off in concentration at the bottom of the cloud, but at the top the concentrations are steady or even increasing, which is exactly what you would expect molecular diffusion to cause.

So the combination of the concentration profile seen in Figure 5.5 (or 5.6) in combination with molecular diffusion creates a situation where the concentration within the gravity current is getting more and more uniform as the cloud travels down channel. If you were to claim that it is trending towards a constant value (which is certainly an oversimplification), and try and speculate what that constant value would be, somewhere around a third of the starting concentration would be a reasonable guess.

Contrast this with what would happen in the case of the alternative release method talked about earlier in this chapter. If you had the pure carbon dioxide piled up against a gate and then

released it, you would have no concentration gradients within the cloud at the beginning, and all of the diffusion would occur at the interface between the gravity current and the air. (This is assuming it is still reasonable to assume there are no other forms of mixing.) A knee jerk reaction may be to say there isn't a significant difference between these two situations. In both you have carbon dioxide (and air) moving from regions of high concentration to low concentration. In both, the cloud is growing in elevation as this occurs. However, they are very different. In this case the cloud would be getting less and less uniform as it travels down channel. The next question which arises is: what are the (potential) consequences of this difference on the hazard potential of an accidental release of a toxic and/or flammable denser-than-air gas? This question will be addressed with Buncefield in mind in Conclusion #3.

Conclusion #3 The potential for diffusion effects to make concentrations more uniform may increase the explosion potential.

The above assertion comes directly from the fact that the cloud in our experiments is getting more uniform as it travels down channel. Earlier in this chapter a rough estimate is given that the cloud is approaching a uniform concentration of about a third of the starting concentration. This, of course, means that the starting concentration will dictate whether there is any increase in the hazard associated with the release.

With this in mind, it was instructive to look at the Buncefield incident in more detail. This was done by taking the COMSOL model used for comparative purposes in Chapter 6, and adjusting it to the dimensions and conditions of Buncefield. We looked at a particular section of the release which is of particular interest due to the fact that the main explosive event took place there. Specifically, this is the section of flow from the western wall of the dike, over the parking lot to

the Northgate building (see Figure 1.1). This is the same section of the release that inspired the design of the channel the experiments were conducted in (Figure 3.5), both because it was an area of interest, and because it is a section of flow which can be treated as linear-2D. The distance from the dyke to the building is 110 meters. The Health & Safety Executive estimated the time of arrival of the gravity current at the building to be approximately 3.5 minutes. This translates to an average velocity of the cloud of around 50 cm per second.

The need to do a 210 second run presented a challenge because it was not defensible to take the curves in Figure 5.5 and extrapolate them beyond 96 seconds. Because of this, it was decided to abandon the transient growth of the concentration and input a constant value for each elevation. The concentration chosen for each elevation was the peak value reached in Figure 5.5. ("Peak value" is differentiated from the ending value only for 2.0, 3.0, 3.5, and 4.0 cm, where there is a drop in concentration at the end of the experiment due to the approach of the floor.) For example, at 3.0 cm elevation, a constant concentration of 85% was input into the model, and at 4.5 cm elevation, a constant value of 41% was input. This simplifying assumption does not invalidate the use of this model, because the purpose of this exercise is to test whether diffusion can increase the percentage of the cloud within the flammability limits when the cloud starts out highly stratified. The stratification does not need to be time dependent in the way that Figure 5.5 is in order to test this.

The next change which needed to be made to the input concentration data was to convert the depth of the cloud from seven cm to one meter (the Buncefield cloud was estimated to be 1-2 meters deep, we chose 1 meter for this model run). This was done in the simplest manner possible. For instance, the 7.0 cm curve was changed to 1 meter, and the 4.0 cm curve was changed to 57 cm using the equation below.

$$\frac{4.0\ cm}{7.0\ cm} * 100\ cm = 57\ cm$$

The rest of the curves in Figure 5.5 were adjusted using the same rationale.

The next task was to delineate within the cloud the region within the flammability limits, the region outside the flammability limits, and to track any changes as the cloud flowed. The British Health & Safety Executive did extensive research (both computer modeling and field experiments) into estimating the initial concentration of the vapor which flowed over the dike [2,3,4,5,17]. Their analysis showed a lot of evaporation (and air entrainment) as the gasoline hit objects on its path from the roof of the tank to the ground, causing what started out as a steady stream to be transformed into droplets. The estimated starting value they reported is 6.8 mol% hydrocarbon with an upper flammability limit of 8.1%, a lower flammability limit of 1.6%, and a stoichiometric condition of 2.7%. Using these values the portion of the cloud within the flammability limits at the outset of the release was calculated. The initial concentration of 6.8% was normalized to be equivalent to the 100% value in Figure 5.5 and the rest of the concentrations are adjusted proportionally. With this rationale, the portion of the cloud within the flammability limit at the beginning of the release would be given by the following calculation.

$$\frac{1.6}{6.8} \times 100\% = 23.5\%$$

This percentage occurs between 5.0 cm and 6.0 cm. At 5.0 cm, the final concentration is 29.5%, and at 6.0 cm, the final concentration is 16%. Assuming that the concentration difference between curves is linear, the depth in Figure 5.5 at which this concentration is achieved is calculated using linear interpolation.

$$5.0\ cm + \frac{23.5\% - 16\%}{29.5\% - 16\%} \times (6.0\ cm - 5.0\ cm) = 5.56\ cm$$

This elevation is then converted to a cloud of 1 meter depth instead of seven cm depth.

$$\frac{5.56\ cm}{7.0\ cm} = .794 \times 100\ cm = 79\ cm$$

Figure 7.1 displays the results of the COMSOL model developed with the rationale above. The top rectangle shows the entire 110 meter run. The beginning and the end are blown up and shown in the boxes below the full graphic. The region colored dark gray is within the flammable limit. The dark contour line within the light gray region denotes a concentration of 1%. The transition from light to dark gray is, again, the transition into the flammable region at a concentration of 23.5%. The contour lines within the flammable region are, starting at the top most one and moving towards the bottom, 30%, 40%, 50%, 60%, 70%, 80%, and 90% concentration. A slight increase in the depth of the flammable region can be discerned between the starting point of the release (bottom left graphic) and end point of the flow, 110 meters away (bottom right graphic). Even though the increase is small, the fact the depth increases instead of decreasing is counterintuitive for a mixing process.

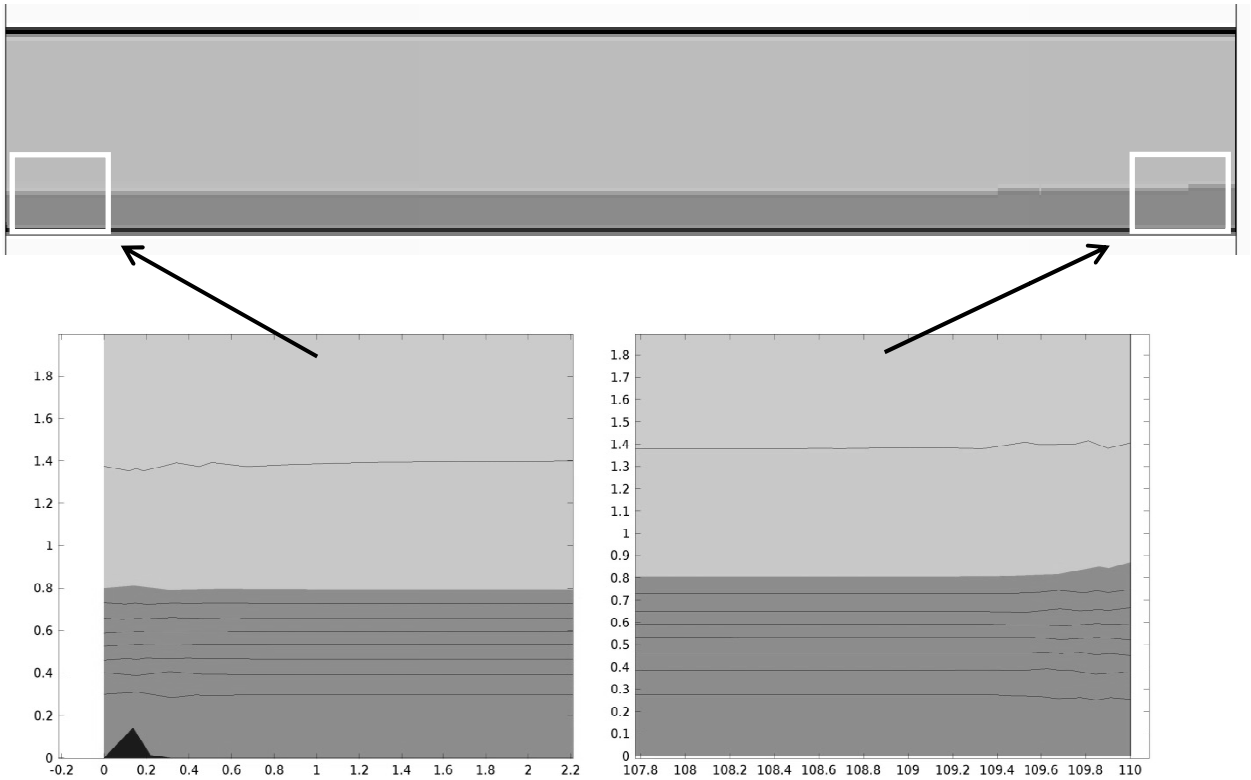

Figure 7.1 COMSOL graphics of a one meter thick cloud travelling 110 meters in three and a half minutes with a starting concentration profile based on the ending values in Figure 5.5.

So the stated claim that molecular diffusion has the potential to increase the depth of the flammable region is borne out in this model.

Conclusion #4 No wind, shallow cloud depths, and long time scales indicate a potential for important diffusion effects.

In the literature review, a series of calculations were worked out using laminarization criteria. These calculations indicated that even for a release of the scale of Buncefield (Re ≈ 100,000), there was likely no turbulent entrainment of air into the cloud, with the possible exception of entrainment behind the head of the gravity current. This result was made much more likely by

the calm conditions which existed at the time of the accident. It is evident that special consideration needs to be given to the potential of accidental releases taking place in no wind conditions. In many locales, such conditions are not unusual, especially in the early morning hours.

The issue of shallow cloud depths, and long time scales are related since molecular diffusion will have a greater net impact on a cloud that is thinner and/or is exposed to air for a longer time. In conclusion #3 it was argued that diffusion can increase the volume of a cloud that is within the flammable region. This is a case of dilution not only not being the solution, but in fact increasing the risk of a release. In the three minute run model run shown in Figure 7.1, the depth of the flammable region kept increasing throughout and it would have kept increasing if it was run longer. Eventually of course, diffusion would eventually cause the cloud too fall below the lower flammability limit, but with this limit being so low (1.6%), this will take a long time.

References

1. *Guidelines for Evaluating the Characteristics of Vapor Cloud Explosions, Flash Fires, and BLEVEs*. American Institute of Chemical Engineers: **1994**; p 387.

2. *The Buncefield Incident 11 December 2005: The Final Report of the Major Incident Incident Investigation Board, Vol. 1*; Buncefield Major Incident Investigation Board: **2008**; p 104.

3. *The Buncefield Incident 11 December 2005: The Final Report of the Major Incident Incident Investigation Board, Vol. 2*; Buncefield Major Incident Investigation Board: **2008**; p 60.

4. *Buncefield Explosion Mechanism*; British Health and Safety Executive: **2009**.

5. Atkinson, G.; Gant, S.; Painter, D.; Shirvill, L.; Ungat, A. *Harards XX: Liquid Dispersal and Vapour Production During Overfilling Incidents*; British Health & Safety Executive: **2008**; p 12.

6. Baik, Jeong-Hyeon, Viscous Effects in Dense Gas Dispersion. Ph.D. Dissertation, University of Arkansas, **1995**.

7. Benjamin, T. B., Gravity Currents and Related Phenomena. *Journal of Fluid Mechanics* **1968,** *31* (2), 209-248.

8. Billeter, L.; Fannelop, T. K., Concentration Measurements in Dense Isothermal Gas Clouds with Different Starting Conditions. *Atmospheric Environment* **1997,** *31* (5), 755-771.

9. Britter, R. E., The Spread of a Negatively Buoyant Plume in a Calm Environment. *Atmospheric Environment* **1979,** *13*, 1241-1247.

10. Britter, R. E.; McQuiad, J. *Workbook on the Dispersion of Dense Gases.*; **1988**.

11. Britter, R. E.; Simpson, J. E., Experiments on the Dynamics of a Gravity Current Head. *Journal of Fluid Mechanics* **1978,** (2), 223-240.

12. Britter, R. E.; Simpson, J. E., A Note on the Structure of the Head of an Intrusive Gravity Current. *Journal of Fluid Mechanics* **1981,** *112*, 459-466.

13. Britter, R.E., Experiments on Some Effects of Obstacles on Dense Gas Dispersion. U.K.A.E.A. Safety and Reliability Directorate Report, SRD R407, **1989**.

14. Cantero, M. I.; Lee, J. R.; Balachandar, S.; Garcia, M. H., On the Front Velocity of Gravity Currents. *Journal of Fluid Mechanics* **2007,** *586*, 1-39.

15. D'Alessio, S. J. D.; Moodie, T. B.; Pascal, J. P.; Swaters, G. E., Gravity Currents Produced by Sudden Release of a Fixed Volume of Heavy Fluid. *Studies in Applied Mathematics* **1996,** *96*, 359-385.

16. Ellison, T. H.; Turner, J. S., Turbulent Entrainment in Stratified Flows. *Journal of Fluid Mechanics* **1959,** *6*, 423-448.

17. Gant, S.E.; Atkinson, G.T. Dispersion of the Vapour Cloud in the Buncefield Incident. *Process Safety and Environmental Protection* **2011**, 89, 391-403

18. Hall, D.J.; Waters, R.J., Investigation of Two Features of Continuously Released Heavy Gas Plumes. Warren Spring Laboratory, Report No. LR 707 (RA), **1989.**

19. Hallworth, M. A.; Huppert, H. E.; Phillips, J. C.; Sparks, S. J., Entrainment into Two-Dimensional and Axisymmetric Turbulent Gravity Currents. *Journal of Fluid Mechanics* **1996,** *308*, 289-311.

20. Henry, N. B., Disaster management in cameroon: The lake nyos disaster experience. *Disaster Prevention and Management* **2012**, *21*(4), 489-506.

21. Hogg, A. J., Lock-Release Gravity Currents and Dam-Break Flows. *Journal of Fluid Mechanics* **2006,** *569*, 61-87.

Hunter D. *The diseases of occupations*, 5th ed. London, England: Hodder and Stoughton, **1975**.

22. Huppert, H. E.; Simpson, J. E., The Slumping of Gravity Currents. *Journal of Fluid Mechanics* **1980,** *99* (4), 785-799.

23. Huppert, H., Gravity Currents: A Personal Perspective. *Journal of Fluid Mechanics* **2006,** *554*, 299-322.

24. Keulegan, G. H., An Experimental Study of the Motion of Saline Water from Locks into Fresh Water Channels. *National Bureau of Standards, U.S. Department of Commerce* **1957,** *Report #5168*.

25. Keulegan, G. H., The Motion of Saline Fronts in Still Water. *National Bureau of Standards, U.S. Department of Commerce* **1958,** *Report #5831*.

26. Kling, G.W.; Tuttle, M.L.; and Evans, W.C., The evolution of thermal structure and water chemistry in Lake Nyos: *Journal of Volcanology and Geothermal Research* **1989**, v. 39, 151-165.

27. Marino, B. M.; Thomas, P. F.; Linden, P. F., The Front Condition for Gravity Currents. *Journal of Fluid Mechanics* **2005,** *536*, 49-78.

28. McQuaid, J., Some Experiments on the Structure of Stably Stratified Shear Flows. Technical Paper P21, Safety in Mines Research Establishment, Sheffield, UK, **1976**.

29. Moodie, T. B., Gravity Currents. *Journal of Computational and Applied Mathematics* **2002,** *144*, 49-83.

30. Peters, W. D.; Venart, J. E. S., Visualization of Rough-Surface Gravity Current Flows Using Laser-Induced Fluorescence. In *9th International Symp*, Carlomagno, G. M.; Grant, I., Eds. **2000**.

31. Rottman, J. W.; Simpson, J. E., Gravity Currents Produced by Instantaneous Releases of a Heavy Fluid in a Rectangular Channel. *Journal of Fluid Mechanics* **1983,** *135*, 95-110.

32. Schmidt, W., Zur Mechanik der Boen. *Meteorologische Zeitschrift* **1911,** *28*, 355-362.

33. Shin, J. O.; Dalziel, S. B.; Linden, P. F., Gravity Currents Produced by Lock Exchange. *Journal of Fluid Mechanics* **2004,** *521*, 1-34.

34. Simpson, J. E., Effects of the Lower Boundary on the Head of a Gravity Current. *Journal of Fluid Mechanics* **1972,** *53* (4), 759-768.

35. Simpson, J. E., Mixing at the Front of a Gravity Current. *Acta Mechanica* **1986,** *63*, 245-253.

36. Simpson, J. E., *Gravity Currents in the Environment and the Laboratory*. Second ed.; Cambridge: **1997**; p 244.

37. Simpson, J. E.; Britter, R. E., The Dynamics of the Head of a Gravity Current Advancing Over a Horizontal Surface. *Journal of the Fluid Mechanics* **1979,** *94* (3), 477-495.

38. Spicer, T.O., *Mathematical Modeling and Experimental Investigation of Heavier-Than-Air Gas Dispersion in the Atmosphere*. Ph.D. Dissertation, University of Arkansas, **1985**.

39. Stretch, D.D, The Dispersion of Slightly Dense Contaminants in a Turbulent Boundary Layer. Ph.D. Thesis, University of Cambridge, **1986**.

40. Venart, J. E. S., In *Buncefield: Reconciliation of Evidence with Mechanisms of Blast*, 23rd International Colloquium on the Dynamics of Explosions and Reactive Systems, Irvine, Ca, Irvine, Ca, **2011**; p 8.

41. Venart, J. E. S.; Rogers, R. J. In *Buncefield: Questions on the Development, Progress, and Severity of the Explosion*, The Sixth International Seminar on Fire and Explosion Hazards, University of Leeds, U.K., Bradley, D., Makhviladze, G., & Molkov, V., Ed. University of New Brunswick: University of Leeds, U.K., **2010**; pp 52-65.

42. von Karman, T., The Engineer Grapples With Non-Linear Problems. *Bulletin of the American Mathematical Society* **1940,** *46*, 615-683.